Load Testing and Load Rating
Eight State Highway Bridges in Iowa

SUBMITTED TO:

Iowa Department of Transportation

BY:

BRIDGE DIAGNOSTICS, Inc.
5398 Manhattan Circle, Suite 100
Boulder, Colorado 80303-4239
(303) 494-3230

November, 1999

Table of Contents

List of Figures

List of Tables

Introduction

Bridge Diagnostics, Inc. was contracted by the Iowa Department of Transportation to perform load testing and load rating on eight highway bridges located primarily in the northern half of the state. Bridge identifications, structure type, and load test dates are provided in Table 1. These bridges were selected for load testing due to deficient load ratings with various load configurations.

Table 1 List of structures.

Bridge Name	Maintenance #	Highway	Structure Type
Robinson Ditch	6723.5R029	I-29	RC Slab - 3 span (17° skew)
West Cedar Cr.	1302.6S020	US-20	RC Slab - 3 span
Lake Creek	1397.5S020	US-20	RC Slab - 3 span
Cedar Creek	7601.2S003	IA-3	Steel beam - 1 span
Cleghorn Ditch	6707.9R029	I-29	RC Slab - 3 span (17° skew)
Des Moines River	4631.1S003	IA-3	Steel beam - 3 span
East Eagle Cr.	9951.4S003	IA-3	Steel beam - PS/C beam hybrid
Elliot Creek	9712.1R020	US-20	Parabolic RC T-beam - 3 span

This main report provides a general discussion of the load testing, structural evaluation, and load rating procedures. Specific details for each bridge are provided in individual report sections. Additional supporting information on load testing, analyses, and load rating are also provided in the attached appendices.

Instrumentation and Testing Procedures

Each bridge was instrumented with between 32 to 40 strain transducers. The transducer locations were selected to capture longitudinal flexure and lateral live-load transfer characteristics of each bridge. Individual instrumentation plans are shown in the following bridge sections.

All sensors were applied in a completely non-destructive manner. Surface grinding was performed to remove paint on steel members and surface dust on concrete members. Note that concrete was **not** removed to expose reinforcement on the RC structures.

Strain measurements on RC members were made with extended gage lengths (12 to 24 inches) to obtain average surface strains. It is important to note that the purpose of the strains was not to directly compute reinforcement steel stress, but simply to measure flexural responses throughout the structure and verify that subsequent analyses would accurately represent the observed live-load distribution.

After each structure was instrumented, load testing was accomplished by recording strain measurements during controlled load applications. Loading was performed by slowly driving a 3-axle dump truck, with known axle weights and dimensions, over the bridge along prescribed paths. During each truck pass, the longitudinal truck position was monitored remotely and recorded with the strain data. Depending on the width of the superstructure, between two and four lateral path-locations were defined so that lateral load distribution behavior could be examined. Truck passes were performed at

least twice along each path to ensure reproducibility of the test procedures and the structure's response behavior. Additional information regarding the semi-static load testing procedures is provided in Appendix A.

Load testing of all eight bridges was performed between the 3rd and 12th of August, 1999. In general, all instrumentation, load testing procedures and instrumentation removal was accomplished in approximately six hours for each bridge. The Iowa Department of Transportation provided all access to the underside of the structures, traffic control, and loading vehicles.

Data Evaluation

All of the field data was initially examined graphically to determine its quality and to provide a *qualitative* assessment of each structure's live-load response. Some of the indicators of data quality included reproducibility between identical truck crossings, elastic behavior (strains returning to zero after truck crossing), and unusual shaped responses that might indicate nonlinear behavior or possible gage malfunctions. Another useful indicator of data integrity was the symmetry of responses, when applicable. For example, strain magnitudes should be similar between symmetrically placed gages and symmetrical truck paths.

In addition to a data "quality check", information obtained during the preliminary investigation was often used to determine appropriate modeling procedures for support conditions and member stiffnesses. For example, the neutral axis locations on the beams and curb elements were examined to assess how these members were interacting with the concrete decks. Composite or non-composite behavior could be immediately established from the strain measurements. In addition, the strain directions and magnitudes observed at gages near abutments were used to determine if negative moment was induced by support conditions.

It should be noted that this qualitative investigation of the data is very important for establishing the direction that the quantitative investigation should take.

Modeling and Analysis

The next phase of the investigation was to develop two-dimensional finite element models for each of the eight superstructures. Once a particular model was developed, the load testing procedures that were used in the field could essentially be "reproduced" through software. A two-dimensional "footprint" of the loading vehicle was applied to each model along the same paths that the actual vehicles crossed the bridge. A direct comparison of strain values could then be made between the analytical predictions and the experimentally measured results. In general, the initial model needed to be "calibrated" until the results matched those measured in the field. The calibration process involved changing member stiffnesses, rotational restraints, and other modeling parameters and is discussed in detail in Appendix B

Load Rating Procedures

The goal of producing accurate models was to use them to predict the actual structure's behavior when subjected to the design loads. This approach is very similar to what is typically done for producing a load rating, except that now an accurate model is being used. All eight bridges were rated using the AASHTO Load Factor technique to develop both inventory and operating limits.

In some cases the rating models were changed from the final "calibrated" models by removing secondary stiffening effects that were considered unreliable for long-term or when heavier loads are applied. For example, rotational end-restraints provided by rocker bearings may "free up" with the passage of a very heavy vehicle. Stiffness parameters that were removed from the calibrated are listed in the individual bridge sections. It was also likely for some structures, that the dead-load distribution was different than the observed live-load performance because of the intended or unintended composite behavior, beam-end restraints, and the addition of continuous RC guardrails. In these cases the models were modified to compute dead-load effects.

Load ratings were completed for the HS-20 design truck and the three Iowa design load configurations as shown in Figure 1. Load ratings were calculated for multiple-lane loading by defining several truck paths that induced critical load responses for the individual components. Load response envelopes containing the critical response from each truck crossing were then generated for each member. Using the principle of superposition, envelopes from truck paths separated by 12 feet were combined to obtain multiple-lane load conditions. Responses from 3-lane loading were reduced by 10% per AASHTO 3.12.1. Additional details on the implemented load rating procedures are provided in Appendix C.

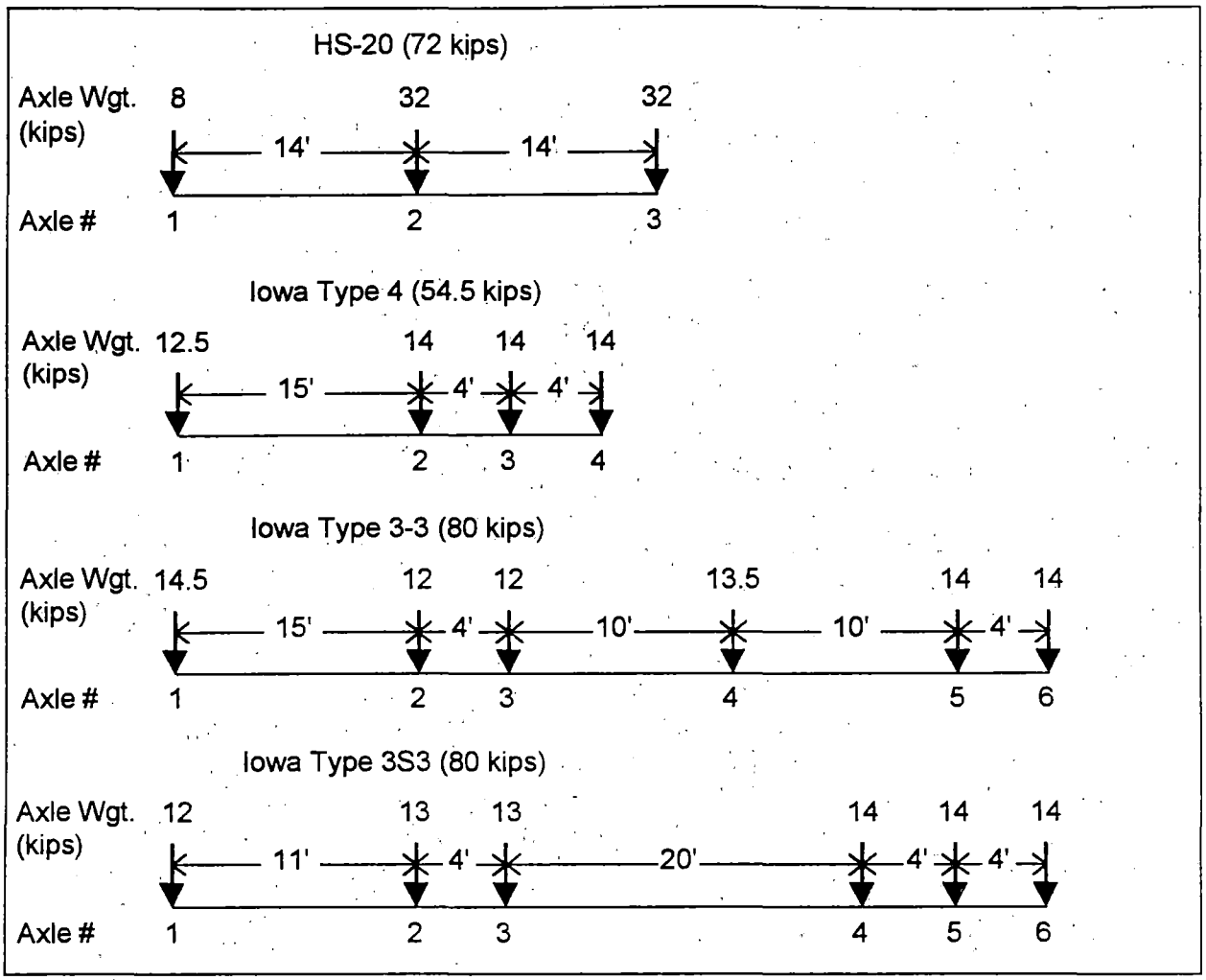

Figure 1 Axle configuration of Iowa rating vehicles.

Summary of Load Rating Results

Table 2 contains the critical (lowest) Inventory and Operating load rating factors obtained from each bridge. All rating factors are based on multiple-lane loading.

Table 2 Controlling load rating factors for Iowa load configurations.

Structure	HS-20		Type 4		Type 3-3		Type 3S3	
	Inv.	Oper.	Inv.	Oper.	Inv.	Oper.	Inv.	Oper.
6723.5R029	1.65	2.75	2.27	3.79	2.05	3.43	1.68	2.80
1302.6S020	1.22	2.04	1.41	2.35	1.88	3.13	1.41	2.35
1397.5S020	1.30	2.16	1.33	2.22	1.85	3.08	1.34	2.24
7601.2S003	2.40	4.01	2.62	4.38	3.10	5.17	2.83	4.72
6707.9R029	1.08	1.80	1.19	1.99	1.27	2.12	1.04	1.73
4631.1S003	1.40	2.33	1.75	2.92	1.43	2.39	1.46	2.44
9951.4S003	1.62	2.71	1.87	3.12	2.00	3.33	2.08	3.48
9712.1R020	.83	1.38	1.02	1.70	0.93	1.56	0.98	1.64

To illustrate how the field verified load ratings compare with those obtained by standard methods (BARS program), Table 3 contains the above HS-20 Inventory and Operating rating values along with the current Iowa DOT load ratings. Iowa DOT ratings are listed for components listed as critical by BDI and BARS.

Table 3 Comparison of BDI and Iowa DOT HS-20 Load Rating Factors.

Structure	HS-20(BDI)		HS-20(DOT)		BDI control	HS-20(DOT)		DOT control
	Inv.	Oper.	Inv.	Oper.	point	Inv.	Oper.	Point (BARS)
6723.5R029	1.65	2.75	0.95	1.57	Pier	0.95	1.57	3.0
1302.6S020	1.22	2.04	0.61	1.02	Span 1	0.60	1.00	2.5
1397.5S020	1.30	2.16	0.68	1.13	Span 1	0.66	1.11	2.5
7601.2S003	2.40	4.01	0.93	1.55	Span 1 int-Bm	0.93	1.55	1.5
6707.9R029	1.08	1.80	1.04	1.73	Pier	1.04	1.73	2.0
4631.1S003	1.40	2.33	0.57	1.07	Span 2 ext-Bm	0.57	1.07	2.5
9951.4S003	1.62	2.71	0.59	1.25	Ext. PS/C Bm	0.36	0.90	1.5
9712.1R020	.83	1.38	0.69	1.14	Pier Ext. BM	0.09	0.14	3.0

Conclusions and Recommendations

In general, the tested bridges had favorable load ratings, indicated by the minimum Inventory rating factors being greater than 1.0. The resulting ratings appear to be representative of each structure's condition and observed performance.

The one bridge that had Inventory rating factors less than 1.0 was the parabolic RC T-beam bridge crossing Elliot Creek in Woodbury County. The relatively low ratings are a function of the design of the bridge as opposed to the structure's performance. Shear and moment capacities of the exterior beams were calculated to be roughly one-half of the interior beam capacities. However, the exterior beams apparently carry a higher percentage of load than was intended (based on the reinforcement details). Therefore the load ratings were controlled by the exterior beam shear and moment capacities while the interior beams had very high ratings for both shear and moment. For load-rating purposes, the vehicle wheel lines were placed two-feet from the face of the curb to generate the critical exterior beam load conditions. Whereas normal truck paths, centered in the lanes, put the wheel lines approximately five-feet from the face of the curb. This may explain why the exterior beams show no sign of distress and perform as well as the interior beams.

Seven of the eight tested structures had RC parapet/guardrails that were not part of the original structure. In each of these cases it was determined that the parapets had a significant effect on the exterior beam or slab edge stiffness and thereby altered the structures' load distribution. This was determined by the measured neutral axis locations of the exterior beams or curbs, and then verified by the calculated load distribution characteristics. On bridges having continuous parapets (without expansion joints) the effects of the parapets were included in the live-load analyses for load rating calculations. In the event that the condition of the parapets are altered, due to environmental effects, impact, overloading, etc., it is likely that the load distributions will be altered as well and rating factors should be modified accordingly. Therefore, the conditions of the parapets should be examined in future inspections. In no case, however, will the loss of parapet stiffness result in a structural failure.

Plans for the widened steel-beam / PS/C bridge (Eagle Creek - 9950.4S003) did not indicate any shear connectors between the steel beams and the concrete deck. During the load test, however, all strain measurements indicated that the beams and deck acted fully composite. Because of the observed condition and the construction details, including the top flanges being embedded in the deck, the deck being bonded to the end-diaphragms and the beam ends being embedded in the end-diaphragms, the bridge was load-rated as a composite structure. It is unlikely that steel/concrete shear interface will fail, however, the condition of the bond lines should be examined during future inspections. In the event of a composite shear failure, the bond will break at the beam-ends and gradually propagate towards midspan of the beam. Given that the structure is highly redundant, a composite shear failure will not result in a structural collapse, therefore it is reasonable to assume composite action for rating purposes.

Bridge 6723.5R029 Robinson Ditch - RC Slab

Description of Structure

Structure Identification	6723.5R029
Location	I-29 over Robinson Drainage Ditch - Monona County
Structure Type	RC Slab - 3 span continuous
Span Length(s)	24'-5", 31'-2", 24'-5"
Skew	17° 9' L.A. (clockwise from perpendicular)
Structure/Slab/Roadway Widths	46'-0", 43'-0", 40'-0"
Slab Thickness	Varies transversely with parabolic curve of top surface. 10 1/2" at slab edge. 17 1/2" at center of roadway
Curb/Parapet Detail	RC curb integral with slab and RC parapet
Visual condition	Slab in excellent condition with minimal flexural or temperature cracks.

Instrumentation and Load Test Details

Date	August 5th 1999
Structural Reference Point	X=0, Y= 0 at intersection of South abutment face and East edge of slab. X direction parallel to roadway.
Test vehicle direction	North bound for all tests (Positive X direction).
Start of data recording	All tests start with front axle at X = -13.6'
Truck position	Record truck position at every wheel revolution (10.808'). *Autoclicker* placed on driver side front wheel.
Lateral truck path(s)	3 truck paths were defined for the load test. The Y position refers to distance between driver side front wheel and East edge of slab. Y1 = 13.7' Y2 = 20.6' Y3 = 36.6'
Measurements	(36) strain gages recorded at 33 Hz
Gage Placement	See Figure 2. All slab gages on bottom of slab. Top parapet gages on top of parapet (42" above bottom of slab). Slab gages placed longitudinally or perpendicular to roadway.
Gage types	BDI Intelliducers with extensions (18" gage length).
Number of test cycles	Data was recorded while the test truck crossed the bridge at crawl speed (5 mph). Each truck path was run twice to check reproducibility. No high-speed passes were performed due to traffic considerations.

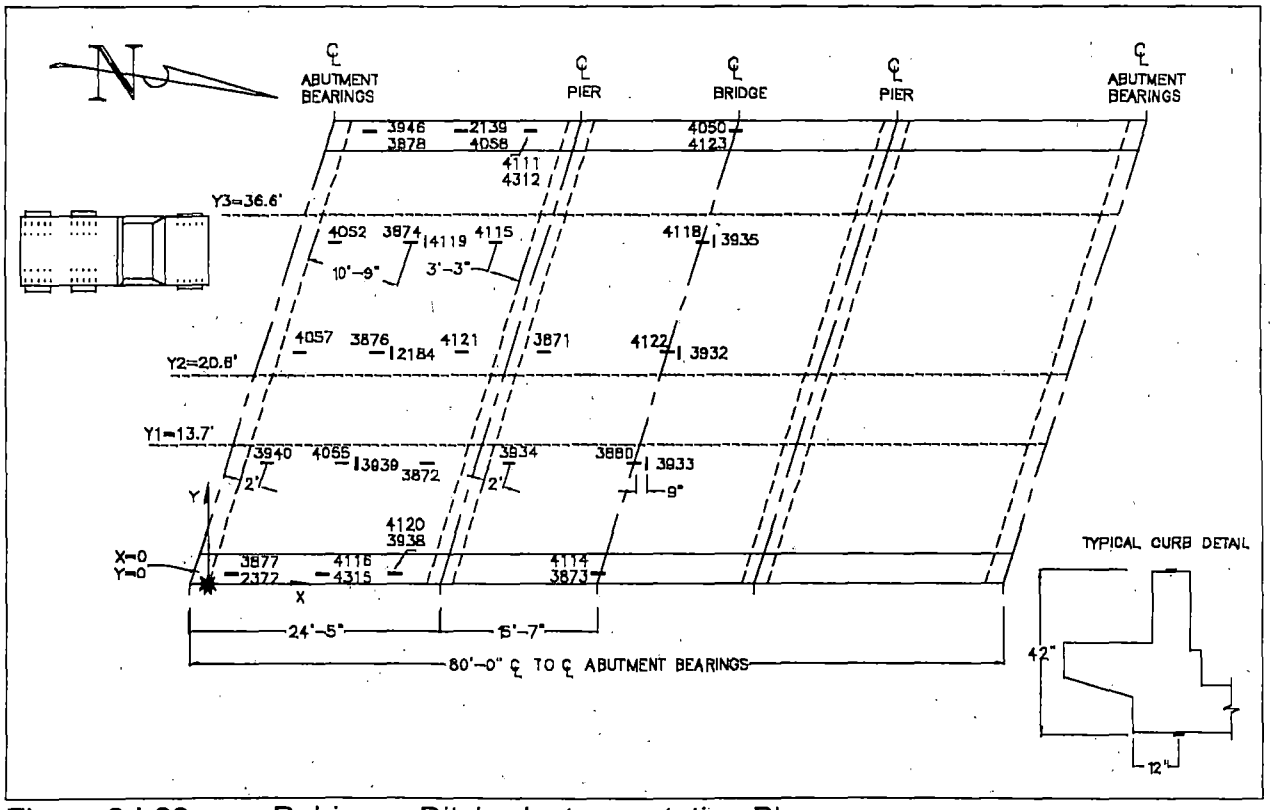

Figure 2 I-29 over Robinson Ditch - Instrumentation Plan.

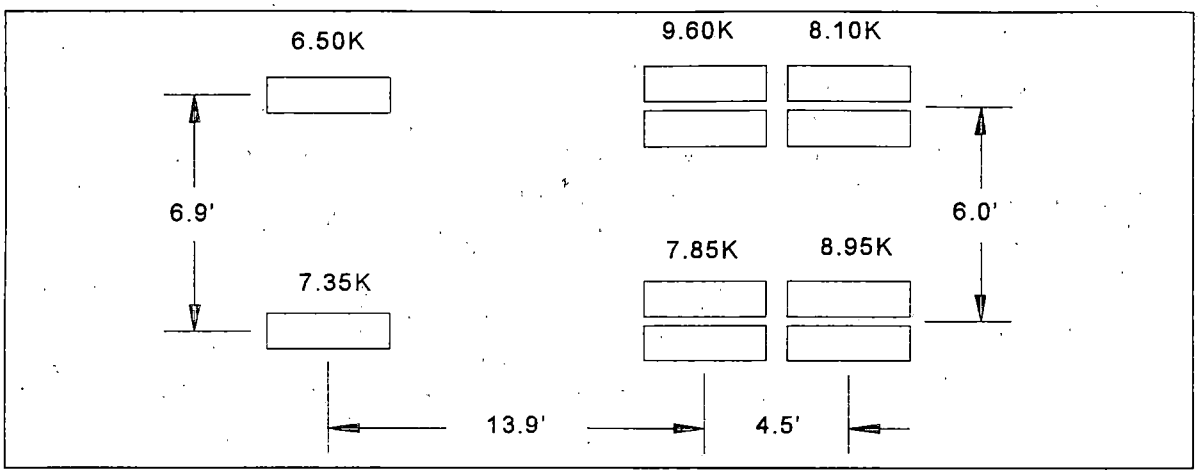

Figure 3 Load Configuration of Test Truck.

Table 4 Load Test Data Files

Truck Path	STS Data File	Comments
Y1	Rob1.dat	Driver-side wheels on right shoulder line
Y1	Rob2.dat	" " " "
Y2	Rob3.dat	Passenger-side wheels on right shoulder line
Y2	Rob4.dat	" " " "
Y3	Rob5.dat	Driver-side wheels on left shoulder line
Y3	Rob6.dat	" " " "

Preliminary Investigation of Test Results

A visual examination of the field data was performed to assess the quality of the data and to make a qualitative assessment of the bridge's live-load response. Conclusions made directly from the field data were:

- Responses from identical truck paths were very reproducible as shown in Figure 4.
- The majority of strain measurements indicated linear-elastic live-load responses. Gages on top of the parapet experienced significant temperature drift relative to the magnitude of live-load strains. The drift was caused by temperature fluctuations and was magnified by aluminum transducer extensions. Normally, temperature fluctuations are not a factor during the short-term live-load tests (30 seconds). However, gages placed on top of the bridge were exposed to sunlight and the temperature change of the transducer and extensions can occur rapidly with changes in cloud cover. Gusty winds can also influence the measurements of gages exposed to solar radiation. Therefore, the top parapet gages were used for qualitative assessment of curb parapet cross-section properties (neutral axis) and not for model calibration.
- Live-load strains were relatively small. Maximum midspan strains were in range of 20 to 30 micro-strain. Assuming a concrete modulus of 4,000 ksi, the maximum midspan strains roughly translate into an average tensile stress of 120 psi at the bottom surface of the slab. Maximum longitudinal steel stresses computed at the gage locations (averaged over 18") equal approximately 600 psi.

- Curb and longitudinal slab strains were relatively consistent with similarly-placed gages.
- Span 2 slab and curb strains were typically 10 to 20 percent less than those measured at the end span strains.
- Strain magnitudes from transverse gages were inconsistent when wheels passed close to the gages. This was a possible indication of high density of longitudinal cracks or that the strain gradient in transverse direction was too steep to be accurately captured with extended gages. Transverse strain measurements were therefore not suitable for model calibration.
- RC parapets and curb were acting integral with the superstructure, essentially providing stiffened edges along the slab. Neutral axes of the parapet were relatively consistent, with the location being 14 to 17 inches from bottom of the slab. Figure 5 shows the consistency of relative strain magnitudes from the top and bottom curb gages. The strain drift on the top curb gage (4114) is due to temperature change, and was verified by the response of the West curb gages. Based on this observation, curbs should be treated as beam line along edge of slab in subsequent analyses since their added stiffness affect the load paths.

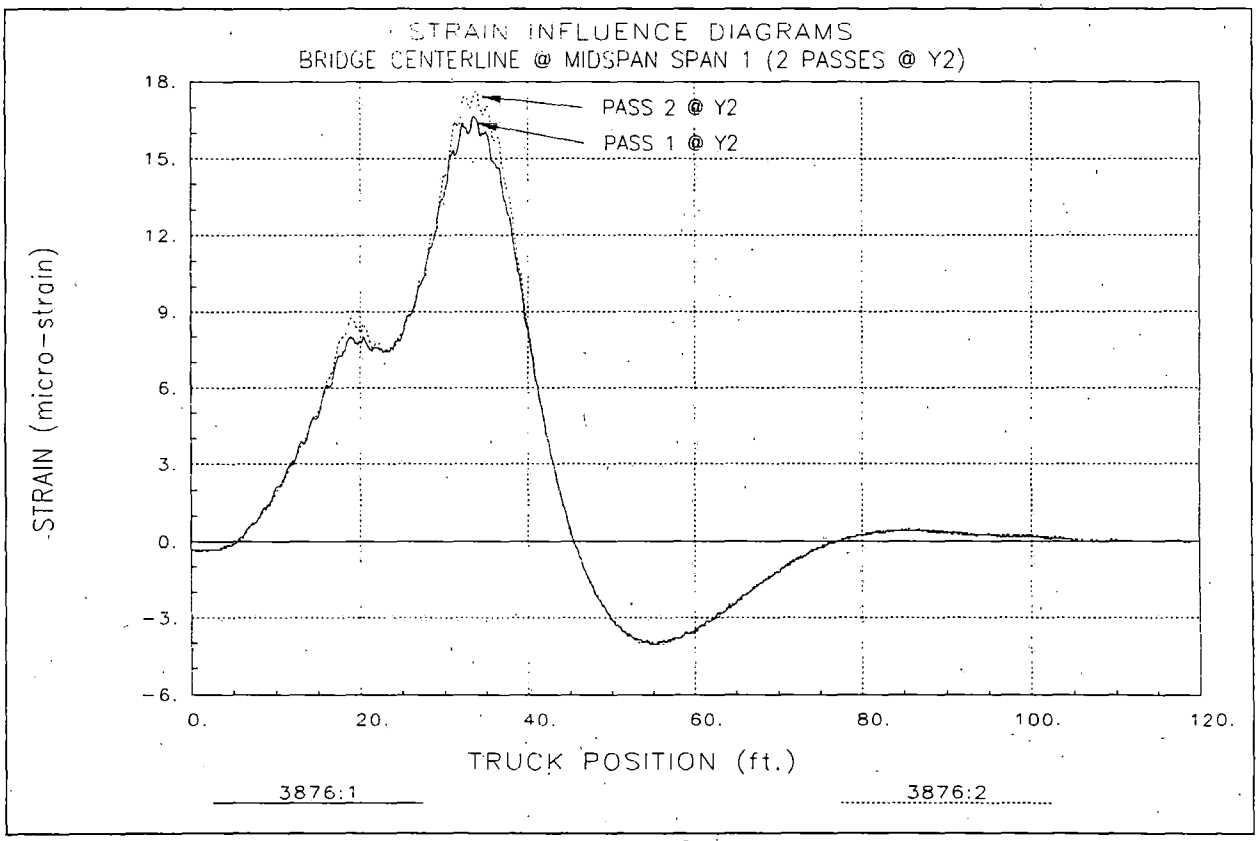

Figure 4 Reproducibility of load test - midspan Span 2.

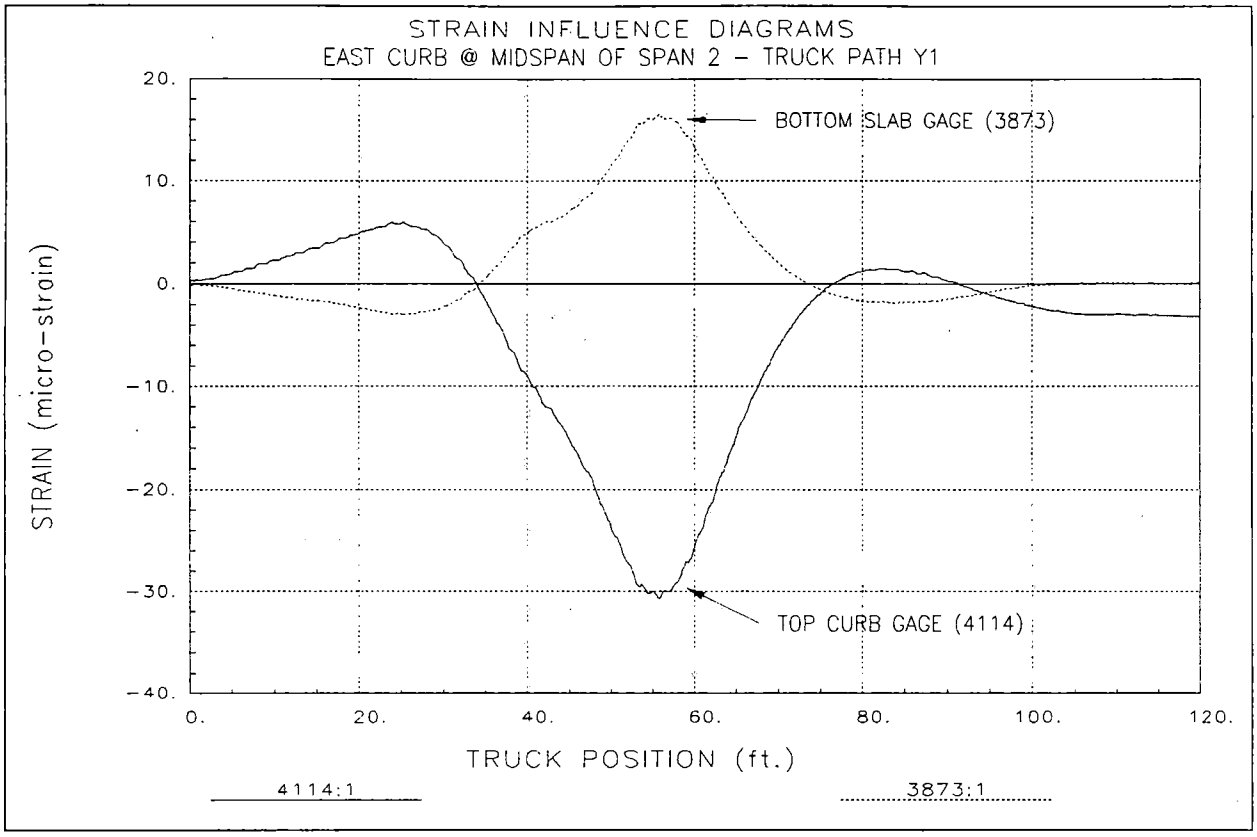

Figure 5 Top and bottom strains at curb - East curb at midspan of Span 2.

Analysis and Model Calibration

Table 5 provides details regarding the structure model and analysis procedures. A discussion of the analysis results is provided along with conclusions regarding the structural performance.

Table 5 Analysis and model details - Robinson Ditch crossing.

Analysis type	Linear-elastic finite element - stiffness method.
Model geometry	Plane grid matching slab plan (see Figure 6)
Model components	• RC slab represented by quadrilateral (skewed) plate elements. Plate thicknesses vary in 1" increments to account for roadway crown. 1" of concrete overlay added to original RC slab thickness. • Curbs simulated by beam elements. Cross-section included parapet, curb, and portion of slab necessary to obtain reasonable neutral axis location (15" from bottom of slab). The beams were assumed to lie in the plane of the deck so the moment-of-inertia properties were computed about the centerline of the slab. • Abutment and pier caps represented by rectangular beam elements. • Elastic spring elements with eccentricity terms used to simulate rotational restraint of pile foundations. Due to construction details, spring used to provide resistance in horizontal translation. The horizontal resistance combined

	with the eccentricity term provides moment resistance.
Live-load	2-D footprint of test truck consisting of 10 vertical point loads. Truck paths simulated by series of load cases with truck moving at 5-foot increments.
Dead-load	Self-weight of slab, curbs, and parapets with additional 15 psf to account for overlay not included in slab thickness. (Used for load rating only)
Data comparison	22 longitudinal strain gage locations defined on model (bottom of slab and curb). Strains computed for 16 truck positions along each path. 22x16x3 = 1056 strain values. Strain records extracted from load test data files corresponding to analysis truck positions.
Model statistics	1000 Nodes 1302 Elements 18 Cross-section/Material types 48 Load Cases 22 Gage locations
Adjustable parameters for model calibration	1 Young's modulus (E_c - ksi) 2 Curb stiffness (I_b - in^4) 3 Abutment pile resistance to horizontal translation (Kx - kips/in) 4 Pier pile resistance to horizontal translation (Kx - kips/in)

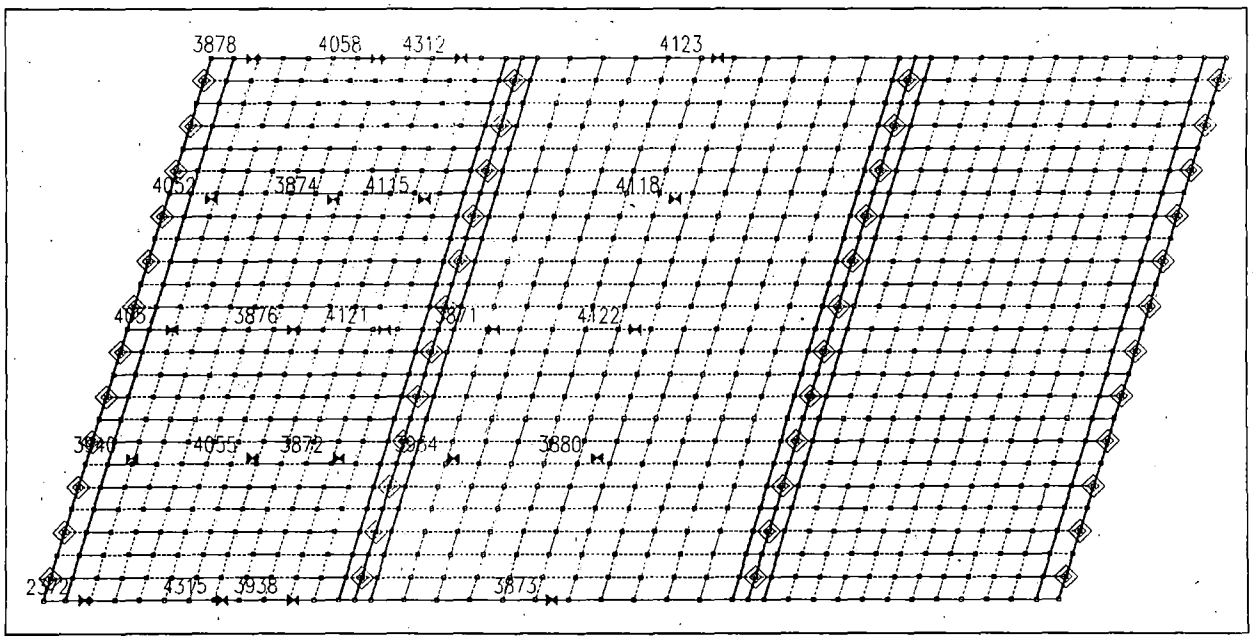

Figure 6 Finite element mesh - I-29 over Robinson Ditch.

A model with the above parameters was defined and the analysis program simulated the load testing process. The accuracy of the model was defined by comparing the 1056 computed and measured strain values. Selected parameters were modified to minimize the comparison error.

The translation spring stiffnesses used to simulate the abutment and pier were aligned parallel to the roadway. The springs were given an eccentricity value equal to the distance between the bottom of the slab and the assumed elastic neutral axis location. The eccentricity term provided a moment-arm such that any translational resistance would induce moment restraint. This method of modeling the support conditions was chosen over rotational springs because it was most representative of the actual construction. Reinforcement dowels, tying the slab to the support elements, were not shown in the plans, therefore a pure moment restraint could not be justified.

Table 6 contains the original stiffness parameters and the final values after the model calibration process. Statistical accuracy values associated with the initial and final models are provided in Table 7. The resulting accuracy terms were in the typical range for RC slab structures.

Table 6 Adjustable Parameter Results

Stiffness Parameter	Units	Initial Value	Final Value
Slab modulus E	ksi	3200	4000
Curb (I)	In^4	117400	105000
Abutment (Kx)	Kips/in	0	550
Pier (Kx)	Kips/in	0	3000

Table 7 Model Accuracy

Statistical Term	Initial Value	Final Value
Absolute Error	1677με	943με
Percent Error	40.5%	13.0%
Scale Error	6.5%	4.1%
Correlation Coefficient	0.93	0.95

Load Rating Calculations

Load rating factors were computed for the slab components of the superstructure using the Load Factor method. A Load Factor of 1.3 was applied to all dead-load affects for both Inventory and Operating load ratings, while load factors 2.17 and 1.3 were applied to live-load responses. Ultimate strength member capacities, based on AASHTO specifications for reinforced concrete beams and slabs, were computed for positive and negative moment regions. Positive moment capacities were obtained for midspan cross-sections and negative moment capacities were computed for slab cross-sections at the face of the pier caps.

Estimated capacity calculations were made for the curb/parapet in positive and negative moment since it was determined that they had significant effect on the load transfer. However, due to lack of structural information on the concrete parapets, the computed capacities are assumed to be overly conservative. It was assumed that the parapet or railing did not contribute to the negative moment capacity of the curb - only the top curb steel was used in ultimate moment computations.

Table 8 contains slab moment capacity calculations for various different slab thicknesses. Grade 40 reinforcement, with a minimum yield stress of 40 ksi, was

assumed based on the age of the structure. A concrete strength of 4 ksi was allowed due the relatively high concrete modulus obtained from the model calibration process. All slab moment capacities are computed for unit width sections (1 in.).

Table 8 Ultimate strength moment capacities for slab sections and curb.

Section	Ultimate Moment Capacities per unit slab width					
t + Cover (in)	d (in)	ρ	+ M (k-in/in)	d' (in)	ρ'	- M (k-in/in)
12 + 1	10.875	.0137	**52.2**	9.81	.0125	**-39.0**
13 + 1	11.875	.0126	**57.6**	10.81	.0113	**-43.4**
14 + 1	12.875	.0116	**63.0**	11.81	.0104	**-47.8**
15 + 1	13.875	.0108	**68.3**	12.81	.0095	**-52.2**
16 + 1	14.875	.0100	**73.7**	13.81	.0089	**-56.6**
17 + 1	15.875	.0094	**79.1**	14.81	.0083	**-61.0**
17.5 + 1	16.375	.0091	**81.8**	15.81	.0080	**-63.2**
Curb/Parapet	40.0	.025	**11681.0**	21.25	.0050	**-3100.0**

Load rating calculations were performed for the HS-20 and the three Iowa rating vehicles by applying the truck configurations to the calibrated model. Due to the width of the roadway, three truck paths were defined. The first path was defined by placing a wheel line 2 feet from the face of the curb. Subsequent truck paths were defined at 12-foot increments. Single lane loading envelopes (critical responses) were generated for every model component by moving the applied rating truck at 2-foot intervals along the length of the bridge. Multiple lane load conditions were obtained by the principle of superposition. The response envelopes were added to generate two and three-lane loading response envelopes. Three-lane load responses were reduced by 10% according to AASHTO specification 3.12.1.

Dead load responses were obtained by computing the self-weight of the structure and adding 15 PSF to account for concrete overlay not included in the slab model components. The model was adjusted prior to dead load application in that spring stiffnesses, providing rotational restraint at support locations, and edge stiffnesses, simulating the curb and parapet effects, were eliminated. Table 9 contains computed dead load and the various rating vehicle live-load forces for each critical slab component. Inventory and operating rating factors for each component are listed in Table 10.

Table 9 Dead load and maximum live load moment on critical slab sections.

Slab Section	Dead-Load M (k-in/in)	HS-20 M (k-in/in)	Type 4 M (k-in/in)	Type 3-3 M (k-in/in)	Type 3S3 M (k-in/in)
12" midspan	8.92	2.72	2.19	1.77	2.02
13" midspan	9.00	4.61	3.73	2.98	3.44
14" midspan	9.21	6.53	5.22	4.26	5.39
15" midspan	11.73	7.71	6.79	5.17	6.54
16" midspan	9.96	9.59	8.14	6.08	7.90
17" midspan	10.69	11.22	9.59	7.19	9.55
17.5" midspan	11.12	11.18	10.44	7.85	9.69
12" pier face	-22.29	-1.21	-0.83	-1.00	-1.27
13" pier face	-13.04	-3.59	-3.18	-3.17	-3.47
14" pier face	-12.17	-5.33	-3.91	-3.90	-4.26
15" pier face	-14.77	-6.47	-5.06	-5.40	-6.10
16" pier face	-14.21	-7.75	-5.89	-6.28	-7.51
17" pier face	-14.41	-9.09	-6.63	-7.29	-8.93
17.5" pier face	-14.03	-9.43	-6.96	-7.60	-9.33

Table 10 Load Rating Factors - Robinson Ditch.

Slab Section	HS-20		Type 4		Type 3-3		Type 3S3	
	Inv.	Oper.	Inv.	Oper.	Inv.	Oper.	Inv.	Oper.
12" midspan	5.18	8.65	6.57	10.97	8.34	13.92	7.32	12.22
13" midspan	3.37	5.63	4.42	7.38	5.53	9.22	4.78	7.99
14" midspan	2.75	4.59	3.45	5.76	4.44	7.42	3.51	5.86
15" midspan	2.39	3.99	2.93	4.90	3.88	6.48	3.07	5.12
16" midspan	2.38	3.97	2.58	4.30	3.44	5.73	2.78	4.63
17" midspan	2.11	3.51	2.38	3.97	3.15	5.26	2.47	4.12
17.5" midspan	2.09	3.49	2.27	3.79	3.02	5.04	2.45	4.08
12" pier face	2.94	4.91	4.26	7.11	3.55	5.93	2.81	4.68
13" pier face	2.61	4.36	3.13	5.22	2.96	4.94	2.70	4.51
14" pier face	2.13	3.55	2.62	4.38	2.45	4.09	2.24	3.74
15" pier face	1.81	3.02	2.43	4.05	2.17	3.62	1.92	3.20
16" pier face	1.74	2.91	2.36	3.94	2.15	3.59	1.80	3.00
17" pier face	1.65	2.75	2.29	3.82	2.05	3.43	1.68	2.80
17.5" pier face	1.69	2.82	2.27	3.80	2.10	3.50	1.71	2.85
Curb @ pier**	1.14	1.90	1.65	2.75	1.37	2.30	1.09	1.81
Critical RF	**1.65**	**2.75**	**2.27**	**3.79**	**2.05**	**3.43**	**1.68**	**2.80**

** Rating of curb/parapet over pier not allowed to govern structure load rating.

Conclusions and Recommendations

The load test and structural assessment results illustrate how components not intended to be structural members often affect the structure's load distribution. The lowest rating factors were obtained for the curb elements in negative moment over the piers. However, due to the over-conservative moment capacity calculation (parapets and railing not contributing), it is not recommended that the curb rating factors be used to

control the superstructure rating. Of the slab components, all rating factors were controlled by the negative moment capacity at the face of the piers.

Due to the high degree of redundancy associated with slab structures, failure of the curb elements will not result in a failure of the entire structure. It is recommended, however, that the condition of the curbs be thoroughly examined during future inspections. Excessive cracking of the parapets and curbs over the piers would be an indication that the bridge has been heavily loaded and that the response behavior of the bridge has changed.

The load rating factors presented in this section are based on the structure's condition at the time of load testing. Any structural degradation must be considered in future load ratings. Note that no effort was made to assess the condition or capacity of the substructure elements such as the abutments or piers.

Bridge 1302.6S020 West Cedar Creek - RC Slab

Description of Structure

Structure Identification	1302.6S020
Location	US 20 over West Cedar Cr. (drainage ditch 83), Calhoun County, Iowa
Structure Type	RC Slab, 3-span continuous
Span Length(s)	21'-4", 27'-4", 21'-4"
Skew	Perpendicular
Structure/Slab/Roadway Widths	36'-0", 34'-0", 30'-0"
Slab Thickness	Varies transversely - parabolic curve at top surface. 11" at edge of slab. 14 1/2" at centerline of bridge.
Curb/Parapet Detail	RC Curb attached with shear keys and stirrups. RC Parapet with expansion joints. Aluminum railing.
Visual condition	Overall appearance is good. Minimal cracking on bottom of slab, no apparent spalling, no exposed reinforcement.

Instrumentation and Load Test Details

Date	August 6th, 1999
Structural Reference Point	South-west corner of slab at inside face of abutment.
Test vehicle direction	East for all truck passes.
Start of data recording	X = -14.64 ft. Face of abutment, back 10', back 1/2 wheel revolution.
Truck position	Record truck position at every wheel revolution (10.808'). *Autoclicker* placed on driver side front wheel.
Lateral truck path(s)	2 truck paths were defined for the load test. The Y position refers to distance between driver side front wheel and south at edge of slab. The two load paths were approximately symmetric about the bridge centerline. Y1 = 5.6 ft Y2 = 28.3 ft (5.7' from north edge of slab)
Measurements	(40) strain gages recorded at 33 Hz
Gage Placement	See Figure 7. 28 locations on bottom of slab, 8 locations on top of curb or parapet, 4 locations on top of slab. Slab gages placed longitudinally or perpendicular to roadway.
Gage types	BDI Intelliducers with extensions (12" gage length).
Number of test cycles	Data was recorded while the test truck crossed the bridge at crawl speed (5 mph). Each truck path was run twice to check reproducibility. No high-speed passes were performed due to traffic considerations.

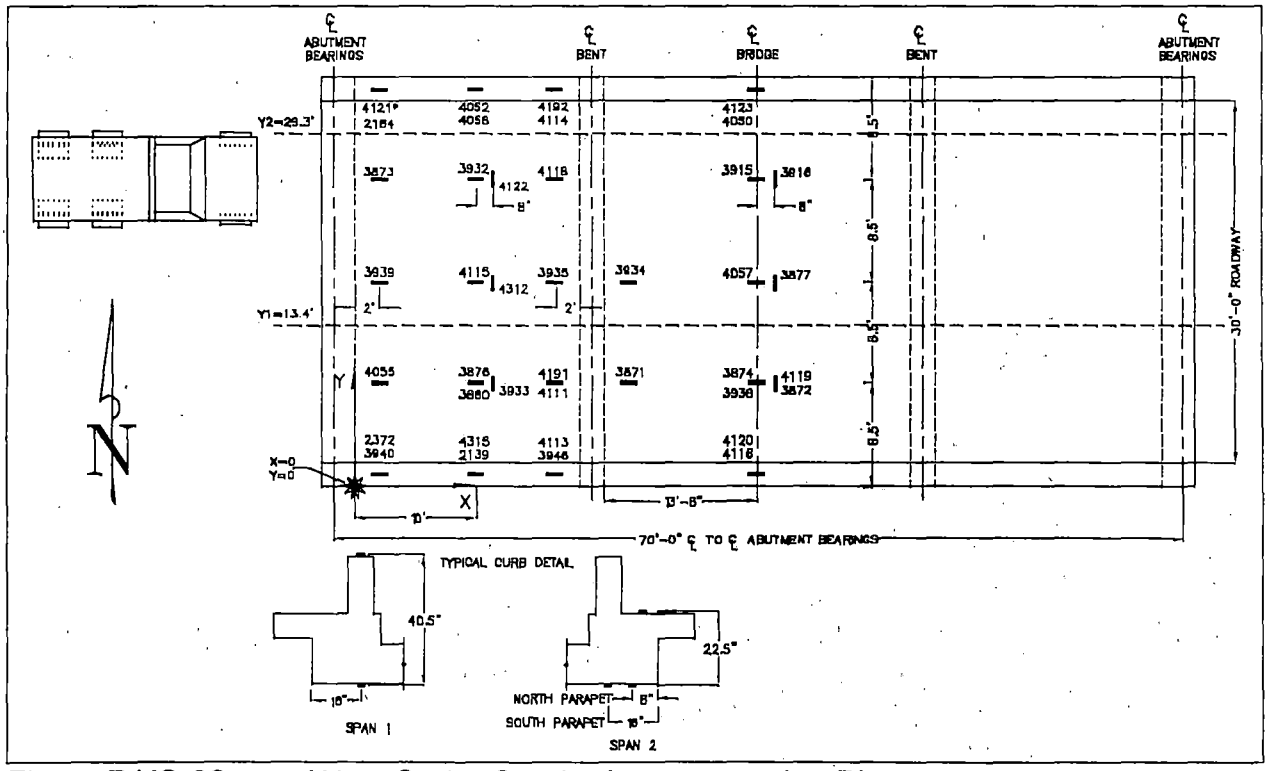

Figure 7 US-20 over West Cedar Creek - Instrumentation Plan.

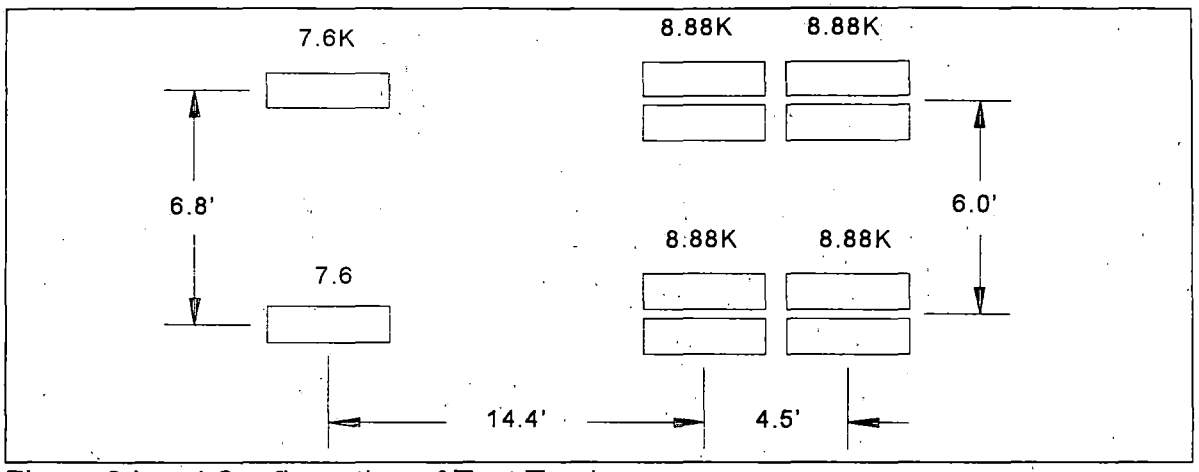

Figure 8 Load Configuration of Test Truck.

Table 11 Load Test Data Files

Truck Path	STS Data File	Comments
Y1	WCED1.DAT	Test truck crossing @ Y1 - crawl speed
Y1	WCED2.DAT	Test truck crossing @ Y1 - crawl speed
Y2	WCED3.DAT	Test truck crossing @ Y2 - crawl speed
Y2	WCED4.DAT	Test truck crossing @ Y2 - crawl speed

Preliminary Investigation of Test Results

A visual examination of the field data was performed to assess the quality of the data and to make a qualitative assessment of the bridge's live-load response. Conclusions made directly from the field data were:

- Symmetry of structure, truck paths, and instrumentation allowed for a direct data comparison of similar gages. Midspan gages located along the structure's centerline measured highly symmetrical responses (Figure 9). The other gages located across the slab provided reasonably consistent strain magnitudes, but not as symmetric as the centerline gages (Figure 10). This is to be expected since the strains are dependent on the local slab properties, which can vary significantly from point to point. Large variations in symmetry were obtained at a few locations.
- Centerline gages near the pier provided less symmetry than the midspan gages, this is an indication that the slab stiffness varies significantly in the negative moment region (Figure 11). Excessive cracking could possibly cause this, or variations may be due to slab repairs. The relatively low strain magnitudes do not indicate a high degree of flexure.
- Neutral axis measurements along the curb varied significantly from location to location. Curb responses near the pier indicated nonlinear behavior, as evidenced by an inconsistent ratio of top and bottom curb strains and peak strains being slightly out of phase to each other (Figure 12). It is evident that the parapet contributes to the curb stiffness, however, parapet contribution should not be allowed during load rating analysis due to the presence of expansion joints and a nonlinear response.

- Strains measured on top of the slab were used to estimate its neutral axis location (Figure 13). All top gages that were exposed to the sun had some drift during the tests and were used for qualitative purposes only.
- Span 2 strain magnitudes were approximately 75% greater than Span 1 strains.
- Strains near abutment indicated minimal end-restraint provided by slab bearing. Strains were typically caused by positive flexure throughout load cycle and in some cases dissipated entirely when truck was on the middle span.

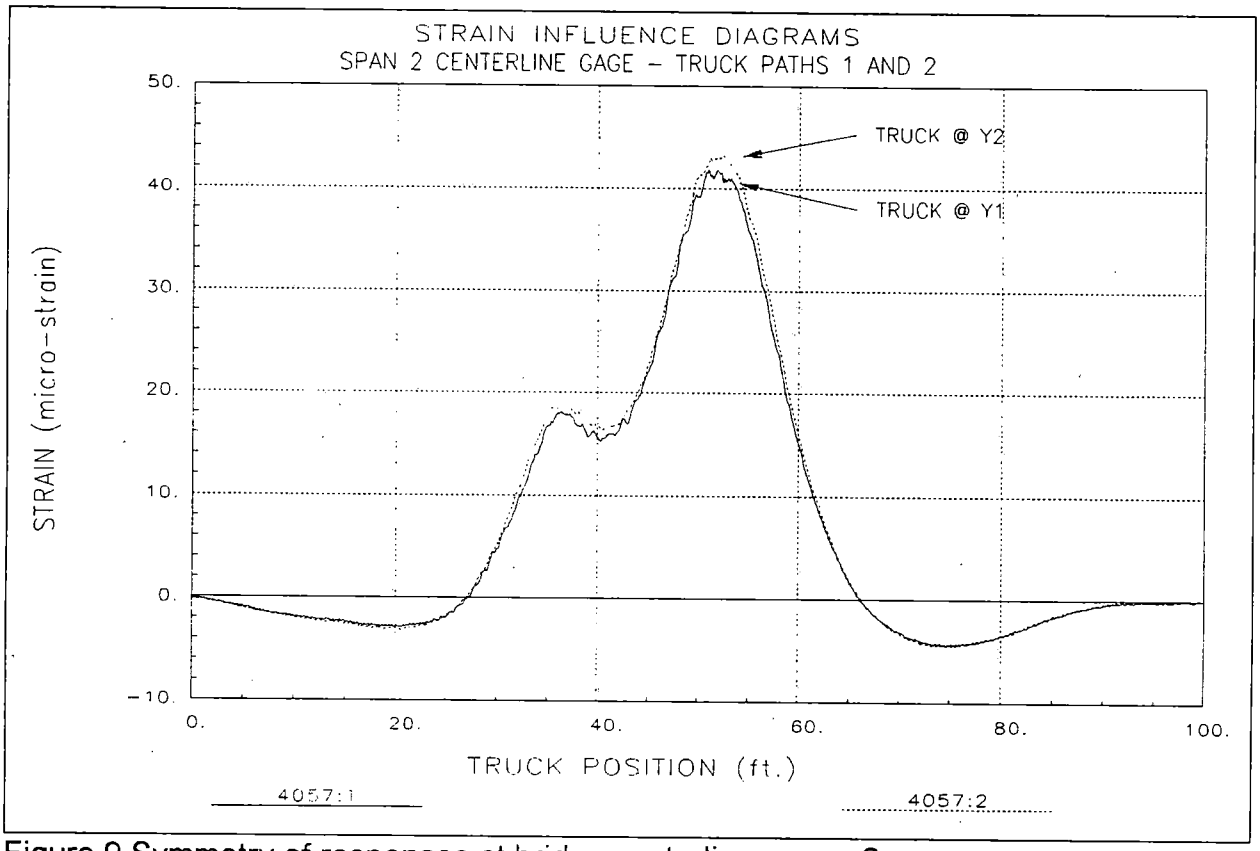

Figure 9 Symmetry of responses at bridge centerline - span 2.

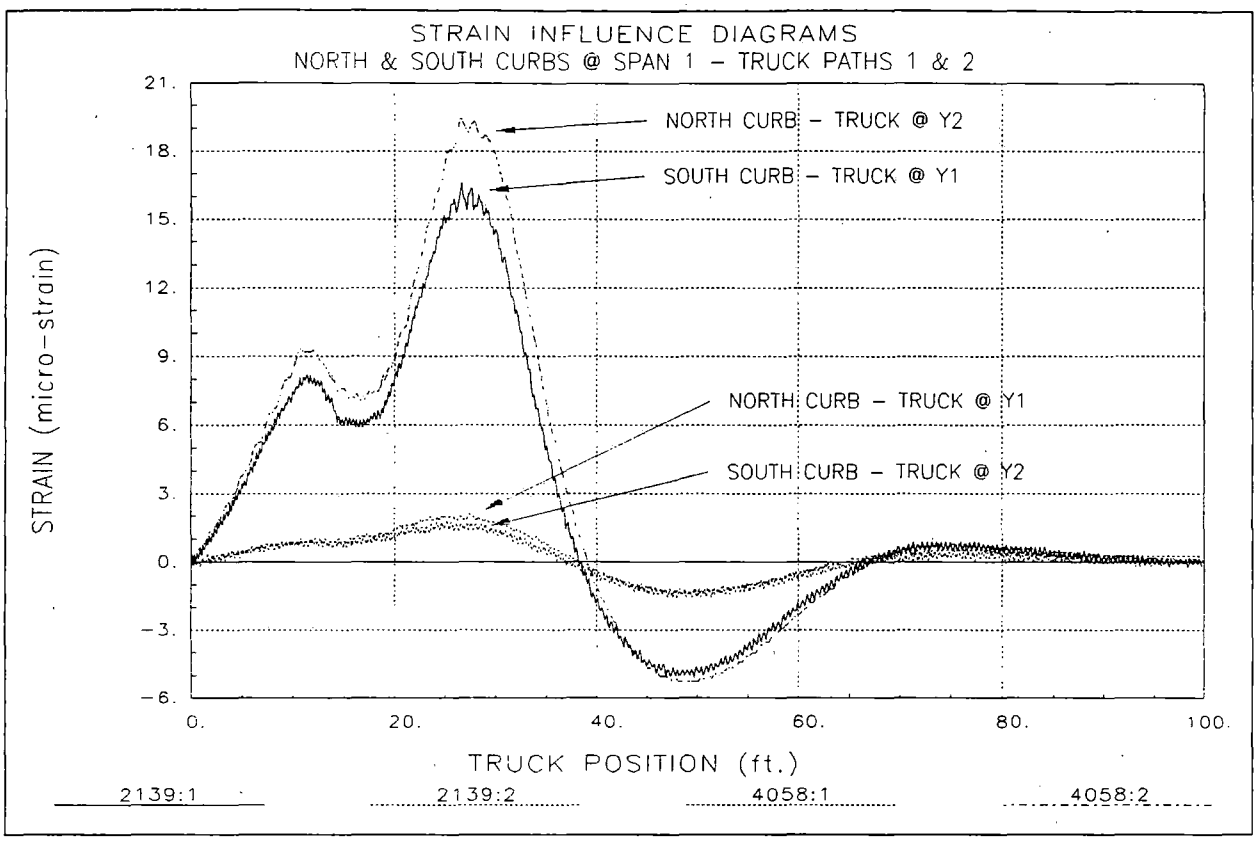

Figure 10 Symmetry of slab edge responses - span 1.

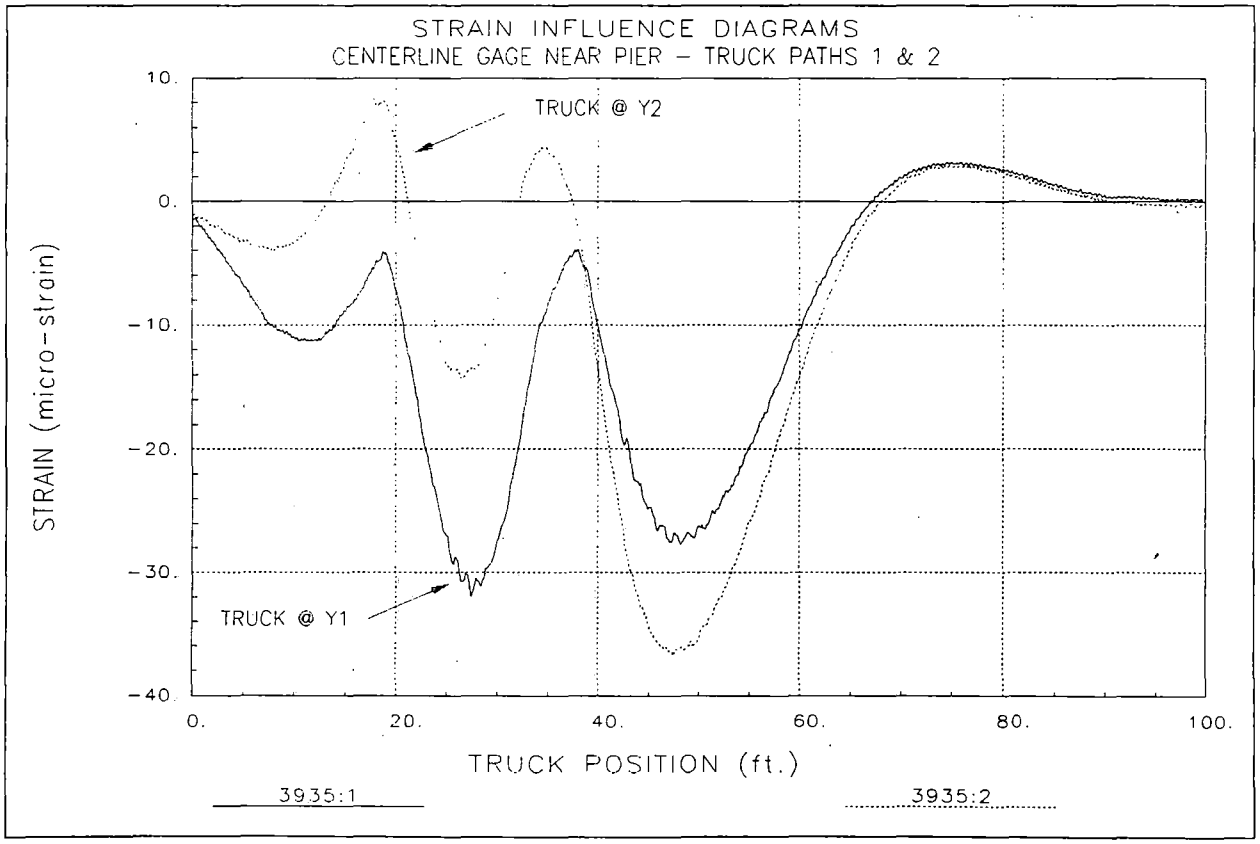

Figure 11 Asymmetrical responses over pier.

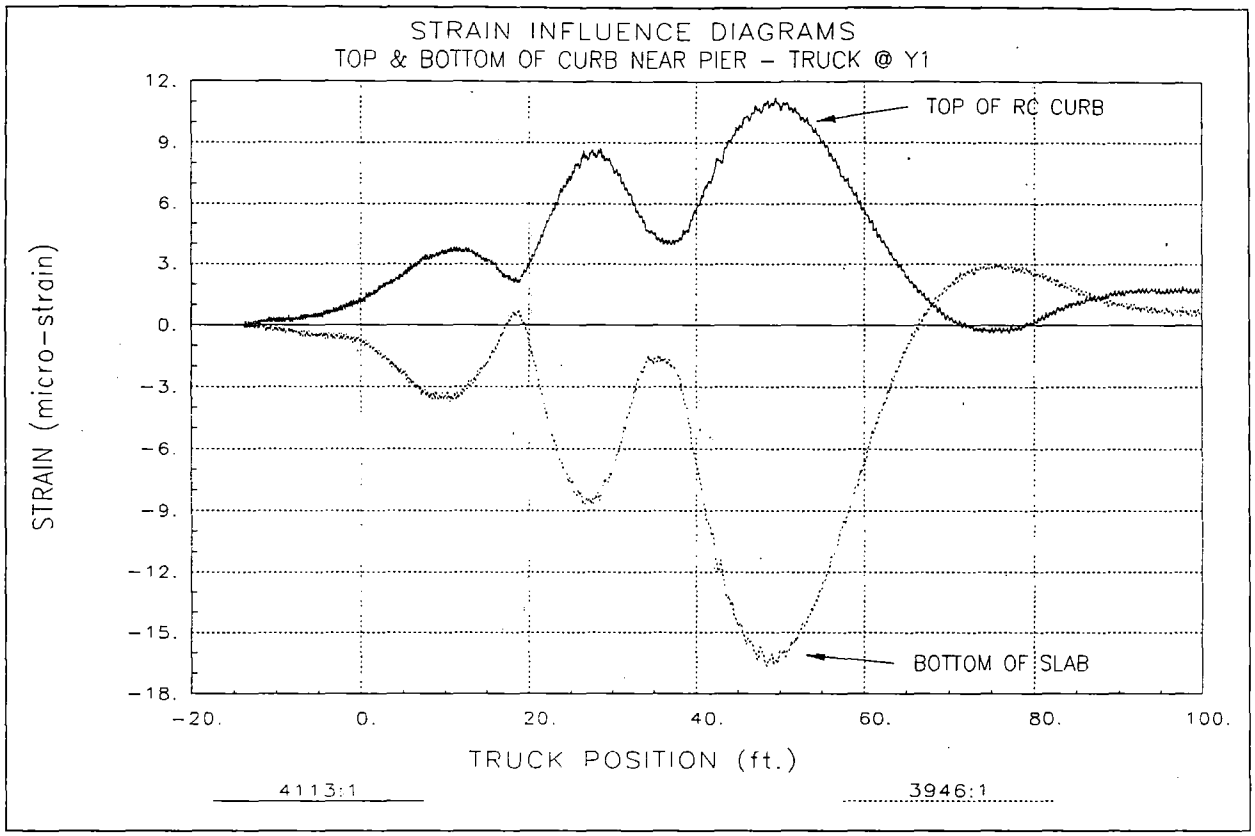

Figure 12 Inconsistent neutral axis measurement along curb.

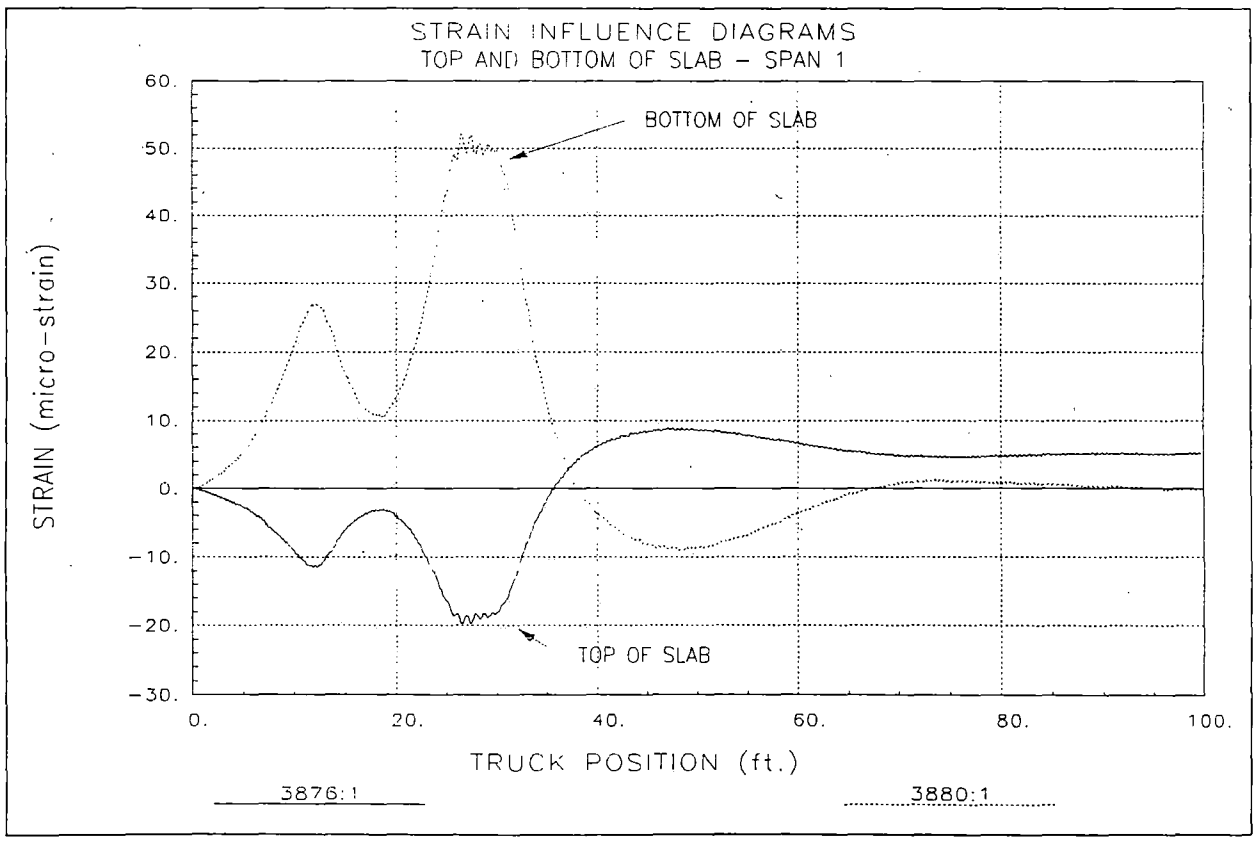

Figure 13 Neutral axis of slab.

Analysis and Model Calibration

Table 12 provides details regarding the structure model and analysis procedures. A discussion of the analysis results is provided along with conclusions regarding the structural performance.

Table 12 Analysis and model details - West Cedar Creek crossing.

Analysis type	Linear-elastic finite element - stiffness method.
Model geometry	Plane grid matching slab plan (see Figure 14)
Model components	• RC slab represented by quadrilateral plate elements. Plate thicknesses vary in 1" increments to account for roadway crown. 1" of concrete overlay added to original RC slab thickness. • Curbs simulated by beam elements. Cross-section included parapet, curb, and portion of slab necessary to obtain reasonable neutral axis location (15" from bottom of slab). • Abutment and pier caps represented by rectangular beam elements. • Elastic spring elements used to simulate pile foundation. Abutment springs resist horizontal translation, whereas pier springs resist rotation and translation.
Live-load	2-D footprint of test truck consisting of 10 vertical point loads. Truck paths simulated by series of load cases with truck moving at 5-foot increments.
Dead-load	Self-weight of slab, curbs, and parapets with additional 15 psf to account for overlay not included in slab thickness. (Used for load rating only)
Data comparison	22 longitudinal strain gage locations defined on model (bottom of slab and curb). Strains computed for 23 truck positions along each path. 22x23x2 = 1012 strain values. Strain records extracted from load test data files corresponding to analysis truck positions.
Model statistics	864 Nodes 1077 Elements 19 Cross-section/Material types 46 Load Cases 22 Gage locations
Adjustable parameters for model calibration	1 Slab stiffness (E_c - ksi) Span 1 2 Slab stiffness (Ec) over pier 3 Slab stiffness (Ec) Span 2 4 Effective Curb stiffness with parapet (I - in^4) 5 Effective cub stiffness at parapet expansion joints (I - in^4) 6 Abutment pile longitudinal resistance (Kx - kips/in) 7 Pier pile rotational resistance (Kr - kip-in/rad)

An initial model with the above parameters was defined and the analysis program simulated the field load test process. The accuracy of the model was defined by

comparing the 1012 computed and measured strain values. Selected parameters were modified to minimize the comparison error.

Table 13 contains the original stiffness parameters and the final values after the model calibration process. Statistical accuracy values associated with the initial and final models are provided in Table 14. The resulting accuracy terms were in the typical range for RC slab structures.

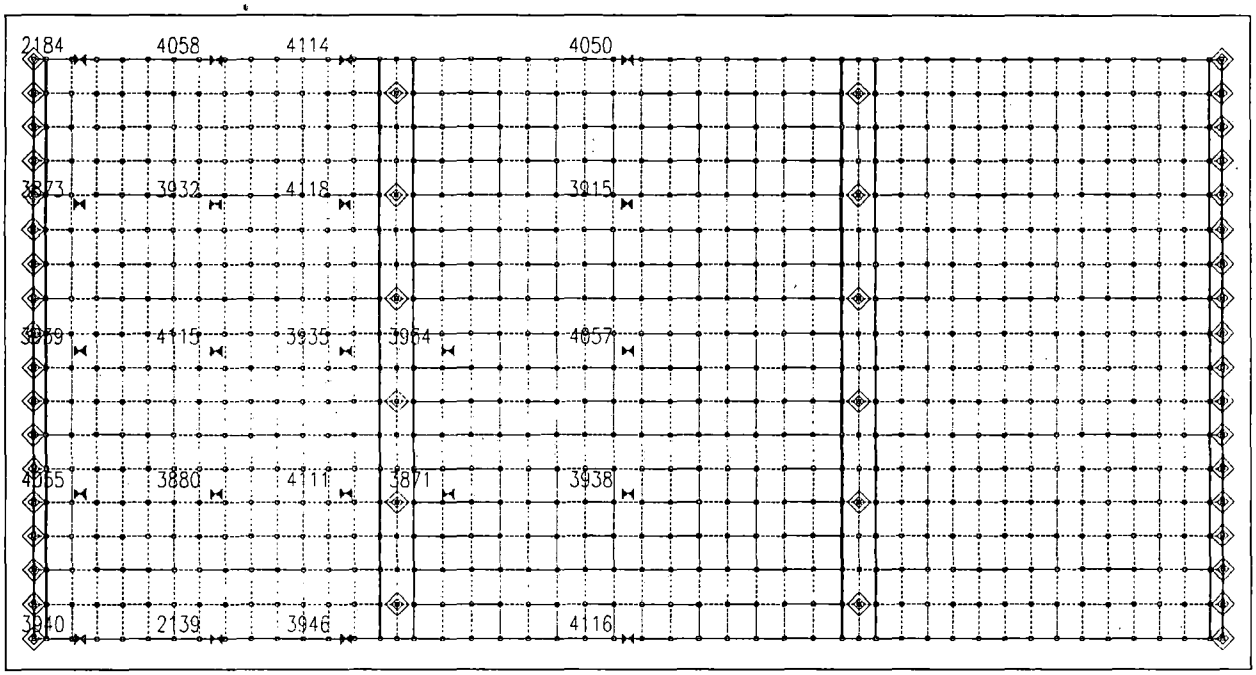

Figure 14 Finite element mesh of bridge - West Cedar Creek.

Table 13 Adjustable Parameter Results

Stiffness Parameter	Units	Initial Value	Final Value
Slab modulus Span 1 E	ksi	3200	3500
Slab modulus @ pier E	ksi	3200	2525
Slab modulus Span 2 E	ksi	3200	2982
Curb/parapet I	in^4	73780	70600
Curb/no parapet I	in^4	23980	25300
Abutment (Kx) of single pile	Kips/in	0	500
Pier (Kr) of single pile	Kip-in/rad	0	400000

Table 14 Model Accuracy

Statistical Term	Initial Value	Final Value
Absolute Error	2865 με	1570 με
Percent Error	20.1 %	9.5 %
Scale Error	11.6 %	4.1 %
Correlation Coefficient	0.91	0.95

Load Rating Calculations

Load rating factors were computed for the structural components of the superstructure using the Load Factor method. A Load Factor of 1.3 was applied to all dead-load effects for both Inventory and Operating load ratings, while load factors 2.17 and 1.3 were applied to live-load responses. Ultimate strength member capacities, based on AASHTO specifications for reinforced concrete beams and slabs, were computed for positive and negative moment regions. Positive moment capacities were obtained for midspan cross-sections and negative moment capacities were computed for slab cross-sections at the face of the pier caps.

Table 15 contains slab moment capacity calculations for various different slab thicknesses. Grade 40 reinforcement, with a minimum yield stress of 40 ksi, was assumed based on the age of the structure. A concrete strength of 4 ksi was allowed due the relatively high concrete modulus obtained from the model calibration process. All slab moment capacities are computed for unit width sections (1 in.).

Table 15 Ultimate strength moment capacities for slab sections and curb.

Section	Ultimate Moment Capacities per unit slab width		
	d (in)	ρ	Mu (k-in/in)
Slab A span 1 12"	10.0	.0105	**35.6**
Slab B span 1 13"	11.0	.0096	**39.4**
Slab C span 1 14"	12.0	.0088	**43.2**
Slab D span 1 14.5"	12.5	.0084	**45.1**
Slab A @ pier 12"	10.0	.0133	**44.2**
Slab B @ pier 13"	11.0	.0121	**49.0**
Slab C @ pier 14"	12.0	.0111	**53.8**
Slab D @ pier 15"	12.5	.0107	**56.2**
Slab A span 2 12"	10.0	.0119	**39.9**
Slab B span 2 13"	11.0	.0108	**44.2**
Slab C span 2 14"	12.0	.0099	**48.5**
Slab D span 2 14.5"	12.5	.0095	**50.7**

Load rating calculations were performed for the HS-20 and the three Iowa rating vehicles by applying the truck configurations to the calibrated model. Due to the width of the roadway, two truck paths were defined. The first path was defined by placing a wheel line 2 feet from the face of the curb with a second truck path 12 feet away. A second pair of truck paths was defined in which the lateral positions were symmetric about the bridge centerline. Single lane loading envelopes (critical responses) were generated for every model component by moving the applied rating truck at 2-foot intervals along the length of the bridge. Multiple lane load conditions were obtained by using the principle of superposition. The response envelopes were added to generate two-lane loading response envelopes.

Dead load responses were obtained by computing the self-weight of the structure and adding 15 PSF to account for concrete overlay not included in the slab model components. The model was adjusted prior to load rating calculations in that spring

stiffnesses, providing rotational restraint at abutment support locations, and the effect of the parapet on the curb stiffness were eliminated. Table 16 contains computed dead load and the various rating vehicle live-load forces for each critical slab component. Inventory and operating rating factors for each component are listed in Table 17.

Table 16 Dead load and maximum live load moment on critical slab sections.

Section	Dead-Load M (k-in/in)	HS-20 M (k-in/in)	Type 4 M (k-in/in)	Type 3-3 M (k-in/in)	Type 3S3 M (k-in/in)
Slab A span 1	3.62	6.07	4.78	3.77	4.76
Slab B span 1	4.52	7.59	6.62	5.07	6.62
Slab C span 1	5.32	9.16	7.64	5.83	7.64
Slab D span 1	6.56	10.63	9.09	6.91	9.10
Slab A @ pier	-6.07	-4.35	-3.75	-3.73	-4.15
Slab B @ pier	-7.23	-6.75	-6.04	-5.51	-6.47
Slab C @ pier	-8.82	-7.84	-6.98	-6.53	-7.66
Slab D @ pier	-8.82	-7.84	-6.98	-6.53	-7.66
Slab A span 2	3.82	5.98	4.49	3.51	4.19
Slab B span 2	4.77	7.46	6.34	4.83	5.99
Slab C span 2	5.70	8.98	7.28	5.58	6.92
Slab D span 2	7.09	10.46	8.75	6.68	8.34

Table 17 Load Rating Factors - West Cedar Creek.

Section	HS-20		Type 4		Type 3-3		Type 3S3	
	Inv.	Oper.	Inv.	Oper.	Inv.	Oper.	Inv.	Oper.
Slab A span 1	1.80	3.01	2.28	3.80	2.96	4.95	2.28	3.81
Slab B span 1	1.57	2.62	1.76	2.95	2.32	3.88	1.76	2.95
Slab C span 1	1.40	2.35	1.67	2.78	2.21	3.69	1.67	2.78
Slab D span 1	**1.22**	**2.04**	**1.41**	**2.35**	**1.88**	**3.13**	**1.41**	**2.35**
Slab A @ pier	2.96	4.94	3.45	5.77	3.47	5.79	3.12	5.20
Slab B @ pier	2.08	3.47	2.32	3.88	2.55	4.25	2.17	3.62
Slab C @ pier	1.91	3.20	2.15	3.59	2.30	3.83	1.96	3.27
Slab D @ pier	2.02	3.38	2.27	3.79	2.43	4.05	2.07	3.46
Slab A span 2	2.07	3.46	2.76	7.73	3.56	5.95	2.95	4.93
Slab B span 2	1.81	3.01	2.11	3.51	2.77	4.62	2.23	3.72
Slab C span 2	1.62	2.71	2.00	3.34	2.61	4.36	2.10	3.50
Slab D span 2	1.41	2.35	1.68	2.81	2.20	3.68	1.77	2.95
Critical RF	**1.22**	**2.04**	**1.41**	**2.35**	**1.88**	**3.13**	**1.41**	**2.35**

Conclusions and Recommendations

Field measurements and the resulting calibrated model indicated that the parapets contributed to the edge stiffness of the slabs. However, due to the presence of expansion joints in the parapets and apparent nonlinear behavior of the parapets, this contribution was not included in the rating analyses. In general, the obtained rating values can be considered slightly conservative. A potential side effect of the expansion joints is the formation of cracks in the curbs due to moment concentrations.

The negative moment region, immediately adjacent to pier caps, is on average more flexible than positive moment regions. While this has little bearing on the moment capacity, it does suggest a higher density of flexural cracks. The presence of flexural cracks on the top of the deck may present a serviceability or maintenance issue since water and road salt can penetrate the slab more easily. Regarding load rating, however, the extra flexibility of the slab near the piers actually reduces the negative moment and increases the midspan moments. This is evident in the load rating results since all of the controlling rating factors were due to positive moment in the end-spans.

Another contributor to the critical region being at the end spans is the apparent lack of end-restraint commonly found in RC slab structures. Additionally, the calculated moment capacities were smaller at midspan of the end spans compared to the interior span or at the pier face.

The load rating factors presented in this report are based on the structure's condition at the time of load testing. Any structural degradation must be considered in future load ratings. Note that no effort was made to assess the condition or capacity of the substructure elements such as the abutments or piers.

Bridge 1397.5S020 Lake Creek - RC Slab

Description of Structure

Structure Identification	1397.5S020
Location	US 20 over Lake Creek Calhoun County, Iowa
Structure Type	RC Slab, 3-span continuous
Span Length(s)	21'-4", 27'-4", 21'-4"
Skew	Perpendicular
Structure/Slab/Roadway Widths	36'-0", 34'-0", 30'-0"
Curb/Parapet Detail	RC Curb attached with shear keys and stirrups. RC Parapet with expansion joints. Aluminum railing.
Visual condition	Overall appearance is good. Minimal cracking on bottom of slab, no apparent spalling, no exposed reinforcement.

Instrumentation and Load Test Details

Date	August 9th, 1999
Structural Reference Point	South-west corner of slab at inside face of abutment.
Test vehicle direction	East for all truck passes.
Start of data recording	X = -14.64 ft. Face of abutment, back 10', back 1/2 wheel revolution.
Truck position	Record truck position at every wheel revolution (10.808'). *Autoclicker* placed on driver side front wheel.
Lateral truck path(s)	2 truck paths were defined for the load test. The Y position refers to distance between driver side front wheel and south at edge of slab. The two load paths were approximately symmetric about the bridge centerline. Y1 = 5.6 ft Y2 = 28.3 ft (5.7' from north edge of slab)
Measurements	(40) strain gages recorded at 33 Hz.
Gage Placement	See Figure 15. 28 locations on bottom of slab, 8 locations on top of curb or parapet, 4 locations on top of slab. Slab gages placed longitudinally or perpendicular to roadway.
Gage types	BDI Intelliducers with extensions (12" gage length).
Number of test cycles	Data was recorded while the test truck crossed the bridge at crawl speed (5 mph). Each truck path was run twice to check reproducibility. No high-speed passes were performed due to traffic considerations.

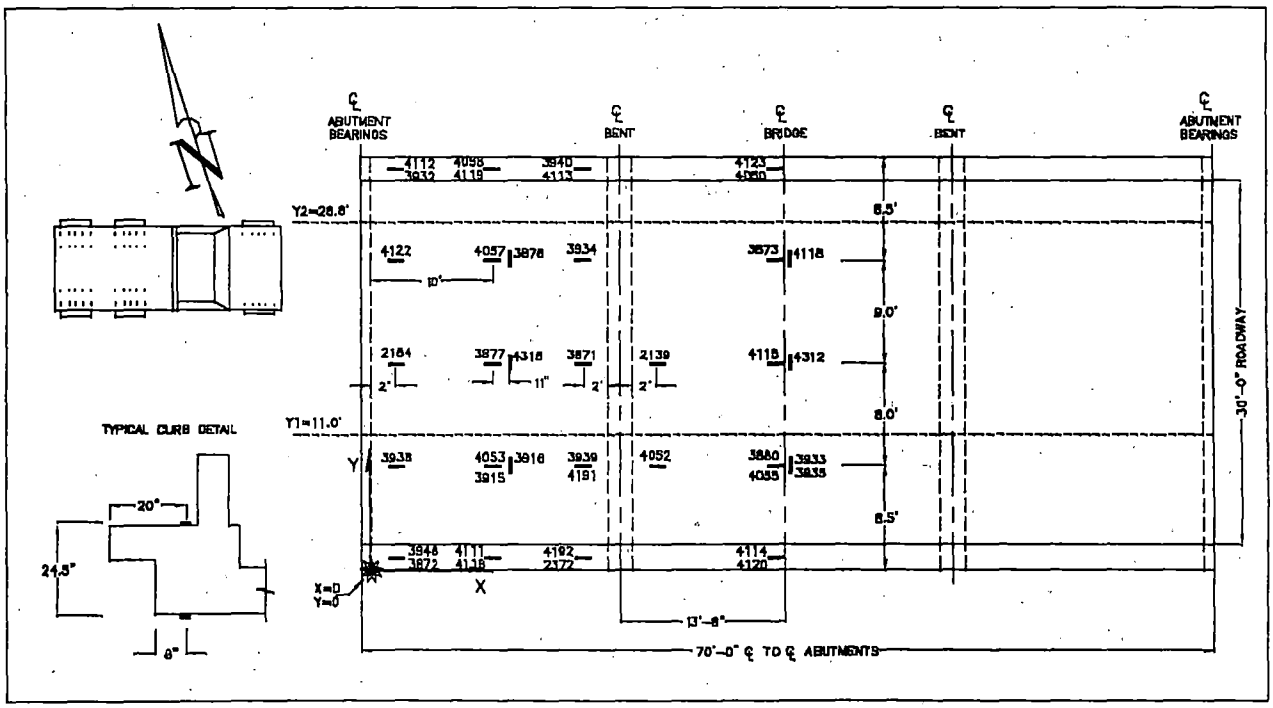

Figure 15 US-20 over Lake Creek - Instrumentation Plan.

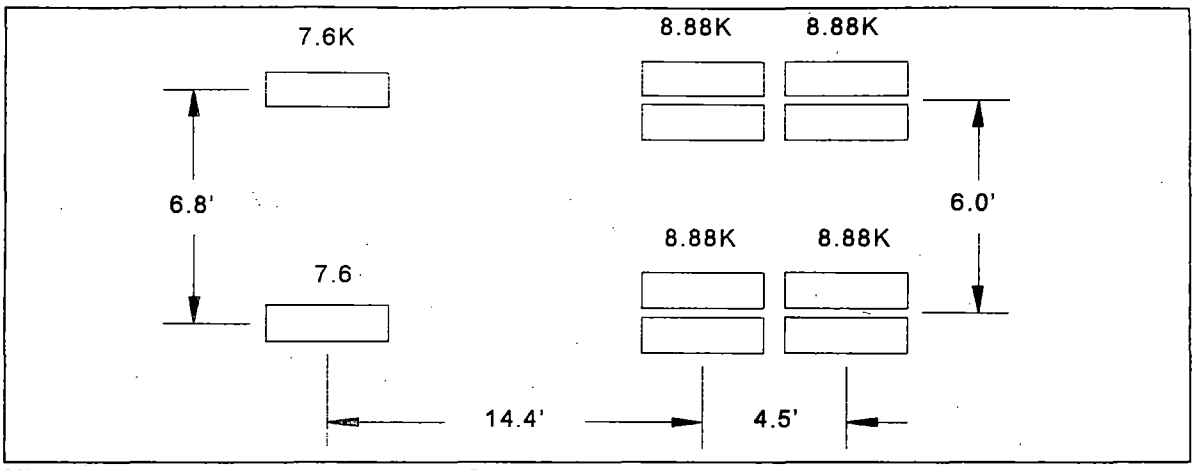

Figure 16 Load Configuration of Test Truck.

Table 18 Load Test Data Files

Truck Path	STS Data File	Comments
Y1	LAKE1.DAT	Test truck crossing @ Y1 - crawl speed
Y1	LAKE2.DAT	Test truck crossing @ Y1 - crawl speed
Y2	LAKE3.DAT	Test truck crossing @ Y2 - crawl speed
Y2	LAKE4.DAT	Test truck crossing @ Y2 - crawl speed

Preliminary Investigation of Test Results

A visual examination of the field data was performed to assess the quality of the data and to make a qualitative assessment of the bridge's live-load response. Conclusions made directly from the field data were:

- Symmetry of structure, truck paths, and instrumentation allowed for a direct data comparison of similar gages. Midspan gages located near the structure's centerline measured relatively symmetrical responses (Figure 17). Due to a construction joint located along the structure centerline, the centerline gages were moved 1' south of centerline. Therefore centerline gage measurements were not expected to be perfectly symmetric. The other gages located across the slab provided reasonably consistent strain magnitudes as well due to the symmetric loading (Figure 18). Large variations in symmetry were obtained at a few locations.
- Centerline gages near the pier provided less symmetry than the midspan gages, this is an indication that the slab stiffness varies significantly in the negative moment region. Excessive cracking could possibly cause this, or variations may be due to slab repairs. The relatively low strain magnitudes do not indicate a high degree of flexure.
- It is evident that the parapet contributes to the curb stiffness, however, parapet contribution should not be allowed during load rating analysis due to the presence of expansion joints.
- Strains measured on top of slab were used to help locate its neutral axis (Figure 19).
- Span 2 strain magnitudes were approximately 50% greater than Span 1 strains.
- Strains near abutment indicate minimal end-restraint provided by slab bearing.

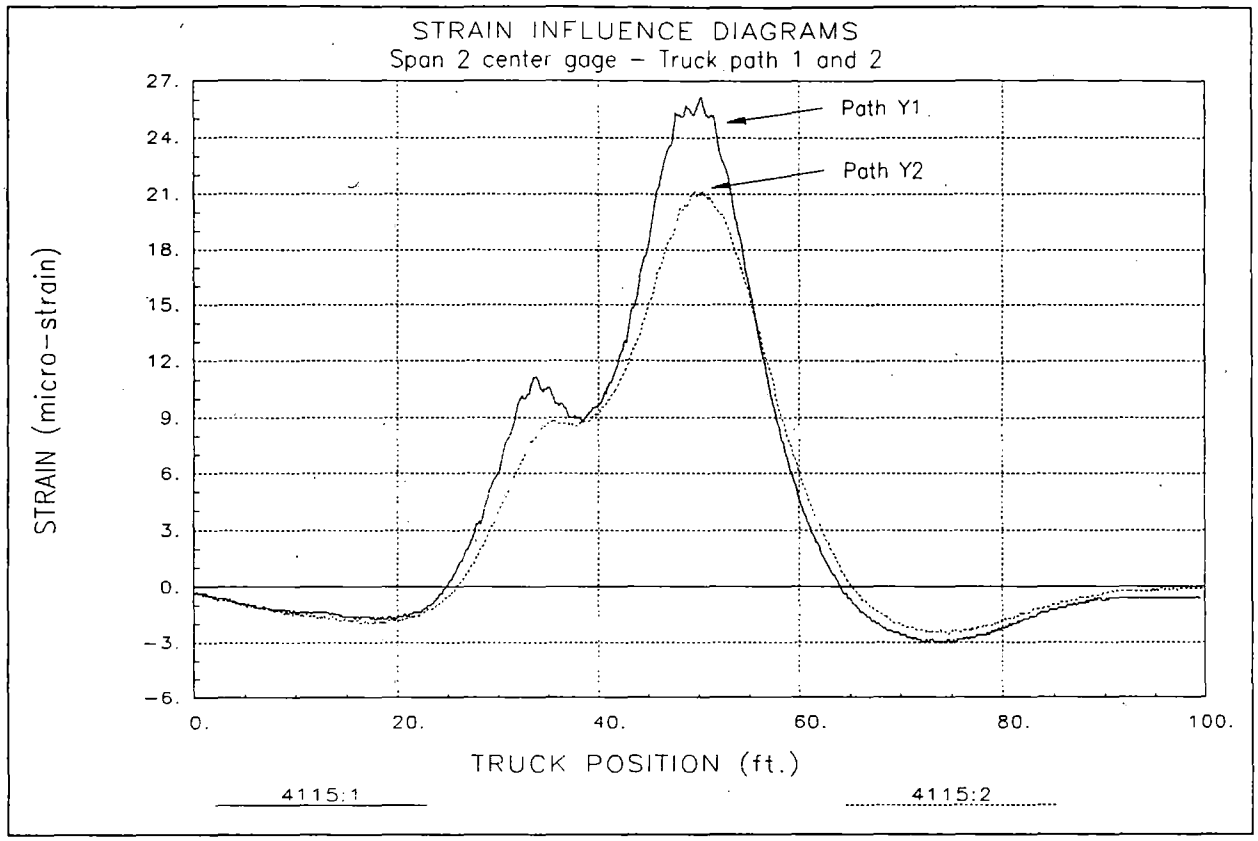

Figure 17 Symmetry of responses at bridge centerline - span 2.

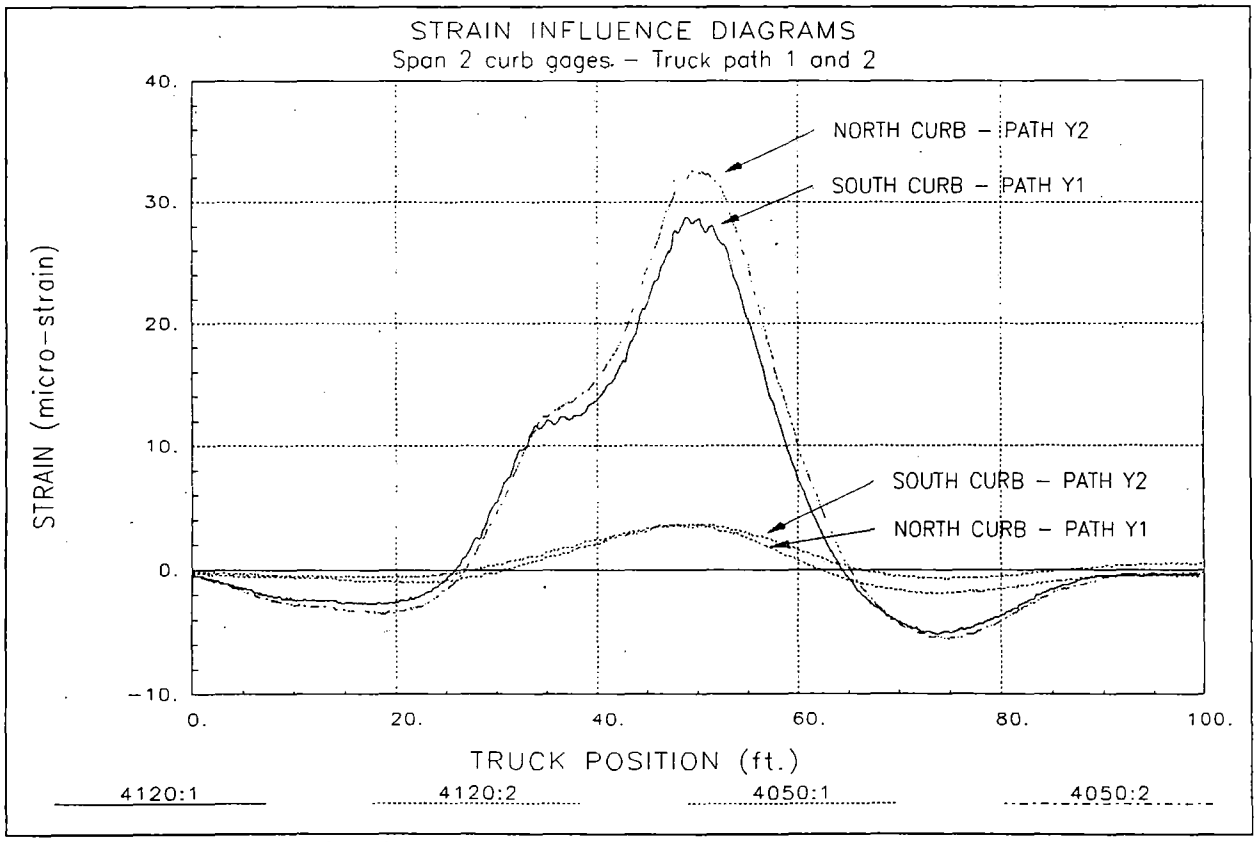

Figure 18 Symmetry of slab edge responses - span 1.

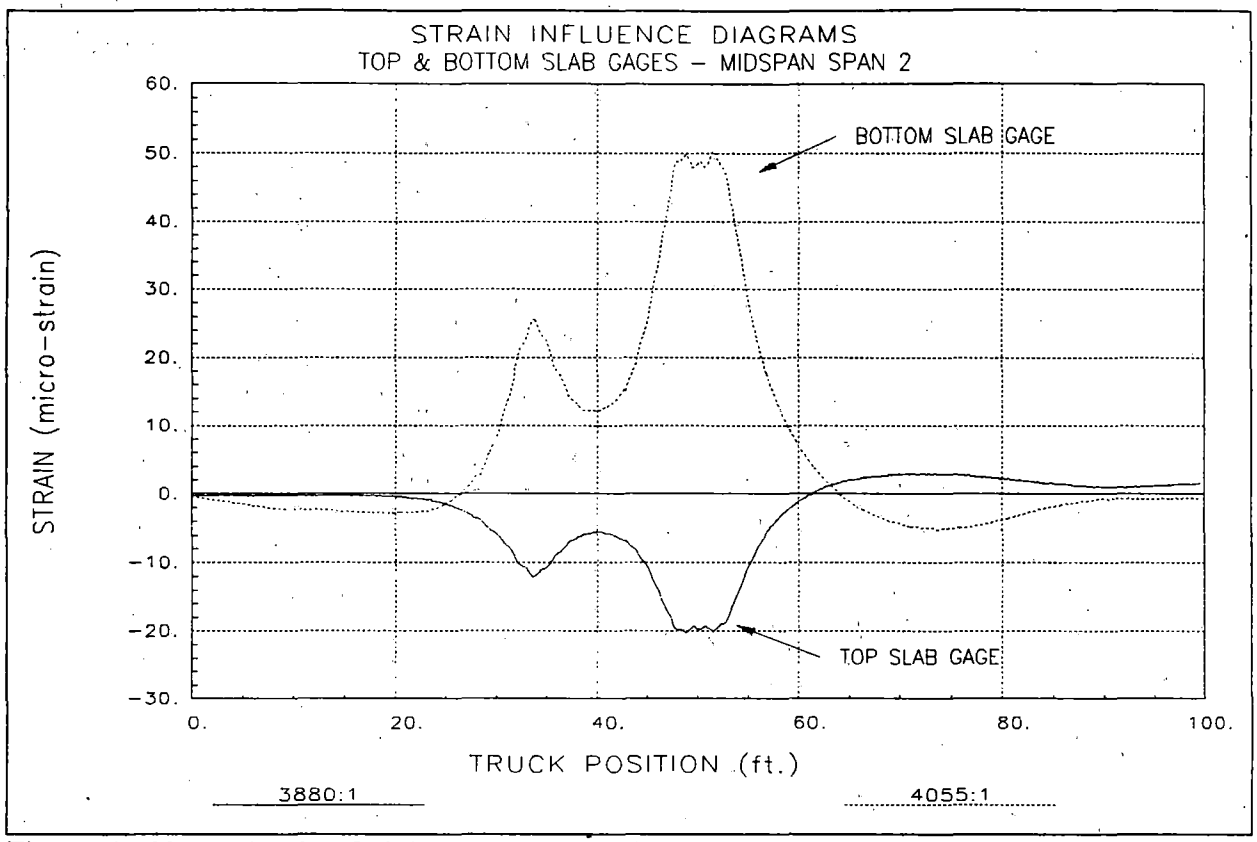

Figure 19 Neutral axis of slab.

Analysis and Model Calibration

Table 19 provides details regarding the structure model and analysis procedures. A discussion of the analysis results is provided along with conclusions regarding the structural performance.

Table 19 Analysis and model details - Lake Creek crossing.

Analysis type	Linear-elastic finite element - stiffness method.
Model geometry	Plane grid matching slab plan (see Figure 20)
Model components	• RC slab represented by quadrilateral plate elements. Plate thicknesses vary in 1" increments to account for roadway crown. 1" of concrete overlay added to original RC slab thickness. • Curbs simulated by beam elements. Cross-section included parapet, curb, and portion of slab necessary to obtain reasonable neutral axis location (13" from bottom of slab). • Abutment and pier caps represented by rectangular beam elements. • Elastic spring elements used to simulate pile foundation.
Live-load	2-D footprint of test truck consisting of 10 vertical point loads. Truck paths simulated by series of load cases with truck moving at 5-foot increments.
Dead-load	Self-weight of slab, curbs, and parapets with additional 15 psf to account for overlay not included in slab thickness. (Used for load rating only)

Data comparison	22 longitudinal strain gage locations defined on model (bottom of slab and curb). Strains computed for 25 truck positions along each path. 22x25x2 = 1100 strain values. Strain records extracted from load test data files corresponding to analysis truck positions.
Model statistics	756 Nodes 963 Elements 21 Cross-section/Material types 50 Load Cases 22 Gage locations
Adjustable parameters for model calibration	1 Slab stiffness (E_c - ksi) Span 1 2 Slab stiffness (E_c) over pier 3 Slab stiffness (E_c) Span 2 4 Effective Curb stiffness without parapet (exp. joints) (I - in^4) 5 Positive moment curb stiffness with parapet (I - in^4) 6 Negative moment curb stiffness with parapet (I - in^4)

A model with the above parameters was defined and the analysis program simulated the field load test process. The accuracy of the model was defined by comparing the 1100 computed and measured strain values. Selected parameters were modified to minimize the comparison error.

Table 20 contains the original stiffness parameters and the final values after the model calibration process. Statistical accuracy values associated with the initial and final models are provided in Table 21. During the calibration process, an attempt was made to simulate the effect of localized cracks on measurements that were obviously influenced. The result was that a much better accuracy was obtained than can normally be achieved for an RC slab.

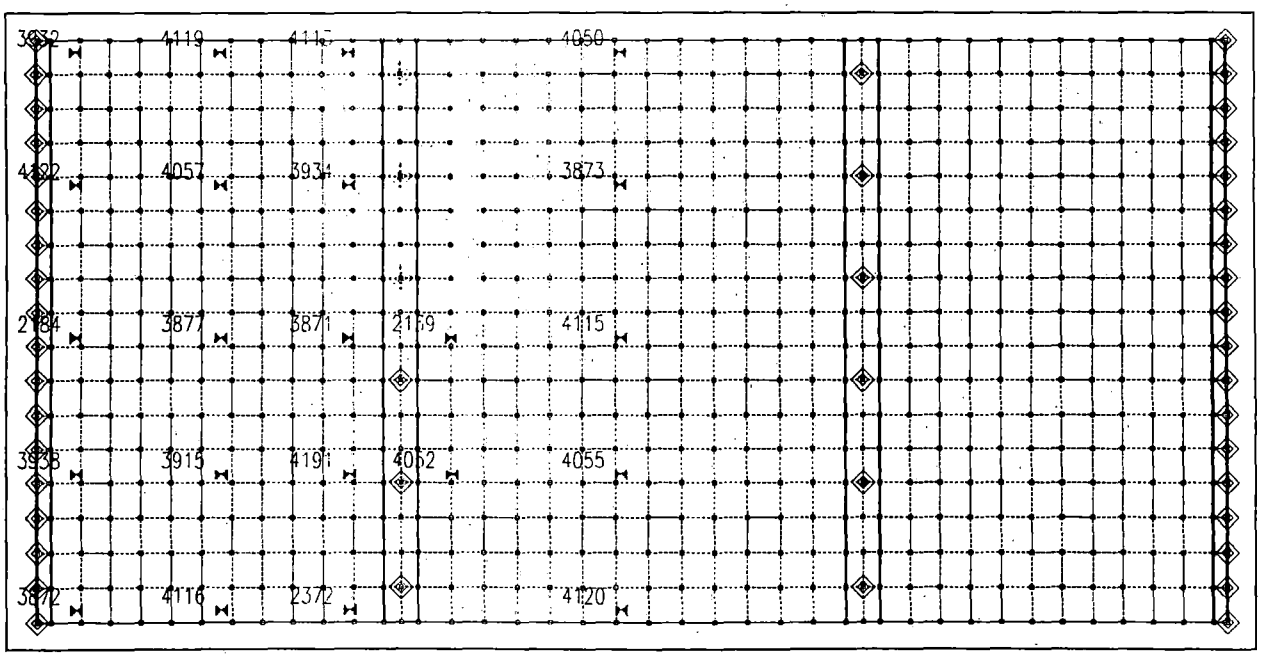

Figure 20 Finite element mesh of bridge - Lake Creek.

Table 20 Adjustable Parameter Results

Stiffness Parameter		Units	Initial Value	Final Value
Slab modulus Span 1	E	ksi	3200	4230
Slab modulus @ pier	E	ksi	3200	2221
Slab modulus Span 2	E	ksi	3200	3145
Curb w/ parapet -M	I	in^4	26912	41667
Curb w/ parapet +M	I	in^4	77100	78062
Curb w/ parapet -M	I	in^4	77100	41667

Table 21 Model Accuracy

Statistical Term	Initial Value	Final Value
Absolute Error	2188 με	1028 με
Percent Error	30.7 %	4.4 %
Scale Error	7.5 %	3.0 %
Correlation Coefficient	0.83	0.98

Load Rating Calculations

Load rating factors were computed for the structural components of the superstructure using the Load Factor method. A Load Factor of 1.3 was applied to all dead-load effects for both Inventory and Operating load ratings, while load factors 2.17 and 1.3 were applied to live-load responses. Ultimate strength member capacities, based on AASHTO specifications for reinforced concrete beams and slabs, were computed for positive and negative moment regions. Positive moment capacities were obtained for midspan cross-sections and negative moment capacities were computed for slab cross-sections at the face of the pier caps.

Table 22 contains slab moment capacity calculations for various different slab thicknesses. Grade 40 reinforcement, with a minimum yield stress of 40 ksi, was assumed based on the age of the structure. A concrete strength of 4 ksi was allowed due the relatively high concrete modulus obtained from the model calibration process. All slab moment capacities are computed for unit width sections (1 in.).

Load rating calculations were performed for the HS-20 and the three Iowa rating vehicles by applying the truck configurations to the calibrated model. Due to the width of the roadway, two truck paths were defined. The first path was defined by placing a wheel line 2 feet from the face of the curb with a second truck path 12 feet away. A second pair of truck paths was defined in which the lateral positions were symmetric about the bridge centerline. Single lane loading envelopes (critical responses) were generated for every model component by moving the applied rating truck at 2-foot intervals along the length of the bridge. Multiple lane load conditions were obtained by the principle of superposition. The response envelopes were added to generate two-lane loading response envelopes.

Table 22 Ultimate strength moment capacities for slab sections and curb.

Section	Ultimate Moment Capacities per unit slab width		
	d (in)	ρ	Mu (k-in/in)
Slab A span 1 12"	10.0	.0105	**35.6**
Slab B span 1 13"	11.0	.0096	**39.4**
Slab C span 1 14"	12.0	.0088	**43.2**
Slab D span 1 14.5"	12.5	.0084	**45.1**
Slab A @ pier 12"	10.0	.0133	**44.2**
Slab B @ pier 13"	11.0	.0121	**49.0**
Slab C @ pier 14"	12.0	.0111	**53.8**
Slab D @ pier 15"	12.5	.0107	**56.2**
Slab A span 2 12"	10.0	.0119	**39.9**
Slab B span 2 13"	11.0	.0108	**44.2**
Slab C span 2 14"	12.0	.0099	**48.5**
Slab D span 2 14.5"	12.5	.0095	**50.7**

Dead load responses were obtained by computing the self-weight of the structure and adding 15 PSF to account for concrete overlay not included in the slab model components. The model was adjusted prior to load rating calculations in that spring stiffnesses, providing rotational restraint at abutment support locations, and the effect of the parapet on the curb stiffness were eliminated. Table 23 contains computed dead load and the various rating vehicle live-load forces for each critical slab component. Inventory and operating rating factors for each component are listed in Table 24.

Table 23 Dead load and maximum live load moment on critical slab sections.

Section	Dead-Load M (k-in/in)	HS-20 M (k-in/in)	Type 4 M (k-in/in)	Type 3-3 M (k-in/in)	Type 3S3 M (k-in/in)
Slab A span 1	2.84	5.30	4.79	3.60	4.76
Slab B span 1	4.49	6.69	6.37	4.66	6.39
Slab C span 1	5.60	8.61	8.22	6.02	8.21
Slab D span 1	6.84	9.90	9.54	6.95	9.55
Slab A @ pier	-5.60	-4.28	-3.68	-3.55	-3.99
Slab B @ pier	-7.36	-6.32	-5.60	-5.17	-6.11
Slab C @ pier	-8.99	-7.72	-6.84	-6.31	-7.47
Slab D @ pier	-10.39	-8.72	-7.94	-7.35	-8.80
Slab A span 2	3.27	4.49	4.39	3.39	4.11
Slab B span 2	4.60	6.06	5.90	4.43	5.57
Slab C span 2	5.78	7.73	7.70	5.88	7.30
Slab D span 2	7.11	8.97	9.02	6.88	8.57

Table 24 Load Rating Factors - Lake Creek.

Section	HS-20		Type 4		Type 3-3		Type 3S3	
	Inv.	Oper.	Inv.	Oper.	Inv.	Oper.	Inv.	Oper.
Slab A span 1	2.13	3.56	2.30	3.85	3.08	5.14	2.34	3.90
Slab B span 1	1.78	2.97	1.86	3.10	2.56	4.27	1.86	3.11
Slab C span 1	1.48	2.47	1.54	2.56	2.12	3.53	1.55	2.59
Slab D span 1	**1.30**	**2.16**	**1.33**	**2.22**	**1.85**	**3.08**	**1.34**	**2.24**
Slab A @ pier	3.06	5.11	3.58	5.98	3.71	6.20	3.30	5.51
Slab B @ pier	2.21	3.69	2.50	4.17	2.71	4.52	2.29	3.82
Slab C @ pier	1.93	3.23	2.18	3.65	2.37	3.95	2.00	3.34
Slab D @ pier	1.74	2.90	1.91	3.18	2.06	3.43	1.72	2.87
Slab A span 2	2.81	4.70	2.88	4.81	3.73	6.22	3.08	5.13
Slab B span 2	2.23	3.73	2.29	3.83	3.06	5.11	2.43	4.06
Slab C span 2	1.88	3.14	1.89	3.15	2.47	4.12	1.99	3.32
Slab D span 2	1.64	2.73	1.63	2.72	2.13	3.56	1.71	2.86
Critical RF	**1.30**	**2.16**	**1.33**	**2.22**	**1.85**	**3.08**	**1.34**	**2.24**

Conclusions and Recommendations

Field measurements and the resulting calibrated model indicated that the parapets contributed to the edge stiffness of the slabs. However, due to the presence of expansion joints in the parapets, this contribution was not included in the rating analyses. In general, the obtained rating values can be considered slightly conservative. A potential side effect of the expansion joints is the formation of cracks in the curbs due to moment concentrations.

The negative moment region immediately adjacent to pier caps, is on average more flexible than positive moment regions. While this has little bearing on the moment capacity, it does suggest a higher density of flexural cracks. The presence of flexural cracks on the top of the deck may present a serviceability or maintenance issue since water and road salt can penetrate the slab more easily. Regarding load rating, however, the extra flexibility of the slab near the piers actually reduces the negative moment and increases the midspan moments. This is evident in the load rating results since all of the controlling rating factors were due to positive moment in the end-spans.

Another contributor to the critical region being at the end spans is the apparent lack of end-restraint commonly found in RC slab structures. Additionally, the calculated moment capacities were smaller at midspan of the end spans compared to the interior span or at the pier face.

The load rating factors presented in this report are based on the structure's condition at the time of load testing. Any structural degradation must be considered in future load ratings. Note that no effort was made to assess the condition or capacity of the substructure elements such as the abutments or piers.

Bridge 7601.2S003 Cedar Creek – Steel Girder

Description of Structure

Structure Identification	7601.2S003
Location	IA 3 Over Cedar Creek – Pocahontas County
Structure Type	Steel Girders - Single Span, Composite
Span Length(s)	41'-3"
Skew	Right
Structure/Roadway Widths	31'-10.5", 30'-0"
Beam Types	(2) Ext. Beams W24x76 composite (2) Int. Beams W27x94 composite
Beam Spacing	3 spaces @ 9'-8 1/4" = 29'-0 3/4"
Curb/Parapet Detail	RC curb integral with slab. RC parapet on curb - not part of original structure. Parapet is continuous over length of bridge and appears to be securely bonded to curb.
Visual condition	Beams in good condition with no apparent corrosion or loss of section.

Instrumentation and Load Test Details

Date	August 10th 1999
Structural Reference Point	X=0, Y= 0 at intersection of South abutment face and centerline of South West girder.
Test vehicle direction	East bound for all tests (Positive X direction).
Start of data recording	All tests start with front axle at X = -15.4'
Truck position	Record truck position at every wheel revolution (10.8'). *Autoclicker* placed on driver side front wheel.
Lateral truck path(s)	2 truck paths were defined for the load test. The Y position refers to distance between driver side front wheel and centerline of SW girder. Y1 = 11.4' Y2 = 25.25'
Measurements	(28) strain gages recorded at 33 Hz
Gage Placement	See Figure 21. Bottom flange gages placed at center of bottom flange. Top gages placed on underside of top flange, 2" from web. Diaphragm gages placed at the edge of top and bottom flanges.
Gage types	BDI Intelliducers
Number of test cycles	Data was recorded while the test truck crossed the bridge at crawl speed (5 mph). Each truck path was run twice to check reproducibility. One high-speed pass was run along path Y1 to measure dynamic response of the bridge.

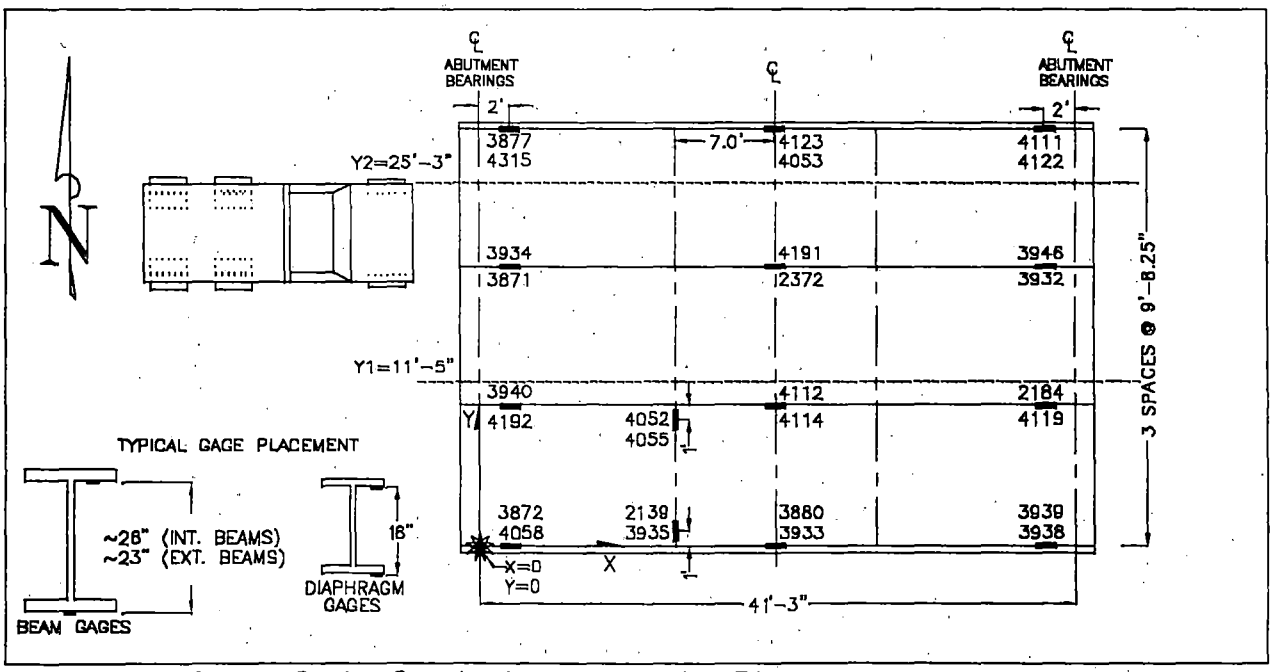

Figure 21 IA 3 over Cedar Creek - Instrumentation Plan.

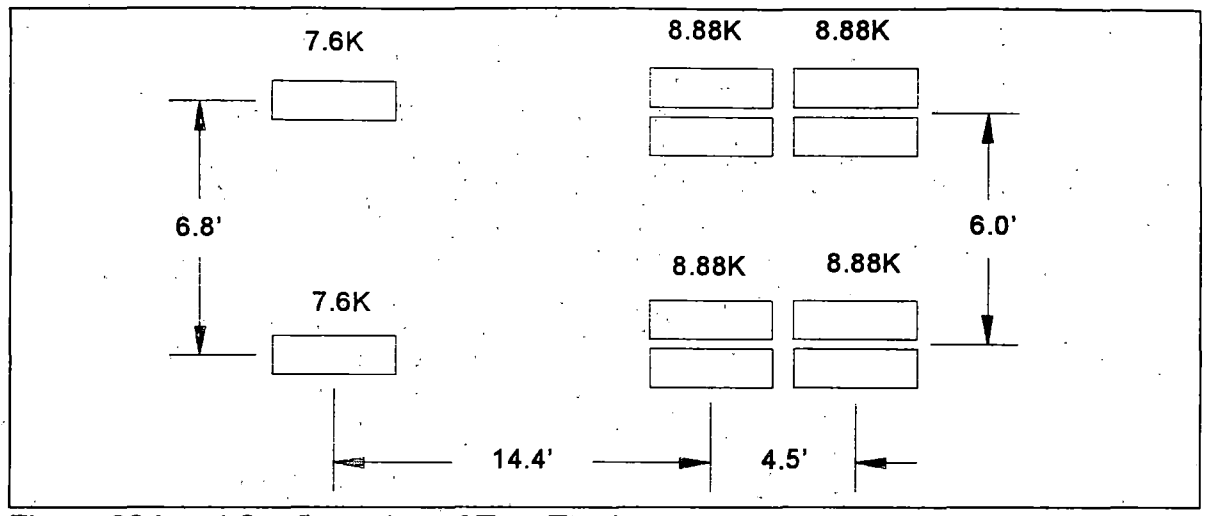

Figure 22 Load Configuration of Test Truck.

Table 25 Load Test Data Files

Truck Path	STS Data File	Comments
Y1	WCED1.dat	Passenger-side wheels on right shoulder line
Y1	WCED2.dat	" " "
Y2	WCED3.dat	Driver-side wheels on left shoulder line
Y2	WCED4.dat	" " "
Y1	WCED5.dat	Passenger-side wheels on right shoulder line High Speed Pass (45 MPH)

Preliminary Investigation of Test Results

A visual examination of the field data was performed to assess the quality of the data and to make a qualitative assessment of the bridge's live-load response. Conclusions made directly from the field data were:

- Responses from identical truck paths were very reproducible as shown in Figure 23.
- The majority of strain measurements indicated linear-elastic live-load responses.
- RC parapets and curb were acting integral with the superstructure, adding stiffness to the exterior beams. This caused the neutral axis locations of the exterior beams to be considerably higher than at the interior beams. The responses of exterior and interior beams are shown in Figure 24 and Figure 25, respectively. Note the differences in the top flange strains. Based on this observation, the effective depth of the composite concrete flange on the exterior beams should be increased in subsequent analysis and modeling.
- Composite behavior was exhibited at all gage locations except for the west-end of the north interior girder, as shown in Figure 26. As all of the other gage locations show composite action, it can be assumed that this non-composite behavior is limited to a small region at the end of the beam. End gages should have been placed further (at least one beam depth) away from the abutment faces.
- By observing flexural responses near the abutments in both sign and relative magnitudes with respect to midspan strains, it was apparent that a large degree of

rotational end-restraint was present. Figure 27 contains top and bottom flange strain histories from the south interior beam near the west abutment. The fact that the bottom flange strains are primarily negative suggests a high degree of rotational resistance. Another interesting observation made from this set of strain histories is the continuity of the bridge with the approach slab. Note the negative moment that is induced as the truck approaches the bridge (-15 to 0 feet on X-axis).

- Neutral axis locations and strain magnitudes from both truck paths were fairly consistent among similarly placed gages.
- Analysis of the data from the high-speed pass produced impact factors ranging from 22 to 29 percent. Figure 28 shows a comparison of the static and dynamic test data.

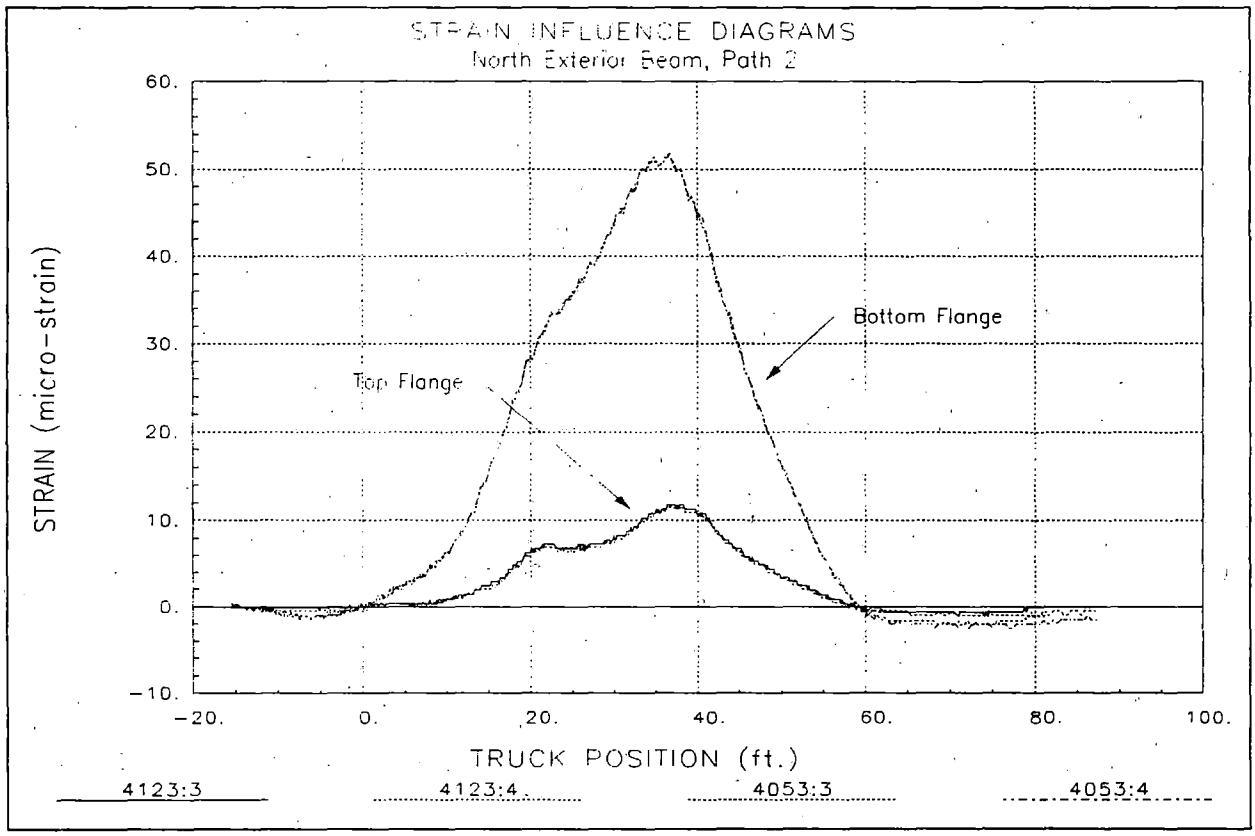

Figure 23 Reproducibility of load test - midspan north exterior beam.

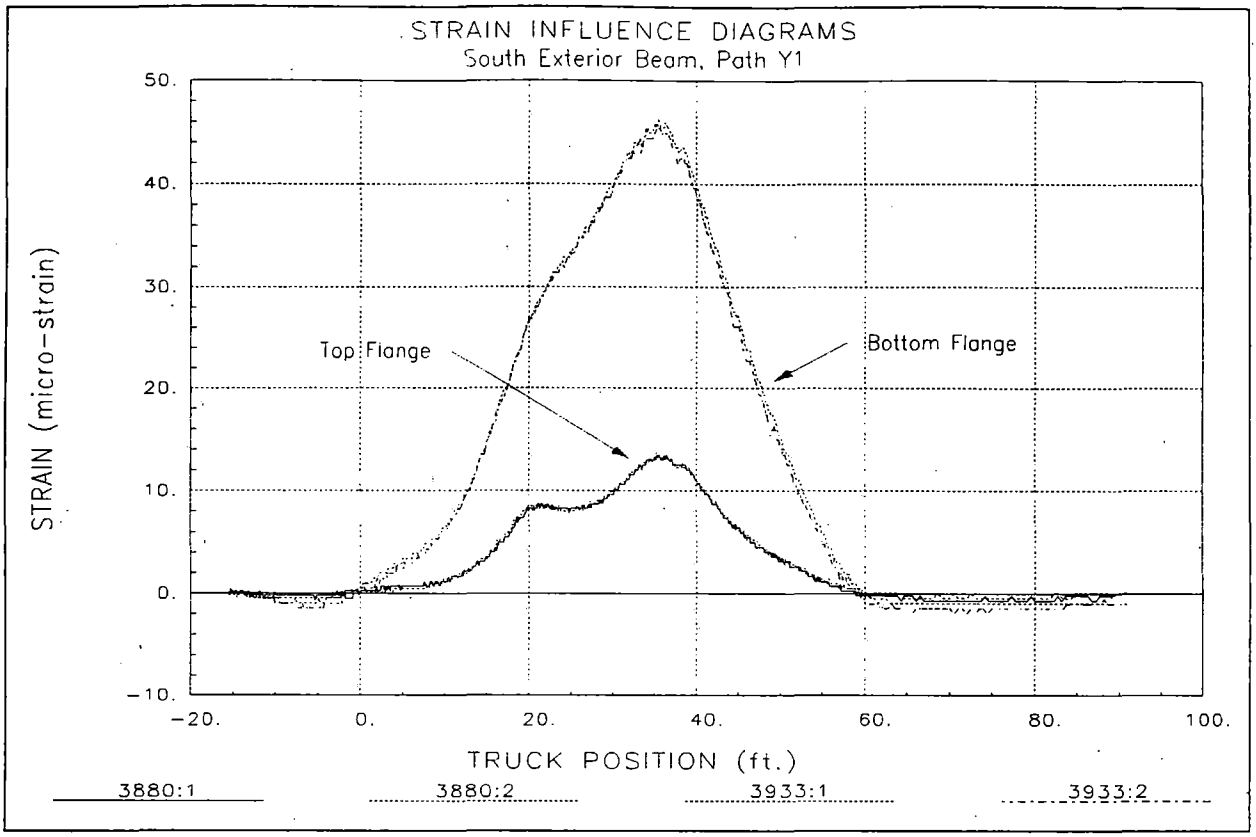

Figure 24 Midspan response of south exterior beam.

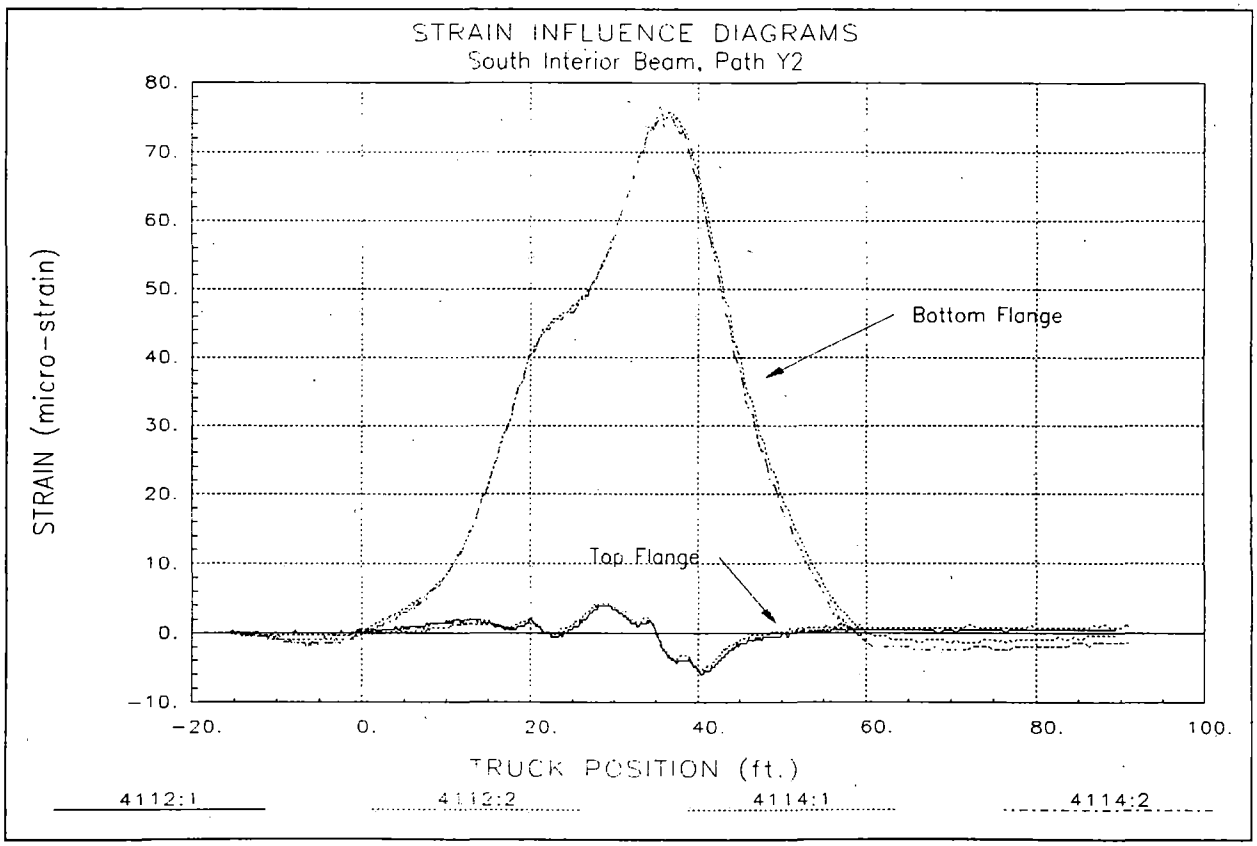

Figure 25 Midspan response of interior beam.

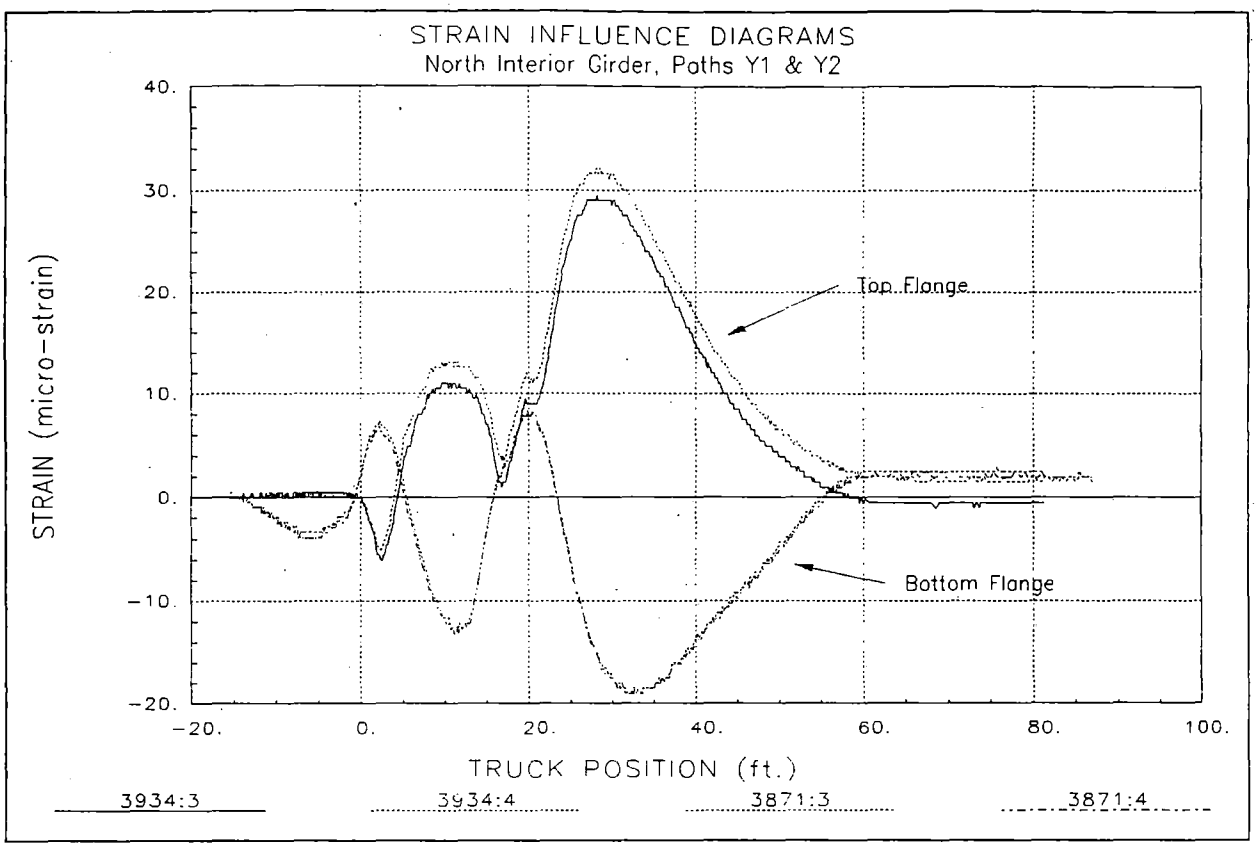

Figure 26 Non-Composite response of north interior beam at west abutment.

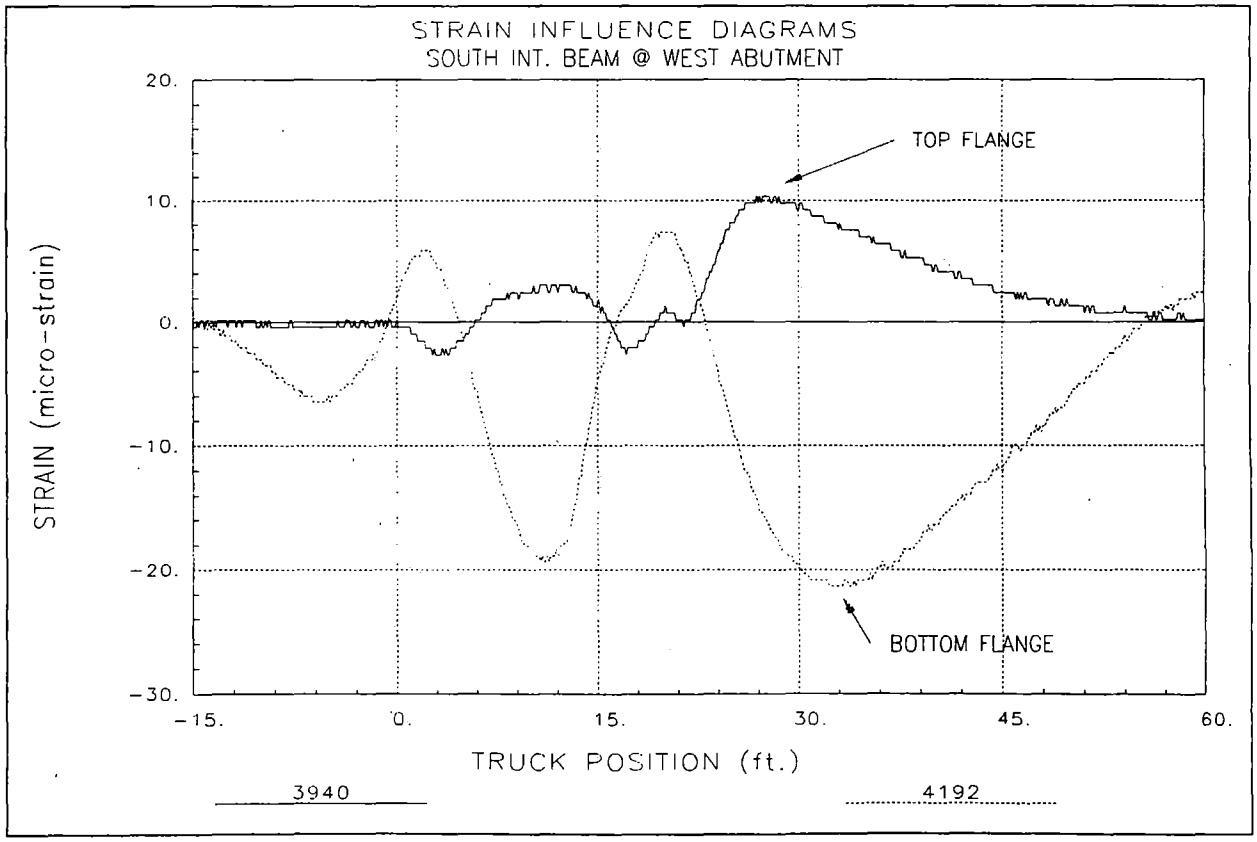

Figure 27 South interior beam near west abutment.

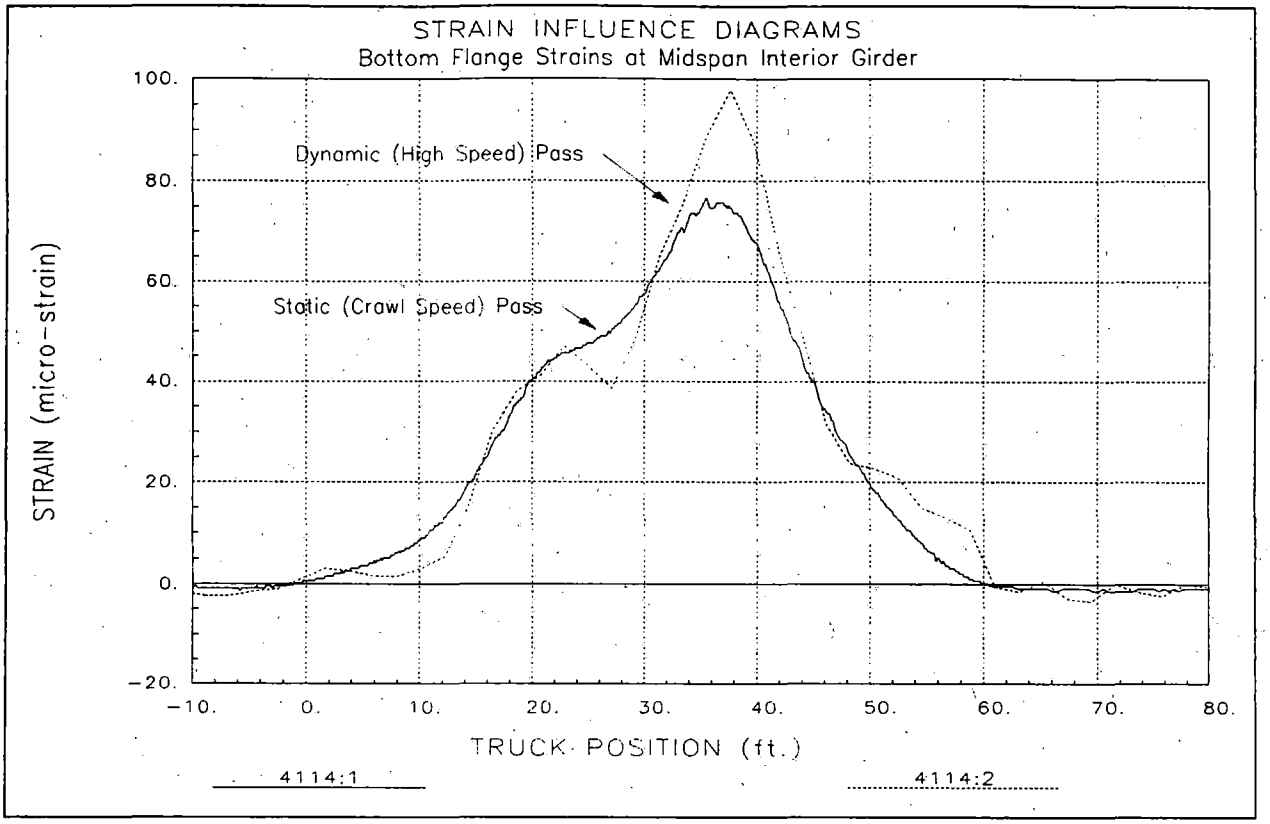

Figure 28 Comparison of static and dynamic test data

Analysis and Model Calibration

Table 5 provides details regarding the structure model and analysis procedures. A discussion of the analysis results is provided along with conclusions regarding the structural performance.

Table 26 Analysis and model details - Cedar Creek.

Analysis type	Linear-elastic finite element - stiffness method.
Model geometry	Plane grid matching framing plan (see Figure 29)
Model components	• RC slab represented by quadrilateral plate elements. • Beam elements corresponding to different cross-sections. • Curbs and parapets simulated within exterior beam elements. • Elastic spring elements used to simulate abutment support.
Live-load	2-D footprint of test truck consisting of 10 vertical point loads. Truck paths simulated by series of load cases with truck moving at 5-foot increments.
Dead-load	Self-weight of beams, slab, curbs, and parapets with additional 15 psf to account for overlay not included in slab thickness. Self weight of structure (not including parapets and overlay) were applied to non-composite model. (Used for load rating only)
Data comparison	16 strain gage locations (bottom flange) defined on model (longitudinal beams and diaphragms). Strains computed for 11 truck positions along each path. 16x11x2 = 352 strain values. Strain records extracted from load test data files corresponding to analysis truck positions.

Model statistics	130 Nodes 200 Elements 13 Cross-section/Material types 22 Load Cases 16 Gage locations
Adjustable parameters for model calibration	1 Young's modulus (E_c - ksi) 2 Exterior beam stiffness - midspan (I_y - in^4) 3 Exterior beam stiffness – near abutment (I_y - in^4) 4 Interior beam stiffness - midspan (I_y - in^4) 5 Interior beam stiffness – near abutment (I_y - in^4) 6 Abutment longitudinal resistance (Kx - kips/in)

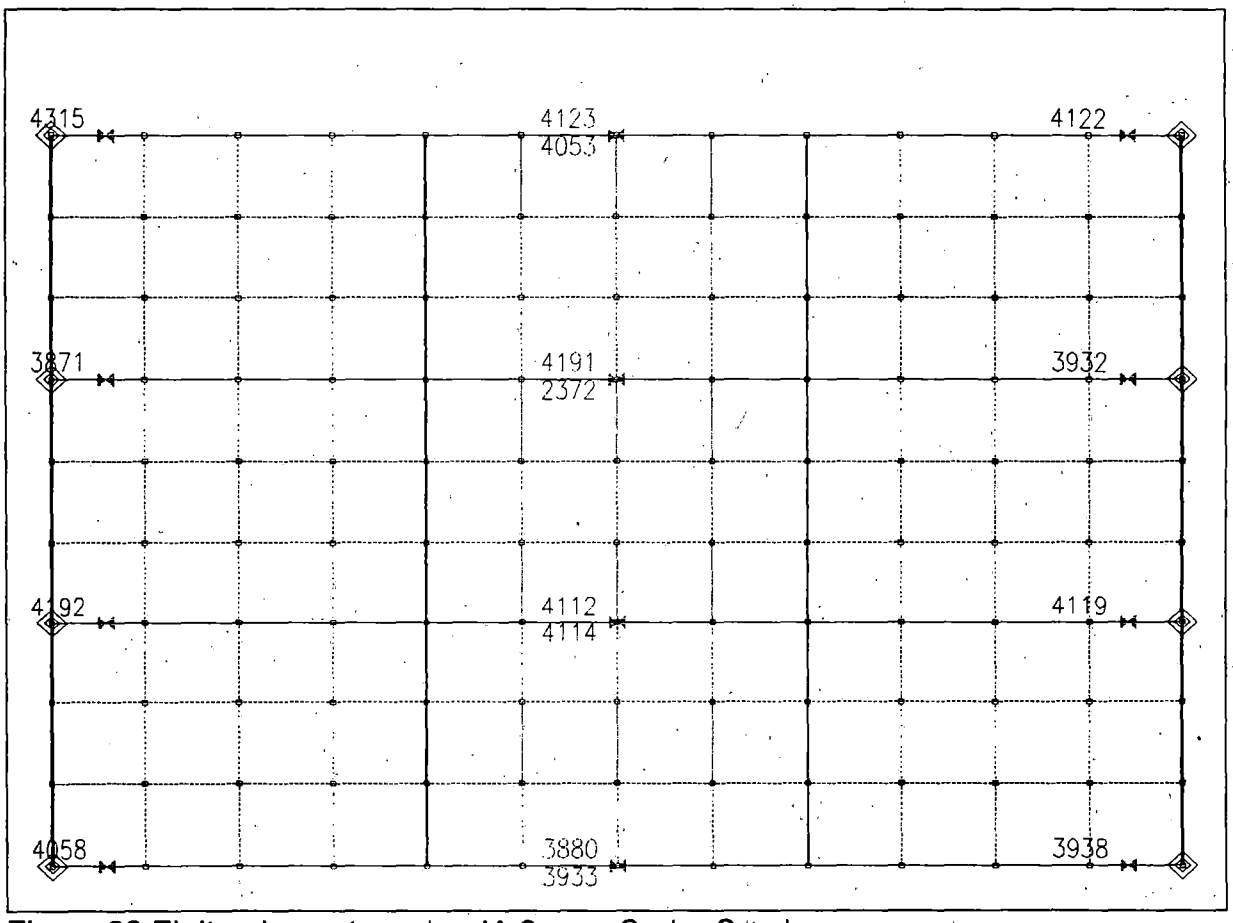

Figure 29 Finite element mesh – IA 3 over Cedar Creek

A model with the above parameters was defined and the analysis program simulated the load test process. The accuracy of the model was defined by comparing the 352 computed and measured strain values. Selected parameters were modified to minimize the comparison error.

The translation spring stiffnesses used to simulate the abutment were aligned parallel to the roadway. The springs were given an eccentricity value equal to the distance between the bottom beam flange and the measured neutral axis location. The eccentricity term provided a moment-arm such that any translational resistance induced

moment restraint. This method of modeling the support conditions was chosen over rotational springs because the apparent arching effect of the beams could be simulated. As far as midspan responses are concerned, both modeling procedures have essentially identical effects. Table 27 contains the original stiffness parameters and the final values after the model calibration process. Statistical accuracy values associated with the initial and final models are provided in Table 28. The resulting accuracy terms were in the typical range for RC slab structures.

Table 27 Adjustable Parameter Results

Stiffness Parameter	Units	Initial Value	Final Value
Slab modulus E	ksi	3600	5813
Exterior beam - midspan (I)	in^4	11703	29460
Exterior beam – near abutment (I)	in^4	7134	15910
Interior beam - midspan (I)	in^4	18433	16660
Interior beam – near abutment (I)	in^4	11613	10490
Abutment (Kx)	Kips/in	0	1769

Table 28 Model Accuracy

Statistical Term	Initial Value	Final Value
Absolute Error	2624.8με	911.4με
Percent Error	36.7%	6.0%
Scale Error	23.2%	4.2%
Correlation Coefficient	0.85	0.97

Load Rating Calculations

Load rating factors were computed for the longitudinal beams using the Load Factor method. A Load Factor of 1.3 was applied to all dead-load affects for both Inventory and Operating load ratings, while load factors 2.17 and 1.3 were applied to live-load responses. Ultimate strength member capacities were computed, based on AASHTO specifications for steel beams except that moment capacities were limited to yield stress rather than plastic moment capacity.

It was assumed that the beams were not shored during construction, therefore the majority of dead load was applied to a non-composite model. Dead load effects were subtracted from the original capacity calculations to obtain composite model capacities. For example moment capacities were obtained by subtracting the non-composite dead load stresses from the yield stress prior to computing a moment capacity for the composite section. Beam end-restraints were also removed from the dead-load model. The yield stress used for the following capacity calculations was 37 ksi based on the available mill reports. Table 29 contains moment and shear capacity calculations for both interior and exterior beam sections.

Table 29 Ultimate moment capacities for composite model components.

Component	Units	Capacity Value
Interior Beam - Moment	k-in	17,570
Exterior Beam - Moment	k-in	29,449
Interior Beam - Shear	kips	245
Exterior Beam - Shear	Kips	203

Load rating calculations were performed for the HS-20 and the three Iowa rating vehicles by applying the truck configurations to the calibrated model. Due to the width of the roadway, two truck paths were defined. The first path was defined by placing a wheel line 2 feet from the face of the curb. The second truck path was defined as being 12 feet from the first path. Single lane loading envelopes (critical responses) were generated for every model component by moving the applied rating truck at 4-foot intervals along the length of the bridge. Multiple lane load conditions were obtained by the principle of superposition. The response envelopes were added to generate two-lane loading response envelopes.

Additional composite model dead load responses included 15 PSF to account for concrete overlay not included in the model components and the self-weight of the RC parapets. Non-composite and composite dead load effects are shown in Table 30. Live-load responses for the HS-20 and three Iowa rating vehicles are listed in Table 31. Load rating factors for critical members are provided in Table 32.

Table 30 Dead load calculations for non-composite and composite structure.

Member	NC Dead-Load	Composite Dead-Load
Interior Beam - Moment (k-in)	3010	355
Exterior Beam - Moment (k-in)	1403	744
Interior Beam - Shear (kips)	21	3.3
Exterior Beam - Shear (kips)	10	7.3

Table 31 Maximum live load moments on critical beam sections.

Member	HS-20	Type 4	Type 3-3	Type 3S3
Interior Beam - Moment (k-in)	2526	2311	1890	2143
Exterior Beam - Moment (k-in)	2896	2603	2270	2349
Interior Beam - Shear (kips)	31.5	26.3	24.3	25.3
Exterior Beam - Shear (kips)	26.7	22.3	21.5	21.4

Table 32 Load Rating Factors – Cedar Creek.

Member	HS-20		Type 4		Type 3-3		Type 3S3	
	Inv.	Oper.	Inv.	Oper.	Inv.	Oper.	Inv.	Oper.
Int. Beam - M	2.40	4.01	2.62	4.38	3.21	5.36	2.83	4.72
Ext. Beam - M	3.49	5.82	3.87	6.47	4.44	7.41	4.29	7.17
Int. Beam - V	2.70	4.51	3.24	5.42	3.51	5.87	3.37	5.62
Ext. Beam - V	2.49	4.16	2.98	4.98	3.10	5.17	3.11	5.19
Critical RF	**2.40**	**4.01**	**2.62**	**4.38**	**3.10**	**5.17**	**2.83**	**4.72**

Conclusions and Recommendations

The relatively high load rating factors indicate that the structure is in good condition and can safely carry all design and rating loads with no restrictions. Conditions providing the favorable rating factors include better than expected lateral distribution, contribution of the concrete parapets in the stiffness of the exterior beams, and the high degree of end-restraint provided by the embedded beam supports. Also the yield stress of 37 ksi listed in the mill report is significantly higher than would normally be allowed based on the age of the structure.

It was observed during examination of the strain data that the composite action between the deck and beams was not present at the west-end of the north interior beam. This is likely caused by deterioration of the deck concrete at the vicinity of the abutment, as opposed to failure of the shear connectors. The negative moments induced by the embedded support detail cause the deck to be in tension and eventually crack. Therefore, composite behavior should not be assumed at the beam-ends, however, this has minimal effect on the structure's performance. Since failure of shear connectors may still be a possibility, it is recommended that the integrity of the deck to steel bond be examined during future inspections.

The deck modulus obtained from the calibration process was greater than can be reasonably assumed. The reason for this is due to the method of construction of the roadway crown compared to the modeling procedure in the analysis. When viewing the cross-section of the bridge, the slab is slightly arched in a parabolic curve. Where as, the finite element model represents the entire structure resides in a single plane. With the real structure the deck's parabolic shape improves the lateral load distribution. During the calibration process, this effect was accounted for by increasing the stiffness of the deck plate elements. While the resulting concrete modulus is not realistic and the presence of high-strength concrete is not implied, the model's resulting load transfer characteristics are accurate.

The load rating factors presented in this report are based on the structure's condition at the time of load testing. Any structural degradation must be considered in future load ratings. Note that no effort was made to assess the condition or capacity of the substructure elements such as the abutments or piers.

Bridge 6707.9R029 - Cleghorn Ditch - RC Slab

Description of Structure

Structure Identification	6707.9R029
Location	I-29 over Cleghorn Drainage Ditch - Monona County
Structure Type	RC-slab 3-span continuous.
Span Length(s)	30'-6", 39'-0", 30'-6"
Skew	30 degrees (counterclockwise) from perpendicular
Structure/Roadway Widths	42'-4", 39'-0"
Curb/Parapet Detail	RC curb attached to slab with shear stirrups and shear keys. Aluminum railing.
Visual condition	Slab appeared to be in good condition. No apparent spalling of concrete or exposed rebar. No excessive cracks in slab or curb.

Instrumentation and Load Test Details

Date	August 4th, 1999
Structural Reference Point	South-west corner of slab at inside face of abutment.
Test vehicle direction	North for all tests.
Start of data recording	-13.1' from line drawn perpendicular to roadway at X=0.0
Truck position	Record truck position at every wheel revolution (10.808'). *Autoclicker* placed on driver side front wheel.
Lateral truck path(s)	3 truck paths were defined for the load test. The Y position refers to distance between driver side front wheel and west slab edge. Y1 = 7.2' Y2 = 23.1' Y3 = 30.0'
Measurements	(36) strain gages recorded at 33 Hz
Gage Placement	See Figure 30. All slab gages on bottom of slab. Top parapet gages on top of parapet (42" above bottom of slab). Slab gages placed longitudinally or perpendicular to roadway.
Gage types	BDI Intelliducers with extensions (18" gage length).
Number of test cycles	Data was recorded while the test truck crossed the bridge at crawl speed (5 mph). Each truck path was run twice to check reproducibility. No high-speed passes were performed due to traffic considerations.

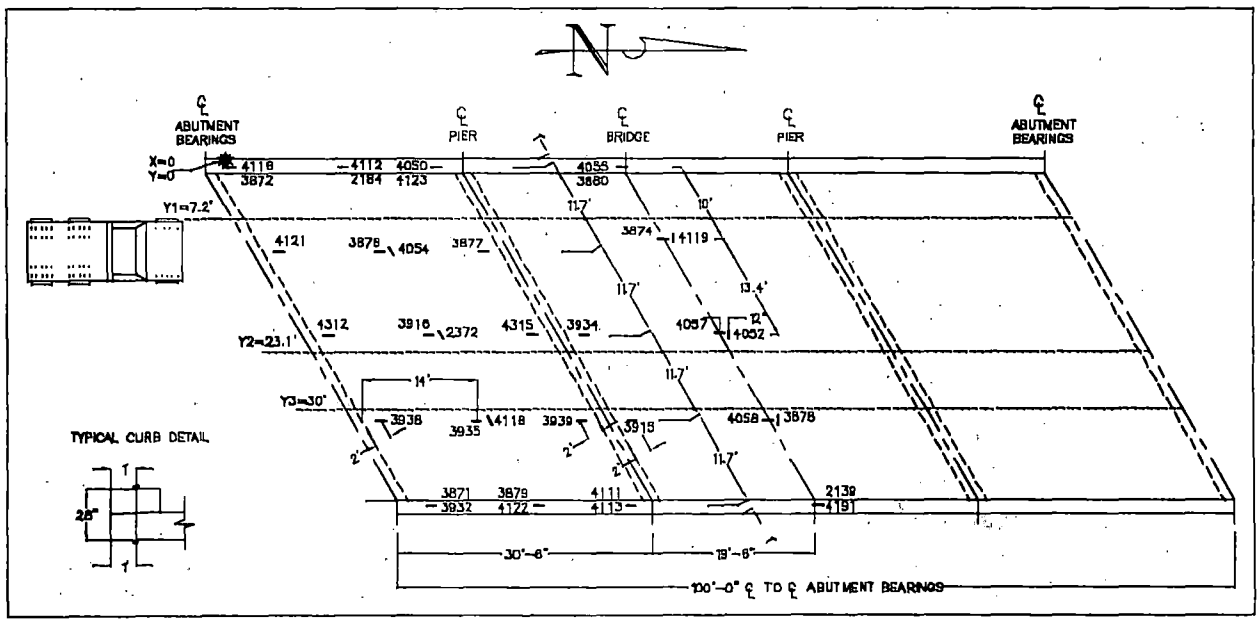

Figure 30 I-29 over Cleghorn Ditch - Instrumentation Plan.

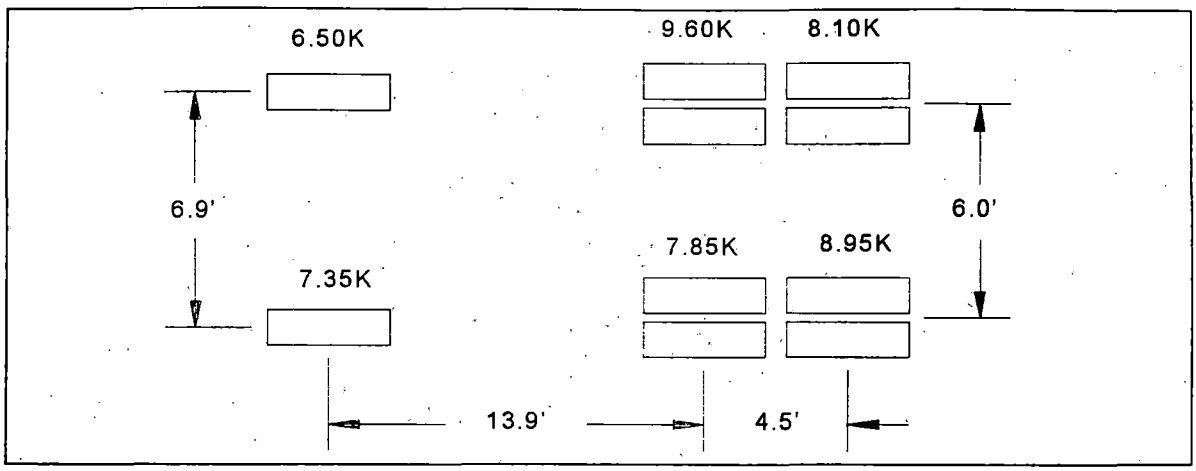

Figure 31 Load Configuration of Test Truck.

Table 33 Load Test Data Files

Truck Path	STS Data File	Comments
Y1	Cleg1.dat	Driver-side wheels on right shoulder line
Y1	Cleg2.dat	" " " "
Y2	Cleg3.dat	Passenger-side wheels on right shoulder line
Y2	Cleg4.dat	" " " "
Y3	Cleg5.dat	Driver-side wheels on left shoulder line
Y3	Cleg6.dat	" " " "

Preliminary Investigation of Test Results

A visual examination of the field data was performed to assess the quality of the data and to make a qualitative assessment of the bridge's live-load response. Conclusions made directly from the field data were:

- Responses from identical truck paths were very reproducible as shown in Figure 32.
- The majority of strain measurements indicated linear-elastic live load responses. Gages on top of the parapet experienced significant drift relative to magnitude of live-load strains. The drift was caused by temperature fluctuations and magnified by aluminum transducer extensions. Therefore top parapet gages were used for qualitative assessment of curb parapet cross-section properties (neutral axis) and not for model calibration.
- Live-load strains were relatively small. Maximum midspan strains were in range of 20 to 30 micro-strain. Assuming a concrete modulus of 4000 ksi, the maximum midspan strains roughly translate into an average tensile stress of 120 psi at the bottom surface of the slab. Maximum longitudinal steel stresses computed at the gage locations (averaged over 18") equal approximately 0.6 ksi.
- Curb and longitudinal slab strains were relatively consistent with similarly placed gages.
- Span 2 strains were typically 2 to 2.5 times greater than end-span strains as shown in Figure 33.

- RC curbs were acting integral with the superstructure providing stiffened edges along the slab. Neutral axes of the parapet were relatively consistent, with the location being approximately 11 inches from the bottom of the slab near the pier and 14 inches at midspan locations. Figure 34 shows the consistency of relative strain magnitudes from the top and bottom curb gages. The strain drift on the top curb gage is due to temperature change, this was verified by the response of the West curb gages. Based on this observation curbs should be treated as beam line along edge of slab in subsequent analyses as they affect the load paths.
- Negative strains measured near the abutments while the truck was on Span 1 indicate a relatively high degree of rotational end-restraint was induced by abutment (see Figure 35).

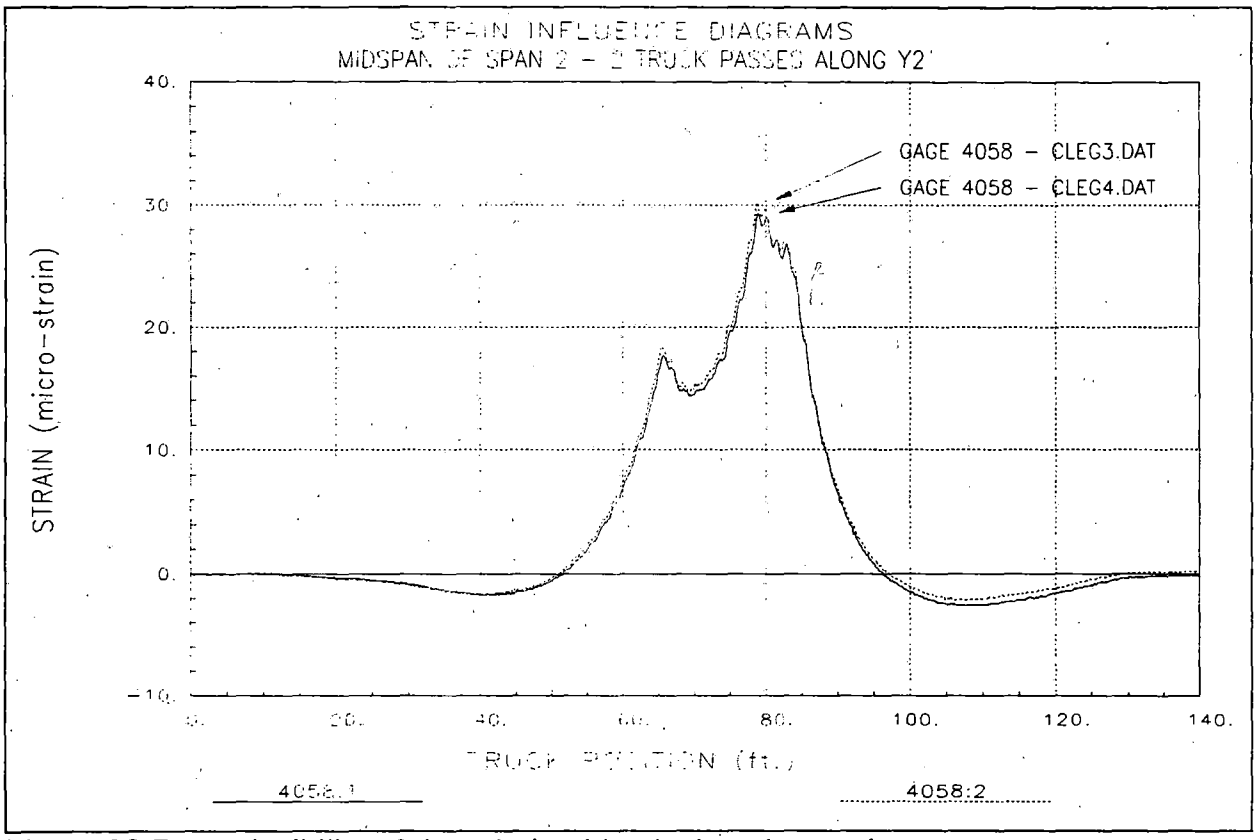

Figure 32 Reproducibility of data during identical truck crossings.

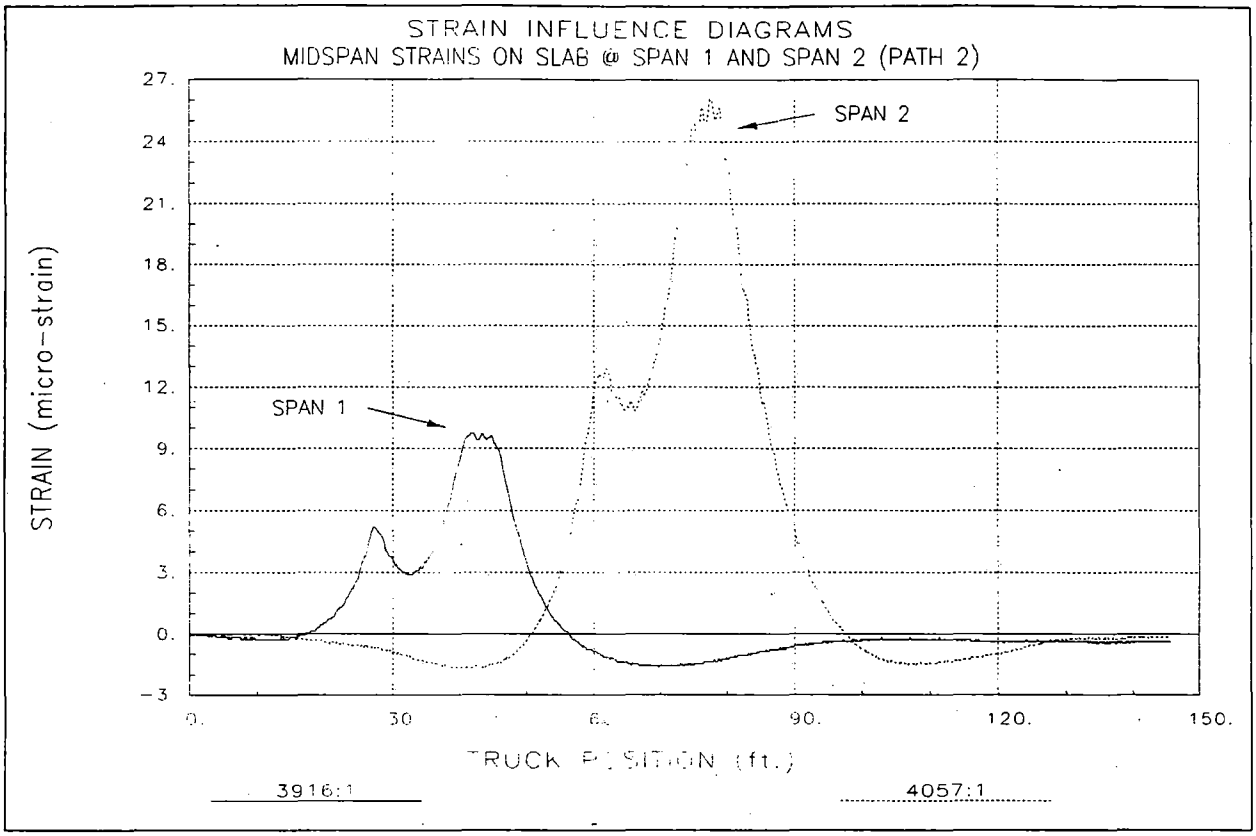

Figure 33 Relative magnitude differences of Span 1 and Span 2 strains.

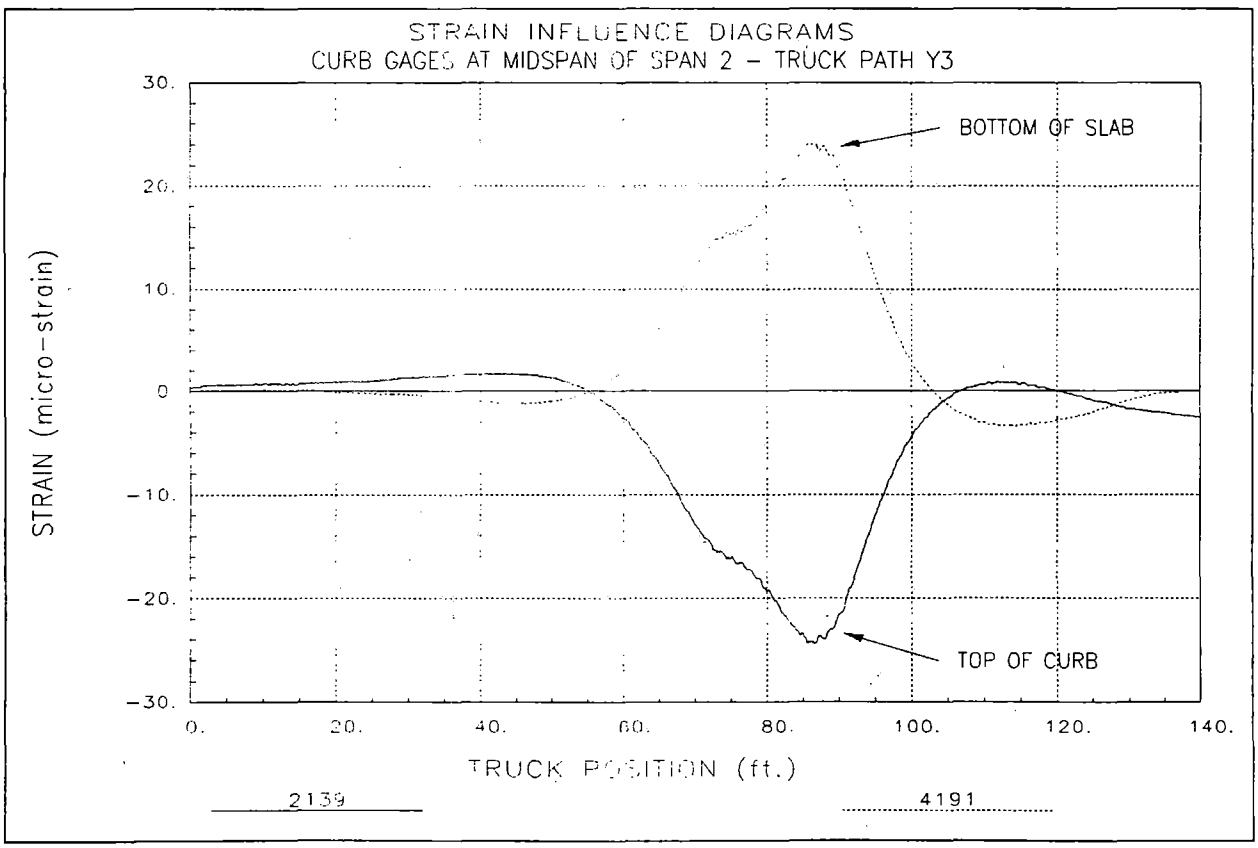

Figure 34 Flexural response of curbs.

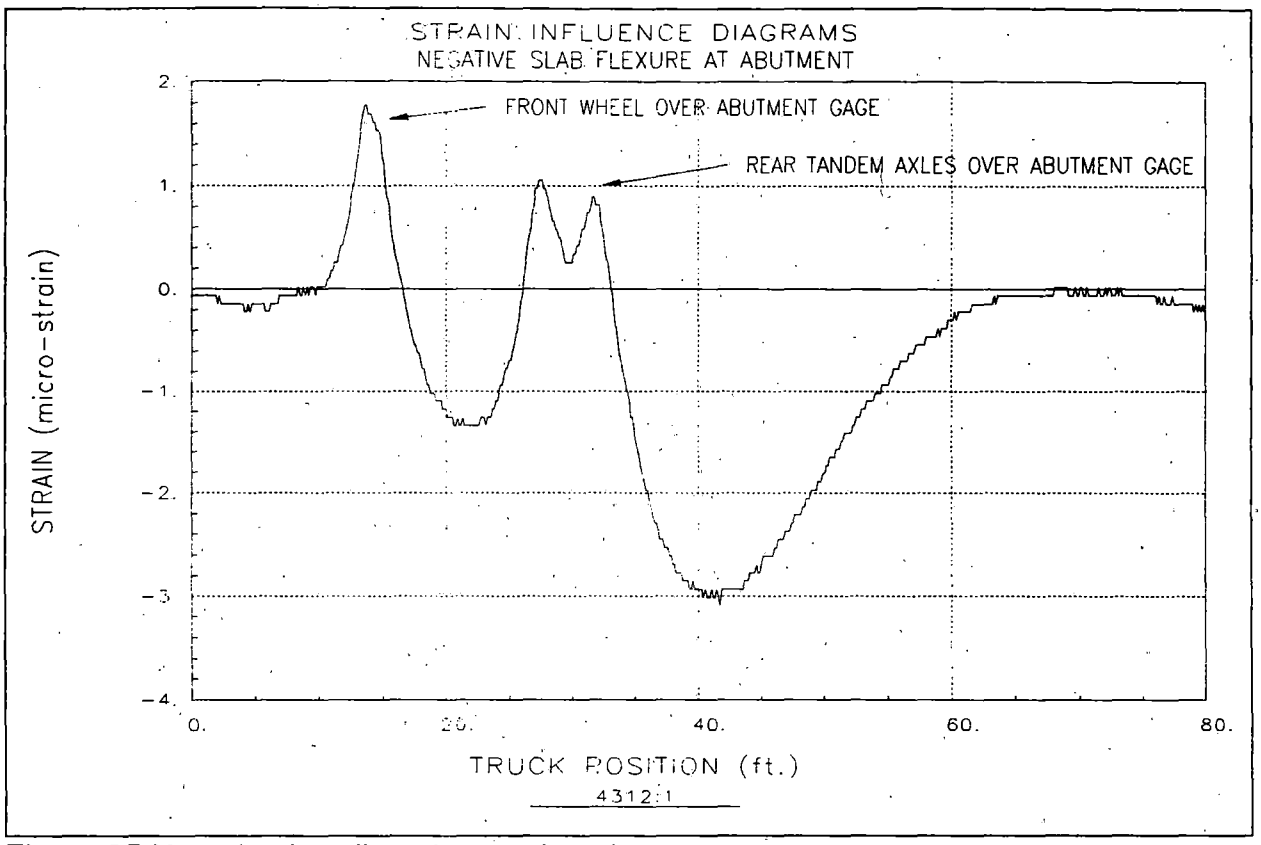

Figure 35 Negative bending observed at abutment.

Analysis and Model Calibration

Table 5 provides details regarding the structure model and analysis procedures. A discussion of the analysis results is provided along with conclusions regarding the structural performance.

Table 34 Analysis and model details - Cleghorn Ditch crossing.

Analysis type	Linear-elastic finite element - stiffness method.
Model geometry	Plane grid matching slab plan (see Figure 36)
Model components	• RC slab represented by quadrilateral (skewed) plate elements. Plate thicknesses vary in 1" increments to account for roadway crown. 1" of concrete overlay added to original RC slab thickness. • Curbs simulated by beam elements. Cross-section included parapet, curb, and portion of slab necessary to obtain reasonable neutral axis location (15" from bottom of slab). • Abutment and pier caps represented by rectangular beam elements. • Elastic spring elements used to simulate pile foundation.
Live-load	2-D footprint of test truck consisting of 10 vertical point loads. Truck paths simulated by series of load cases with truck moving at 5-foot increments.
Dead-load	Self-weight of slab, curbs, and parapets with additional 15 psf to

	account for overlay not included in slab thickness. (Used for load rating only)
Data comparison	22 longitudinal strain gage locations defined on model (bottom of slab and curb). Strains computed for 16 truck positions along each path. 22x16x3 = 1056 strain values. Strain records extracted from load test data files corresponding to analysis truck positions.
Model statistics	468 Nodes 662 Elements 17 Cross-section/Material types 99 Load Cases 24 Gage locations
Adjustable parameters for model calibration	1 Young's modulus - span 1 (E_c - ksi) 2 Young's modulus - at pier face (E_c - ksi) 3 Young's modulus - span 2 (E_c - ksi) 4 Curb stiffness positive moment (I_b - in^4) 5 Curb stiffness negative moment (I_b - in^4) 6 Abutment pile longitudinal resistance (Kx - kips/in) 7 Pier pile longitudinal resistance (Kx - kips/in)

A model with the above parameters was defined and the analysis program simulated the load test process. The accuracy of the model was defined by comparing the 2376 computed and measured strain values. Selected parameters were modified to minimize the comparison error.

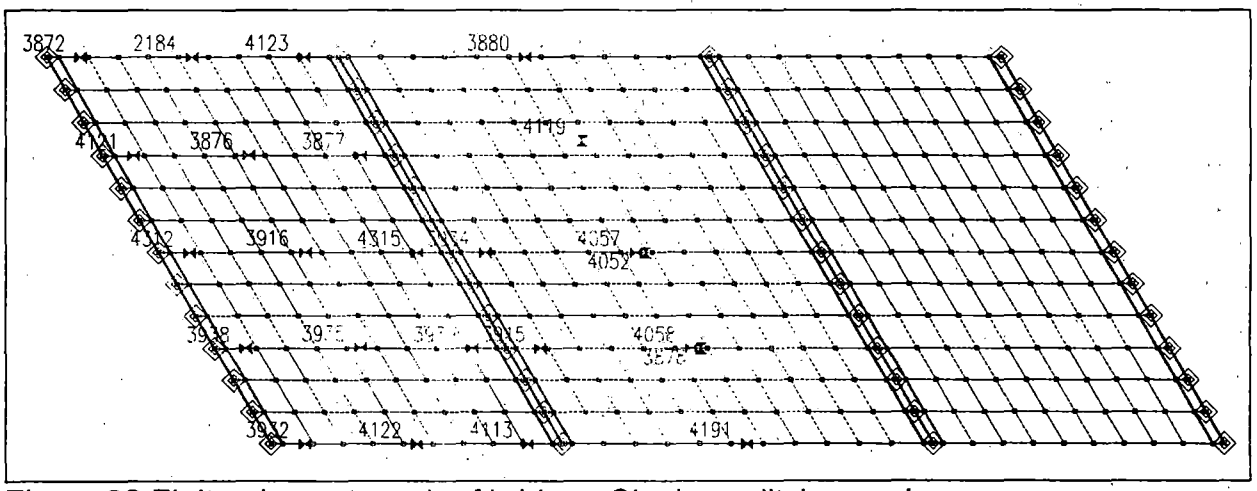

Figure 36 Finite element mesh of bridge - Cleghorn ditch crossing.

Because the measurements indicated that the curbs were acting integrally with the slab, they were represented as beam elements along the edge of the slab. The measured neutral axes values were relatively consistent, but varied between negative and positive moment regions. Therefore separate beam properties were assigned to the two regions. The initial moment of inertia values were based on the gross-dimensions of the curb plus sufficient width of slab such that the calculated neutral axis was close to the measured neutral axis.

Table 35 contains the original stiffness parameters and the final values after the model calibration process. Statistical accuracy values associated with the initial and final models are provided in Table 36. The resulting accuracy terms were in the typical range for RC slab structures.

Table 35 Adjustable Parameter Results

Stiffness Parameter	Units	Initial Value	Final Value
Deck Span 1 E	ksi	3200	4500
Deck @ pier E	ksi	3200	3800
Deck Span 2 E	ksi	3200	2600
Curb +M (I)	In^4	47500	30000
Curb -M (I)	In^4	54900	55000
Abutment (Kx)	Kips/in	0	4300
Pier (Kx)	Kips/in	0	430

Table 36 Model Accuracy

Statistical Term	Initial Value	Final Value
Absolute Error	3068 με	2366 με
Percent Error	24.2%	15.5%
Scale Error	7.2%	5.3%
Correlation Coefficient	.9050	.9329

Load Rating Calculations

Load rating factors were computed for the structural components of the superstructure using the Load Factor method. A Load Factor of 1.3 was applied to all dead-load affects for both Inventory and Operating load ratings, while load factors 2.17 and 1.3 were applied to live-load responses. Ultimate strength member capacities, based on AASHTO specifications for reinforced concrete beams and slabs, were computed for positive and negative moment regions. Positive moment capacities were obtained for midspan cross-sections and negative moment capacities were computed for slab cross-sections at the face of the pier caps.

Estimated capacity calculations were made for curb elements since it was determined that they had a significant effect on the load transfer. However, since the curbs were not intended to be structural elements, rating factors obtained for the curbs were not allowed to control the overall load ratings.

Table 37 contains slab moment capacity calculations for various different slab thicknesses. Grade 40 reinforcement, with a minimum yield stress of 40 ksi, was assumed based on the age of the structure. A concrete strength of 4 ksi was allowed due the relatively high concrete modulus obtained from the model calibration process. All slab moment capacities are computed for unit width sections (1 in.).

Table 37 Ultimate strength moment capacities for slab sections and curb.

Section	Ultimate Moment Capacities per unit slab width		
	d (in)	ρ	M (k-in/in)
Span 1 midspan east edge	14.81	.0123	**90.1**
Span 1 midspan center	15.81	.0115	**96.5**
Span 1 midspan west edge	16.81	.0108	**102.9**
Deck at Face of Pier	13.31	.0104	**62.4**
Span 2 midspan east edge	14.81	.0132	**96.1**
Span 2 midspan center	15.81	.0123	**102.7**
Span 2 midspan west edge	16.81	.0116	**116.6**
Curb Midspan	25.81	.017	**7340 k-in**
Curb at pier	25.31	.005	**-895 k-in**

Load rating calculations were performed for the HS-20 and the three Iowa rating vehicles by applying the truck configurations to the calibrated model. Due to the width of the roadway, three truck paths were defined. The first path was defined by placing a wheel line 2 feet from the face of the curb. Subsequent truck paths were defined at 12-foot increments. Single lane loading envelopes (critical responses) were generated for every model component by moving the applied rating truck at 2-foot intervals along the length of the bridge. Multiple lane load conditions were obtained by the principle of superposition. The response envelopes were added to generate two and three-lane loading response envelopes. Three-lane load responses were reduced by 10% according to AASHTO specification 3.12.1.

Dead load responses were obtained by computing the self-weight of the structure and adding 15 PSF to account for concrete overlay not included in the slab model components. The model was adjusted prior to dead load application in that spring stiffnesses, providing rotational restraint at support locations, and edge stiffnesses, simulating the curb and parapet effects, were eliminated. Table 9 contains computed dead load and the various rating vehicle live-load forces for each critical slab component. Inventory and operating rating factors for each component are listed in Table 10.

Table 38 Dead load and maximum live load moment on critical slab sections.

Section	Dead-Load M (k-in/in)	HS-20 M (k-in/in)	Type 4 M (k-in/in)	Type 3-3 M (k-in/in)	Type 3S3 M (k-in/in)
Span 1 A	17.26	9.28	9.20	5.88	6.75
Span 1 B	12.09	10.15	9.25	5.85	6.92
Span 1 C	9.32	10.57	9.84	6.86	7.53
Deck at Pier A	-21.55	-11.33	-10.22	-8.24	-10.64
Deck at Pier B	-22.11	-10.33	-9.15	-9.29	-11.02
Deck at Pier C	-20.66	-11.58	-10.13	-9.72	-11.93
Span 2 A	11.61	9.01	7.73	5.91	6.77
Span 2 B	11.47	9.92	8.91	6.77	8.13
Span 2 C	10.50	10.76	9.97	7.46	8.97
Curb Midspan	0.00	602.10	586.80	448.70	513.60
Curb at pier	0.00	-450.70	401.50	-355.60	-424.90

Table 39 Load Rating Factors - Cleghorn Ditch.

Section	HS-20		Type 4		Type 3-3		Type 3S3	
	Inv.	Oper.	Inv.	Oper.	Inv.	Oper.	Inv.	Oper.
Span 1 A	2.58	4.31	2.61	4.35	4.08	6.81	3.68	6.14
Span 1 B	2.82	4.71	3.08	5.14	4.82	8.04	4.36	7.29
Span 1 C	3.04	5.08	3.22	5.37	4.62	7.71	4.31	7.19
Slab @ Pier A	1.08	1.80	1.19	1.99	1.35	2.25	1.15	1.91
Slab @ Pier B	1.15	1.93	1.40	2.34	1.28	2.14	1.08	1.81
Slab @ Pier C	1.09	1.82	1.24	2.08	1.27	2.12	1.04	1.73
Span 2 A	3.18	5.31	3.45	5.76	4.51	7.53	3.94	6.58
Span 2 B	3.14	5.24	3.49	5.83	4.59	7.67	3.83	6.39
Span 2 C	3.39	5.66	3.74	6.24	4.85	8.10	4.03	6.73
Curb Midspan	4.45	7.43	4.57	7.62	5.97	9.97	5.22	8.71
Curb at pier	0.70	1.18	.79	1.32	.89	1.49	.75	1.25
Critical RF	**1.08**	**1.80**	**1.19**	**1.99**	**1.27**	**2.12**	**1.04**	**1.73**

Conclusions and Recommendations

The load test and structural assessment results illustrate how components not intended to be structural members often affect the structure's load distribution. The lowest rating factors were obtained for the curb elements in negative moment over the piers. However, since the curbs were not intended to be structural elements and failure of the curbs will not cause failure of the structure, it is not recommended that the curb rating factors be used to control the structure rating.

Of the slab components, all rating factors were controlled by negative moments at the face of the piers. The large difference between the positive and negative moment rating factors is due to three factors. First of all, the calculated negative moment capacity at the pier faces was considerably less in magnitude than at the positive moment capacities calculated for midspan locations. The relatively low moment capacities at the face of the piers were due to the lack of development length on every 3rd bar. Therefore only 2 out of 3 bars were utilized in the capacity calculation at the face of the piers. Additionally, since the dead load moments at the pier faces were large compared to the

midspan moments, the remaining negative moment live-load capacity was relatively small. Ironically, the negative moment rating factors were reduced again, because load test results indicated that the slab in the negative moment region was in good condition and relatively stiff. Because the structure is continuous, the negative moment increases with the stiffness of the slab over the piers. As flexural cracks develop in the vicinity of the pier and the slab becomes more flexible, the load rating will actually improve because the applied moments in this region will decrease.

This condition is relatively common with continuous RC structures (slabs in particular) and is due to the limitations of a linear-elastic analysis. With this in mind, the resulting critical load rating factors can be considered conservative and not indicative of what loads would induce a structural failure. The critical rating factors can still be considered reasonable though because they are representative of the loads limits that would induce large permanent deflections.

Since it is likely that excessive cracks would appear in the curbs if the bridge were loaded near its operating limit, it is recommended that the condition of the curbs be thoroughly examined during future inspections. The presence of cracks would indicate that the structure's load distribution characteristics have changed.

The load rating factors presented in this section are based on the structure's condition at the time of load testing. Any structural degradation must be considered in future load ratings. Note that no effort was made to assess the condition or capacity of the substructure elements such as the abutments or piers.

Bridge 4631.1S003 East Fork Des Moines River – Steel Girder

Description of Structure

Structure Identification	4631.1S003
Location	IA 3 Over East Fork Des Moines River – Humboldt County
Structure Type	3-Span Continuous, Composite Steel Girders
Span Length(s)	97'-6", 125'-0", 97'-6"
Skew	Perpendicular
Structure/Roadway Widths	34'-0" / 28'-0"
Beam spacing	4 beams spaced at 8'-11"
Beam depth(s)	Interior Beams: W36x245 with cover plates Exterior Beams: W36x194 with cover plates
Curb/Parapet Detail	RC curb with embedded steel channels and steel handrail. Curbs directly over exterior beam line.
Deck	8" RC deck with 1 to 3 inches over concrete overlay. Parabolic deck crown of 3" obtained with differential beam elevations.
Visual condition	Beams in good condition with no apparent corrosion or loss of section.

Instrumentation and Load Test Details

Date	August 11th 1999
Structural Reference Point	X=0, Y= 0 at intersection of East abutment face and center line of South girder.
Test vehicle direction	West bound for all tests (Positive X direction).
Start of data recording	All tests start with front axle at X = -15.4'
Truck position	Record truck position at every wheel revolution (10.8'). *Autoclicker* placed on driver side front wheel.
Lateral truck path(s)	2 truck paths were defined for the load test. The Y position refers to distance between driver side front wheel and center line of S girder. Y1 = 2.0' Y2 = 18.5'
Measurements	(40) strain gages recorded at 33 Hz
Gage Placement	See Figure 37. Bottom flange gages placed at center of bottom flange. Top gages placed on underside of top flange, 2" from web. Diaphragm gages placed at the edge of top and bottom flanges.
Gage types	BDI Intelliducers
Number of test cycles	Data was recorded while the test truck crossed the bridge at crawl speed (5 mph). Each truck path was run twice to check reproducibility. One high-speed pass was run.

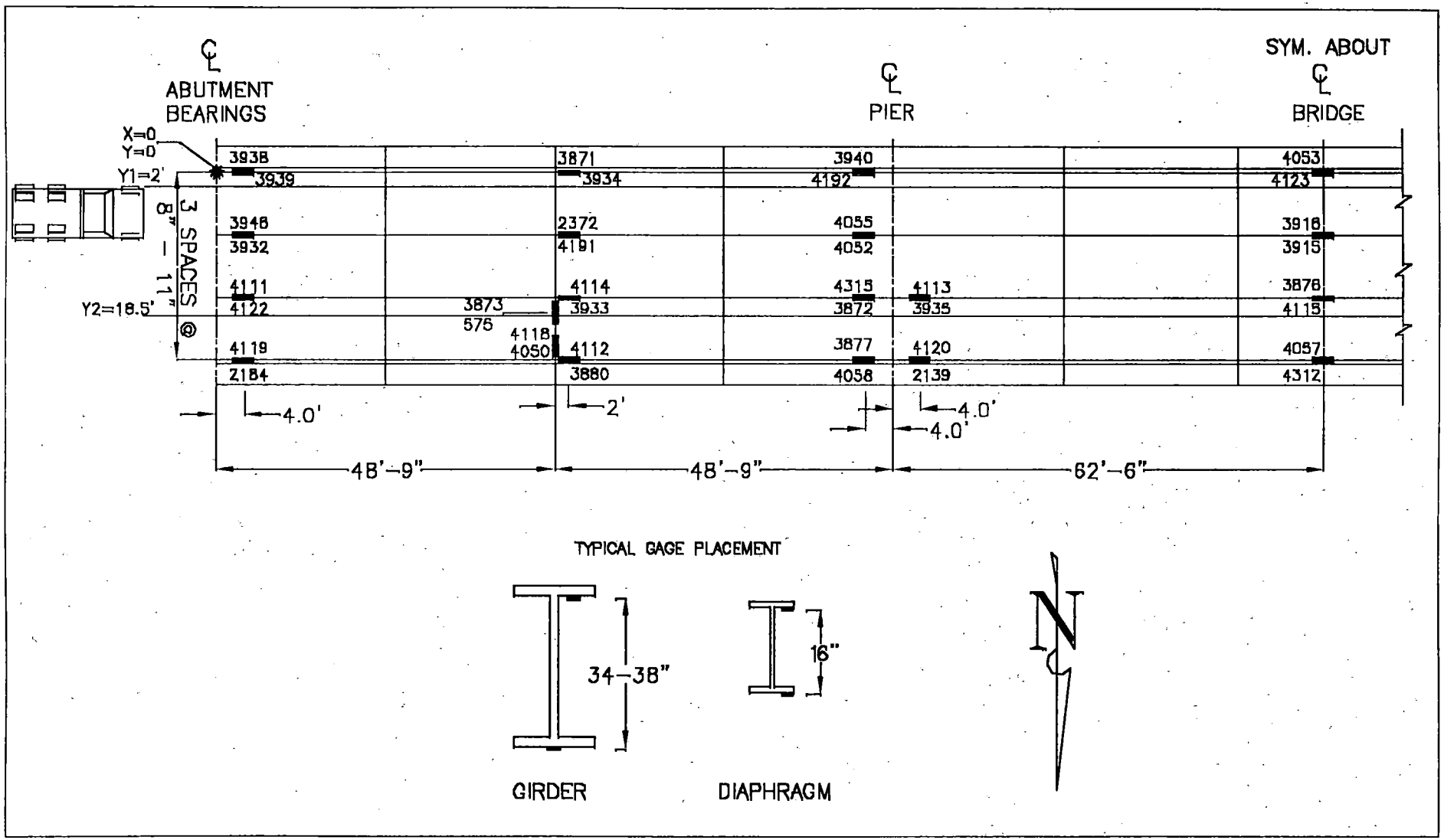

Figure 37 IA 3 over East Fork Des Moines River - Instrumentation Plan.

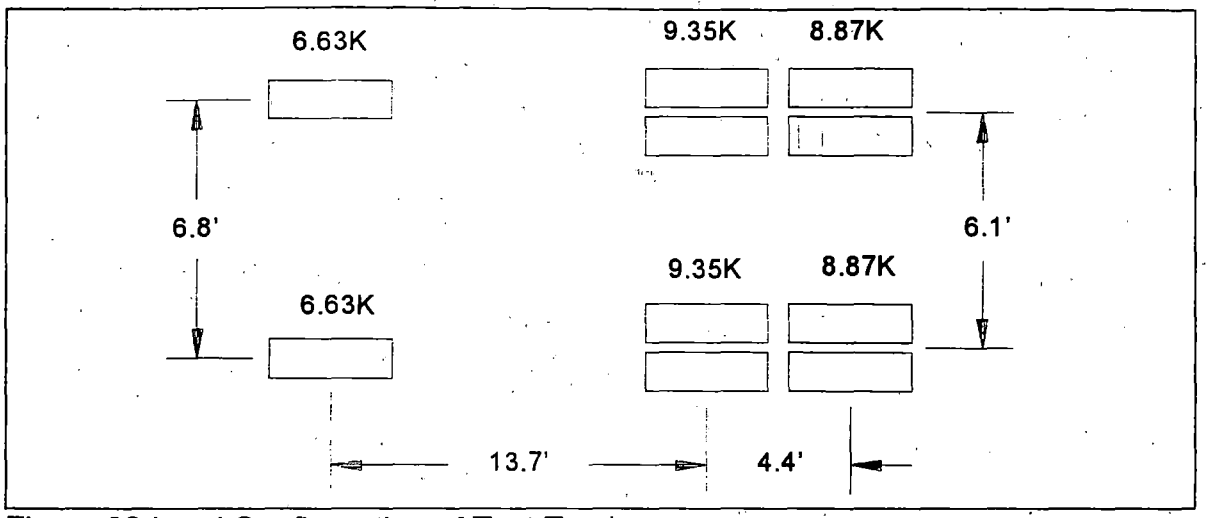

Figure 38 Load Configuration of Test Truck.

Table 40 Load Test Data Files

Truck Path	STS Data File	Comments
Y2	DMR1.dat	Passenger-side wheels on right shoulder line (missed 1st click).
Y2	DMR2.dat	Passenger-side wheels on right shoulder line
Y2	DMR3.dat	" " "
Y1	DMR4.dat	Driver-side wheels on left shoulder line
Y1	DMR5.dat	" " "
Y2	DMR6.dat	Passenger-side wheels on right shoulder line High Speed Pass (55 MPH)

Preliminary Investigation of Test Results

A visual examination of the field data was performed to assess the quality of the data and to make a qualitative assessment of the bridge's live-load response. Conclusions made directly from the field data were:

- Responses from identical truck paths were very reproducible as shown in Figure 39. It is difficult to differentiate between the two passes, indicating nearly identical responses.
- All strain measurements indicated linear-elastic live-load responses.
- RC/Steel channel curbs were acting integral with the superstructure, adding stiffness to the exterior beams. This caused the neutral axis locations of the exterior beams to be considerably higher than predicted by traditional composite analysis. The strain history of an exterior beam at the middle of the center span is shown in Figure 40. Based on this observation, the effective area/depth of the composite concrete block should be increased in subsequent analysis and modeling.
- Analysis of the data from the high-speed pass produced an impact factor of approximately 21 percent. This indicates that the AASHTO (I = 50/(L+125)) value of 22 percent is reasonable. However, since dynamic data was only obtained from a single truck during a single high-speed pass it is not likely that the maximum

impact/dynamic response was measured. An impact factor of 30% is recommended for subsequent load rating. Figure 41 shows a comparison of the static and dynamic test data.

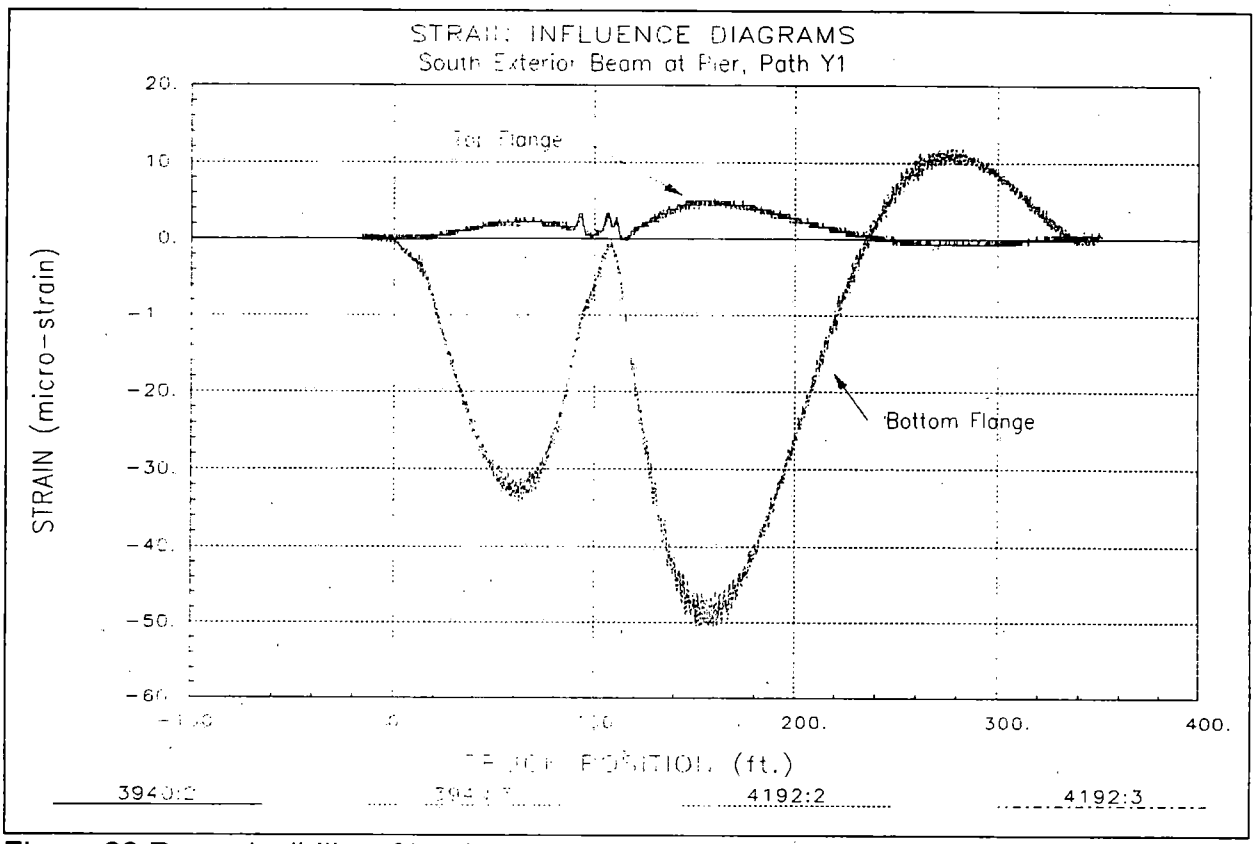

Figure 39 Reproducibility of load test - responses from two identical truck passes.

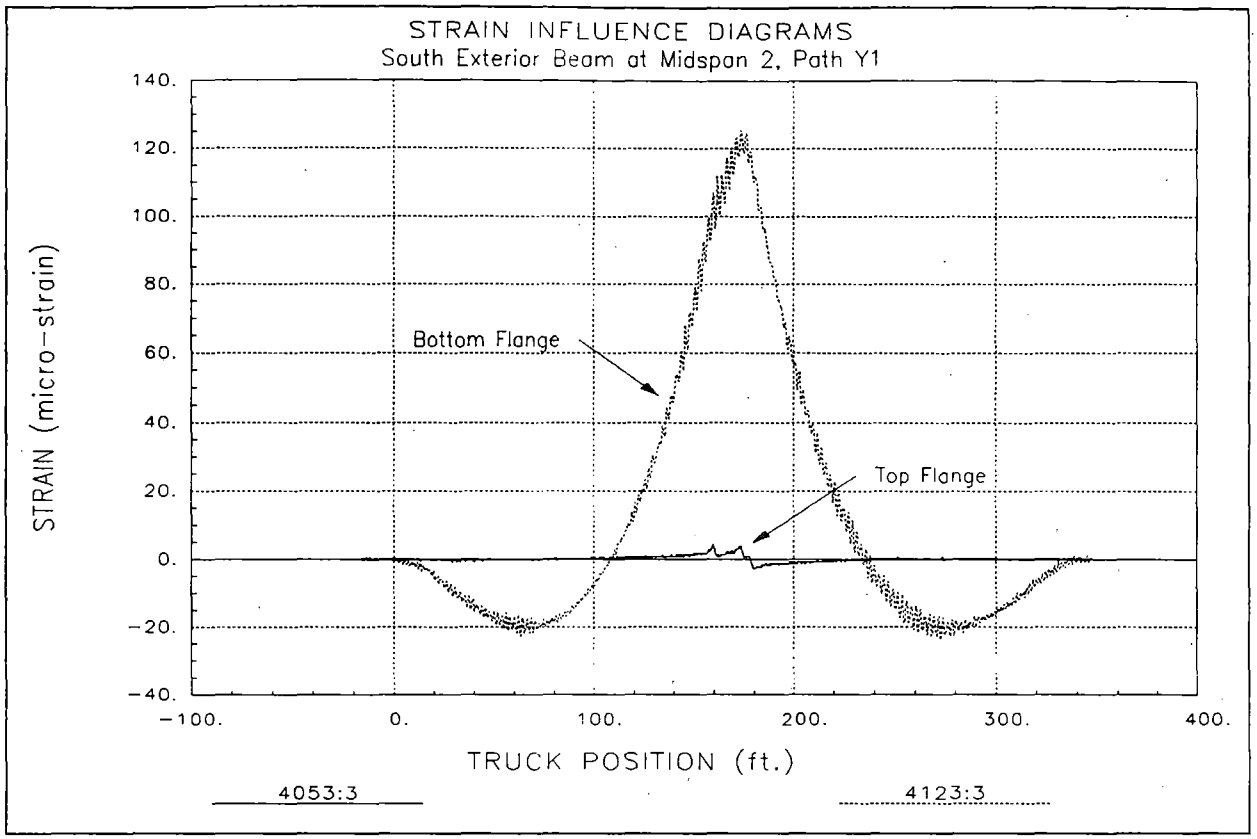

Figure 40 Midspan Exterior Beam Strain Response

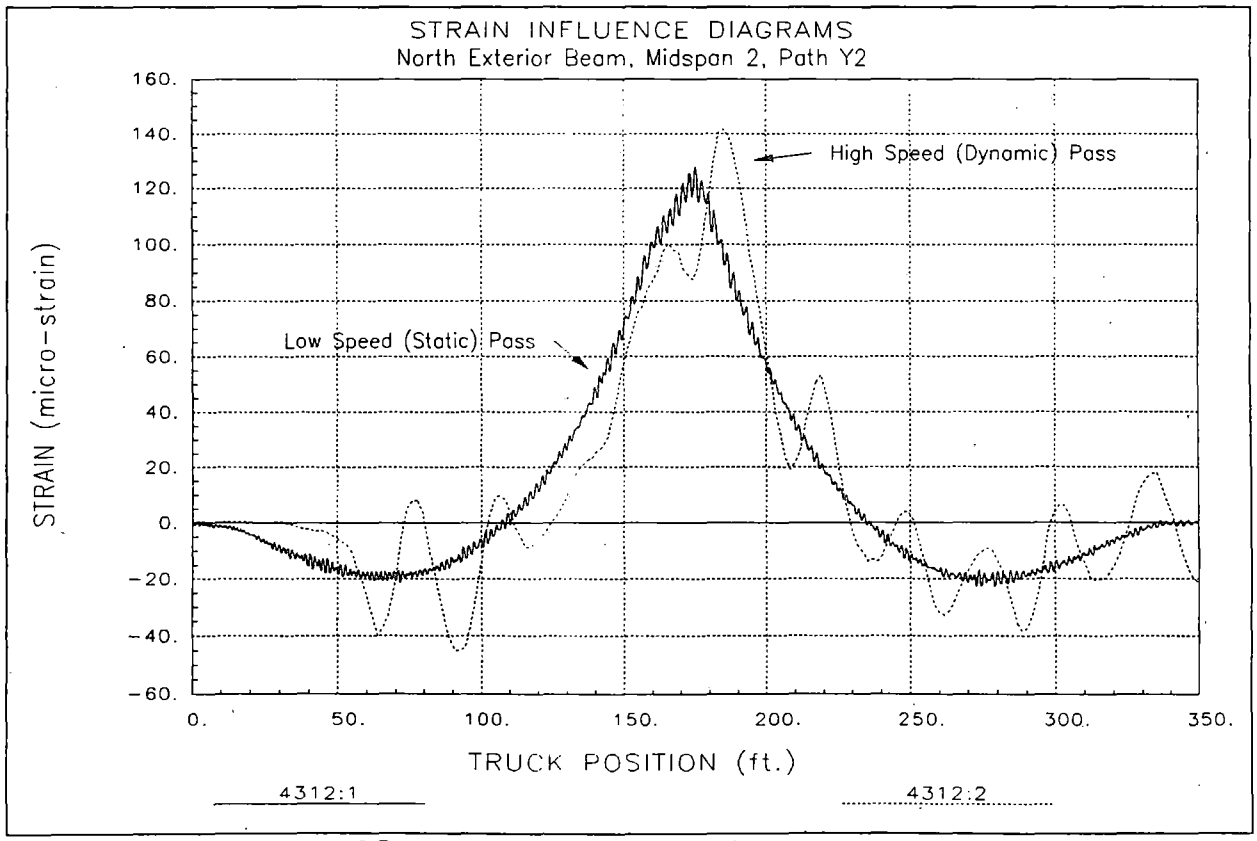

Figure 41 Comparison of Static and Dynamic Loading

Analysis and Model Calibration

Table 41 provides details regarding the structure model and analysis procedures. A discussion of the analysis results is provided along with conclusions regarding the structural performance.

Table 41 Analysis and model details – Des Moines River crossing.

Analysis type	Linear-elastic finite element - stiffness method.
Model geometry	Plane grid matching framing plan (see Figure 42)
Model components	• RC slab represented by quadrilateral plate elements. • Beam elements corresponding to different sections. • Curbs simulated by separate beam elements.
Live-load	2-D footprint of test truck consisting of 10 vertical point loads. Truck paths simulated by series of load cases with truck moving at 10-foot increments.
Dead-load	Self-weight of beams, slab, curbs, and parapets with additional 15 psf to account for overlay not included in slab thickness. (Used for load rating only)
Data comparison	40 strain gage locations defined on model (longitudinal beams and diaphragms). Strains computed for 34 truck positions along each path. 40x34x2 = 2720 strain values. Strain records extracted from load test data files corresponding to analysis truck positions.
Model statistics	726 Nodes 1140 Elements 20 Cross-section/Material types 69 Load Cases 40 Gage locations
Adjustable parameters for model calibration	1 Young's modulus (E_c - ksi) 2 Exterior beam stiffness – midspan (I_y - in^4) 3 Exterior beam stiffness – near abutment (I_y - in^4) 4 Exterior beam stiffness – near pier (I_y - in^4) 5 Interior beam stiffness – midspan (I_y - in^4) 6 Interior beam stiffness – near abutment (I_y - in^4) 7 Interior beam stiffness – near pier (I_y - in^4)

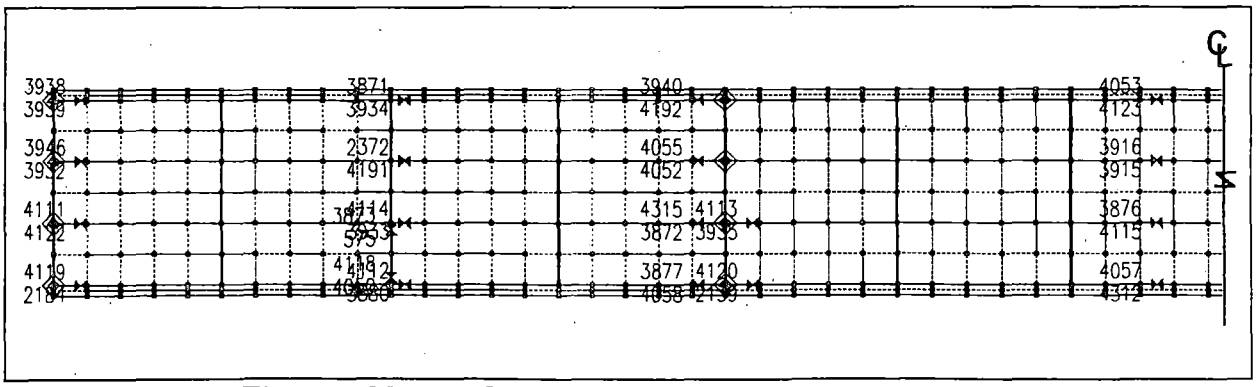

Figure 42 Finite Element Mesh – Des Moines River

A model with the above parameters was defined and the analysis program simulated the load test process. The accuracy of the model was defined by comparing the 2720 computed and measured strain values. Selected parameters were modified to minimize the comparison error.

Typically, all bridges show some level of moment resistance at the supports, making it necessary to include rotational or longitudinal springs in their respective models. The data from this bridge, however, indicated negligible moment restraint at the abutments and piers. Considering this and the rocker support conditions at both locations, no support moment restraint was added to the model.

Table 42 contains the original stiffness parameters and the final values after the model calibration process. Statistical accuracy values associated with the initial and final models are provided in Table 43. The resulting accuracy terms were in the typical range for steel structures.

Table 42 Adjustable Parameter Results

Stiffness Parameter	Units	Initial Value	Final Value
Deck modulus E	ksi	3,600	5,775
Exterior beam – midspan (I)	In^4	40,982	47,530
Exterior beam – near abutment (I)	In^4	36,354	42,160
Exterior beam – near pier (I)	In^4	70,055	81,250
Interior beam – midspan (I)	In^4	52,775	56,500
Interior beam – near abutment (I)	In^4	44,973	48,150
Interior beam – near pier (I)	In^4	71,338	76,380

Table 43 Model Accuracy

Statistical Term	Initial Value	Final Value
Absolute Error	5359.8με	2546.6με
Percent Error	8.2%	2.0%
Scale Error	10.4%	3.2%
Correlation Coefficient	0.98	0.99

Load Rating Calculations

Load rating factors were computed for the longitudinal beams using the Load Factor method. A Load Factor of 1.3 was applied to all dead-load affects for both Inventory and Operating load ratings, while load factors 2.17 and 1.3 were applied to live-load responses. Ultimate strength member capacities were computed, based on AASHTO specifications for steel beams, except that moment capacities were limited to yield stress of the extreme fiber rather than plastic moment capacities. Positive moment capacities were obtained for midspan cross-sections, negative moment capacities were computed for cross-sections at the piers, and shear capacities were calculated for the sections at the abutments and piers.

The modeling and calibration phase of the analysis yielded neutral axis values for the beams near the piers that indicated composite behavior even in negative moment.

However, for rating purposes, the beam cross sections in negative moment regions were computed as non-composite sections. Also, the majority of dead load was applied to a non-composite model. The non-composite dead-load stresses were subtracted from the original yield stress, at each critical section, to obtain composite member capacities. A yield stress of 35 ksi was assumed, based on the provided mill test reports. Table 8 contains the resulting moment and shear capacities for the composite model.

Table 44 Ultimate strength moment capacities for beam sections.

Member	Ultimate Strength Capacity	
	Moment (K in)	Shear (Kips)
Exterior Beam		
Midspan (Span 1)	35,292	N/C
Midspan (Span 2)	36,639	N/C
Near Abutment	N/C	528
Near Pier	-39,338	528
Interior Beam		
Midspan (Span 1)	44,408	N/C
Midspan (Span 2)	46,082	N/C
Near Abutment	N/C	542
Near Pier	-49,451	542

Load rating calculations were performed for the HS-20 and the three Iowa rating vehicles by applying the truck configurations to the calibrated model. Due to the width of the roadway, two truck paths were defined. The first path was defined by placing a wheel line 2 feet from the face of the curb. The second truck path was defined as being 12 feet from the first path. Single lane loading envelopes (critical responses) were generated for every model component by moving the applied rating truck at 8-foot intervals along the length of the bridge. Multiple lane load conditions were obtained by the principle of superposition. The response envelopes were added to generate two-lane loading response envelopes.

Dead load responses were obtained by applying 22 PSF to account for concrete overlay not included in the deck model components and the railing. Note that the non-composite dead-load effects were subtracted from the member capacities prior to running the rating analyses. Table 9 contains computed dead load and the various rating vehicle live-load forces for each critical beam section. Inventory and operating rating factors for each component are listed in Table 46.

Table 45 Dead load and maximum live load forces on critical beam sections.

Member	Units	Dead-Load*	HS-20	Type 4	Type 3-3	Type 3S3
Exterior Beam						
Mid – (Span 1) Mom.	K in	1,102	8,446	6,861	8,216	8,059
Mid – (Span 2) Mom.	K in	1,241	8,882	7,104	8,668	8,478
Abutment Shear	Kips	35.6	33.8	26.0	31.3	31.5
Pier Moment	K in	-5,632	-5,377	-4,134	-5,677	-5,632
Pier Shear	Kips	62.0	35.8	28.4	35.8	35.5
Interior Beam						
Mid – (Span 1) Mom.	K in	1,357	8,769	7,282	8,405	8,249
Mid – (Span 2) Mom.	K in	1,502	9,242	7,510	8,830	8,590
Abutment Shear	Kips	45.1	37.4	28.8	33.9	34.5
Pier Moment	K in	-5,978	-5,696	-4,370	-6,028	5,978
Pier Shear	Kips	83.8	40.1	32.3	39.3	39.4

* Composite dead-load only - non-composite dead-load effects subtracted from member capacities.

Table 46 Load Rating Factors – Des Moines River.

Member	HS-20		Type 4		Type 3-3		Type 3S3	
	Inv.	Oper.	Inv.	Oper.	Inv.	Oper.	Inv.	Oper.
Exterior Beam								
Midspan 1 Mom.	1.41	2.36	1.75	2.92	1.46	2.44	1.49	2.49
Midspan 2 Mom.	1.40	2.33	1.75	2.92	1.43	2.39	1.46	2.44
Abutment Shear	5.06	8.45	6.58	10.98	5.45	9.10	5.42	9.04
Pier Moment	2.43	4.05	3.16	5.27	2.30	3.84	2.32	3.87
Pier Shear	4.43	7.39	5.61	9.37	4.43	7.40	4.47	7.46
Interior Beam								
Midspan 1 Mom.	1.71	2.85	2.08	3.47	1.80	3.00	1.83	3.06
Midspan 2 Mom.	1.69	2.83	2.08	3.48	1.77	2.96	1.82	3.04
Abutment Shear	4.58	7.65	5.94	9.92	5.06	8.45	4.97	8.29
Pier Moment	2.87	4.78	3.73	6.23	2.71	4.52	2.73	4.56
Pier Shear	3.81	6.36	4.76	7.94	3.89	6.49	3.90	6.50
Critical RF	**1.40**	**2.33**	**1.75**	**2.92**	**1.43**	**2.39**	**1.46**	**2.44**

Conclusions and Recommendations

The analysis results from the initial model were reasonably accurate, indicating that the structure is behaving in a normal manner. The slight modifications to model parameters to improve the comparison with measured strains included a 7% increase in interior beam stiffness, 15% stiffness increase in the exterior beams, and a substantial increase in the effective deck stiffness. The resulting deck modulus should not be considered accurate from a material standpoint. The transverse crown of the deck improved the lateral distribution properties of the deck. This geometry effect was compensated for, in the plane model, by increasing the effective deck stiffness.

The structure exhibited relatively large dynamic effects compared to the shorter bridges that were tested. The measured dynamic response of 21% was approximately equal to the factor computed from the AASHTO impact formula. However, only a single high-speed truck pass was recorded. It is likely that different vehicle speeds and different trucks could induce greater dynamic responses. Therefore, an impact factor of 30% was applied to the live-load for all load-rating calculations.

The load rating factors presented in this report are based on the structure's condition at the time of load testing. Any structural degradation must be considered in future load ratings. Note that no effort was made to assess the condition or capacity of the substructure elements such as the abutments or piers.

Bridge 9951.4S003 Eagle Creek– Steel and PS/Concrete Beams

Description of Structure

Structure Identification	9951.4S003
Location	IA 3 Over Eagle Creek – Wright County
Structure Type	Single Span, Widened structure Original: Steel Beams Widened Section: Prestressed Concrete Beams
Span Length(s)	Original: 40'-0" Widened Section: 40'-0" up to 52'-0" @ Exterior beams
Beam Spaces	10 spaces at 4'-3 1/4"
Skew	Perpendicular
Structure/Roadway Widths	Original: 28'-0" / 24'-0" Widened : 46'-6" / 44'-0"
Curb/Parapet Detail	RC curb integral with slab and RC parapet
Visual condition	Beams in good condition with minimal corrosion and loss of section.

Instrumentation and Load Test Details

Date	August 12th 1999
Structural Reference Point	X=0, Y= 0 at intersection of West abutment face and center line of South exterior PS/C girder.
Test vehicle direction	East bound for all tests (Positive X direction).
Start of data recording	All tests start with front axle at X = -15.4'
Truck position	Record truck position at every wheel revolution (10.8'). *Autoclicker* placed on driver side front wheel.
Lateral truck path(s)	4 truck paths were defined for the load test. The Y position refers to distance between driver side front wheel and centerline of S girder: Y1 = 10.0' Y2 = 16.8' Y3 = 33.5' Y4 = 40.3'
Measurements	(40) strain gages recorded at 33 Hz
Gage Placement	See Figure 43. Bottom flange gages placed at center of bottom flange. For steel beams, top gages placed on underside of top flange, 2" from web. For concrete beams, top gages placed on side of top flange.
Gage types	BDI Intelliducers
Number of test cycles	Data was recorded while the test truck crossed the bridge at crawl speed (5 mph). Each truck path was run twice to check reproducibility. One high-speed (50 mph) pass was also run along path Y2.

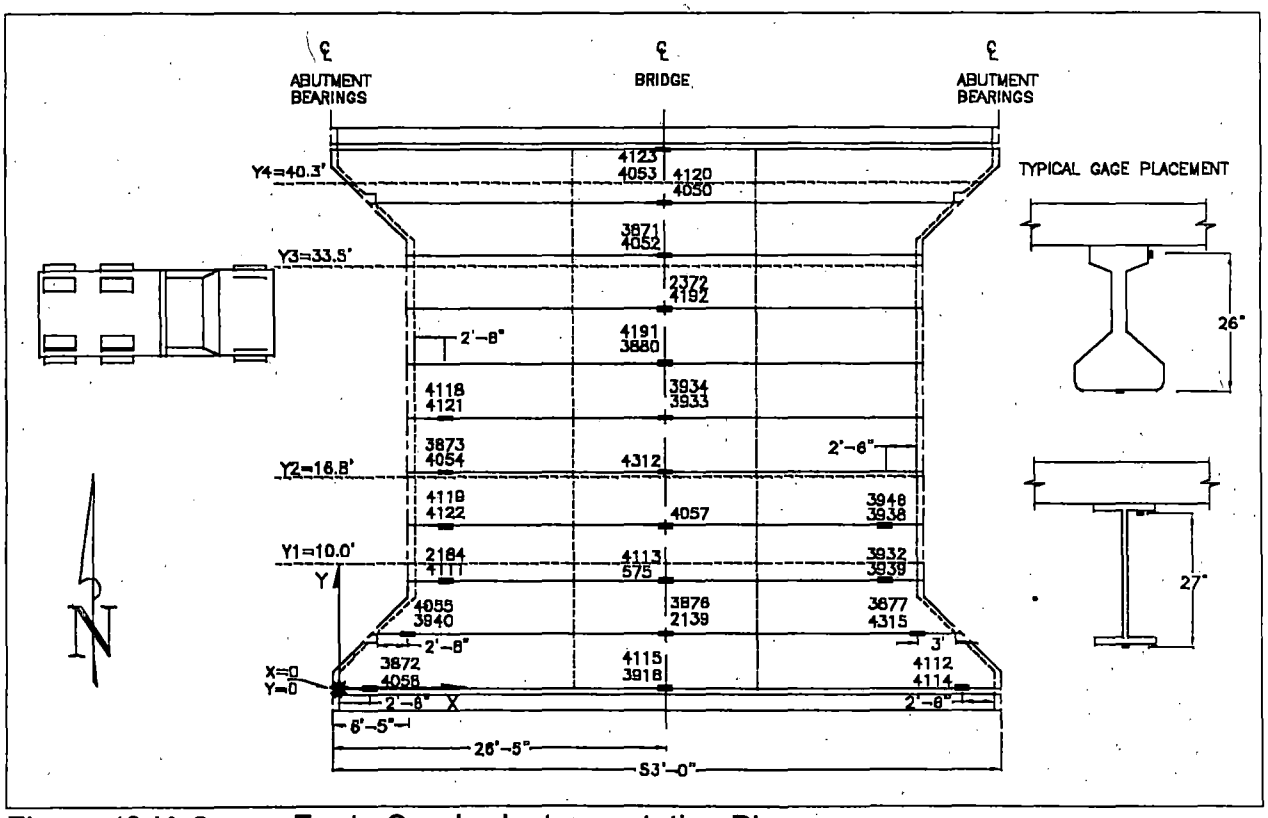

Figure 43 IA 3 over Eagle Creek - Instrumentation Plan.

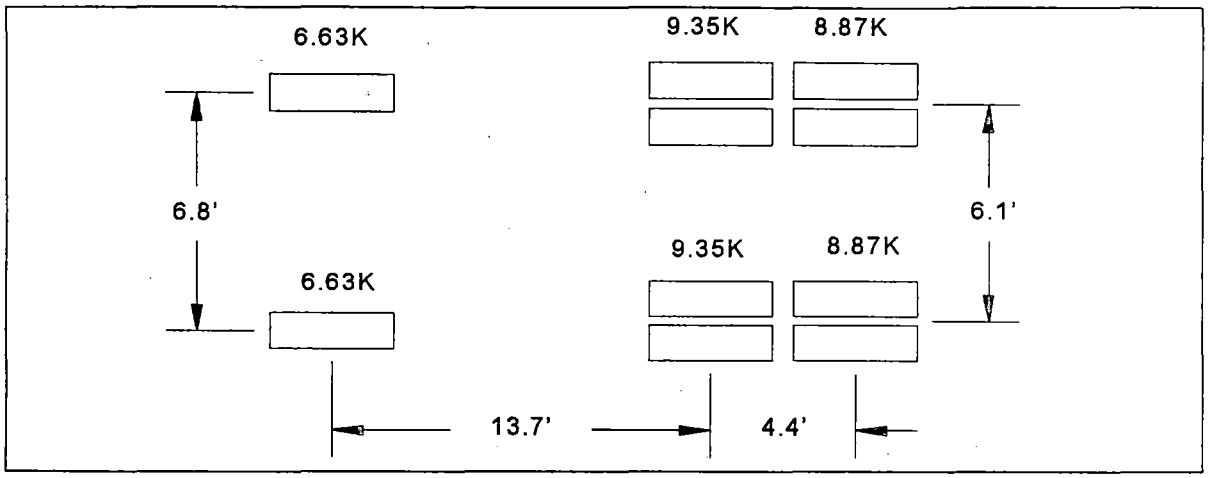

Figure 44 Load Configuration of Test Truck.

Table 47 Load Test Data Files

Truck Path	STS Data File	Comments
Y1	EAGLE1.dat	Driver-side wheels on right shoulder line
Y1	EAGLE2.dat	" " "
Y1	EAGLE3.dat	Passenger-side wheels on right shoulder line
Y1	EAGLE4.dat	" " "
Y2	EAGLE5.dat	Driver-side wheels on left shoulder line
Y2	EAGLE6.dat	" " "
Y2	EAGLE7.dat	Passenger-side wheels on left shoulder line
Y2	EAGLE8.dat	" " "
Y1	EAGLE9.dat	Passenger-side wheels on right shoulder line High Speed Pass (50 MPH)

Preliminary Investigation of Test Results

A visual examination of the field data was performed to assess the quality of the data and to make a qualitative assessment of the bridge's live-load response. Conclusions made directly from the field data were:

- Responses from identical truck paths were very reproducible as shown in Figure 45.
- The majority of strain measurements indicated linear-elastic live-load responses. All gages returned to the zero point when the truck drove off of the bridge.
- Contrary to the non-composite design, the steel beams all exhibited composite behavior, as shown in Figure 46.
- Because the beams were embedded in concrete at the supports, the torsional stiffness of the abutment had an effect on the gages located near the end of the beams. This produced positive moment responses instead of the expected negative moment (due to the rotational restraint) when the truck was far away from the beam. Figure 47 shows a typical strain history of a gage pair located near to an abutment.
- Analysis of the data from the high-speed pass produced an impact factor of approximately 20 percent. This proves the AASHTO value of 30 percent to be conservative. Figure 48 shows a comparison of the static and dynamic test data.

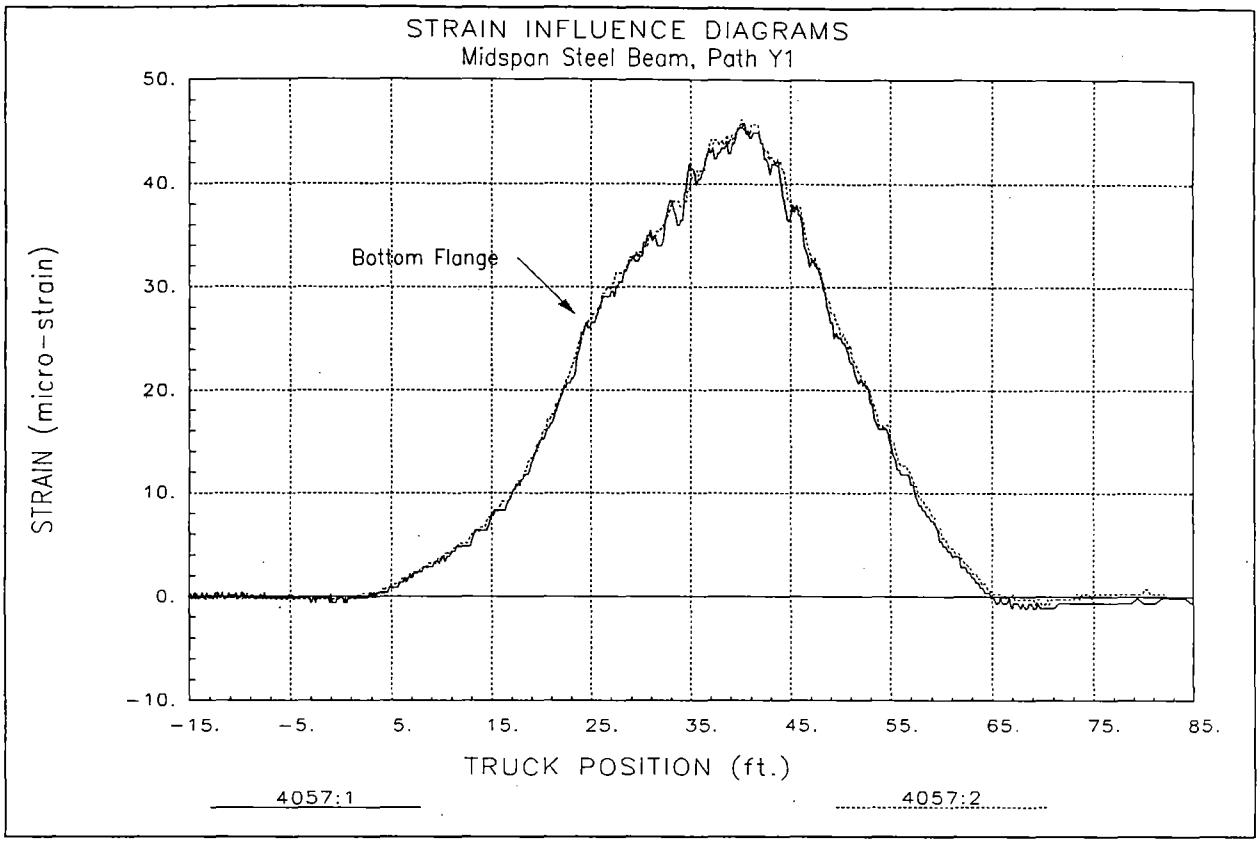

Figure 45 Reproducibility of load test

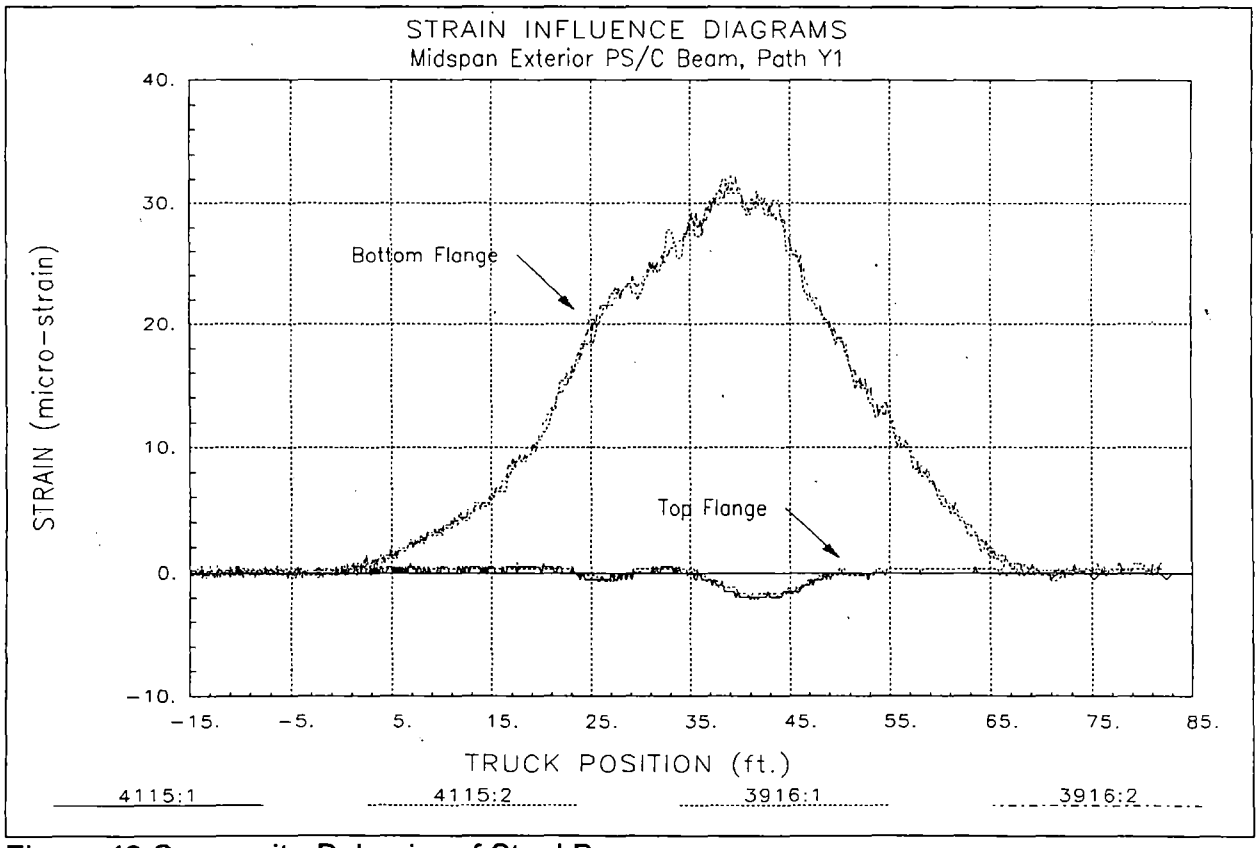

Figure 46 Composite Behavior of Steel Beams

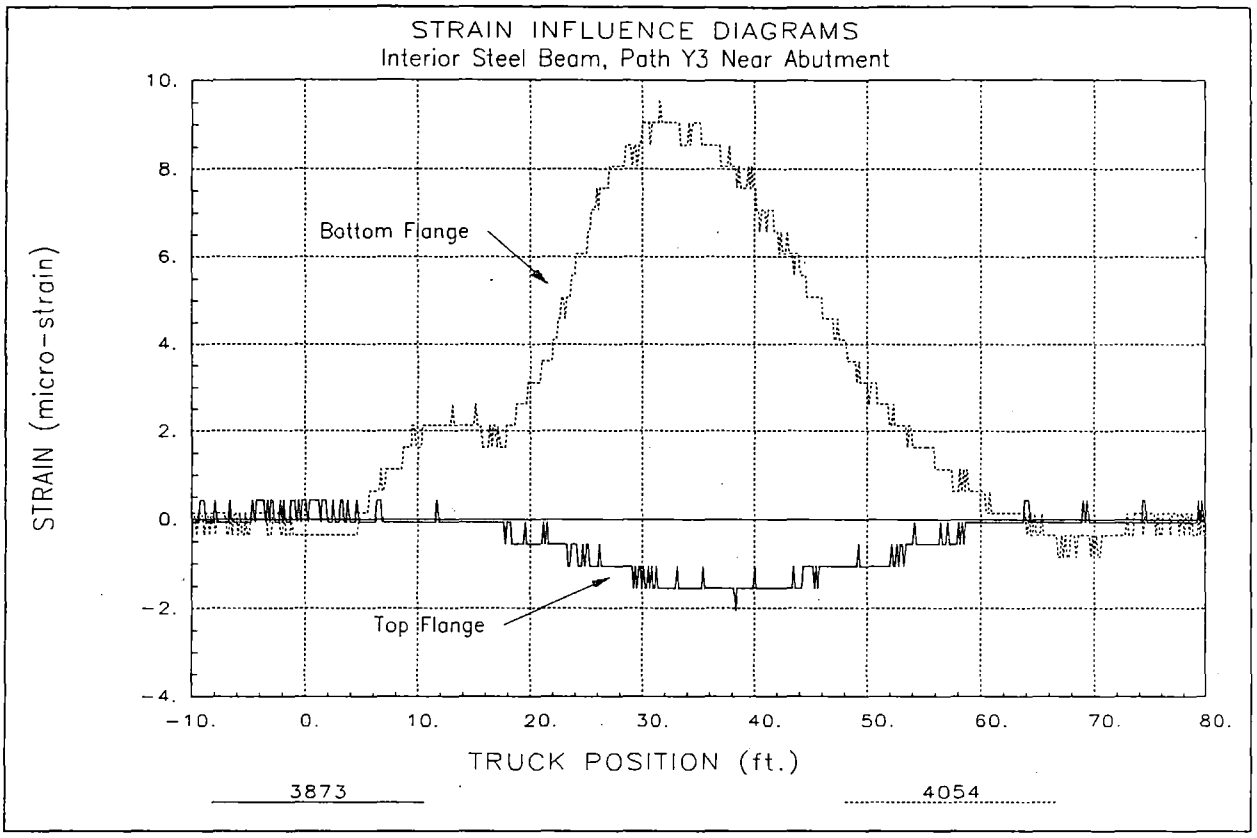

Figure 47 Strain History of Steel Beam Near Abutment

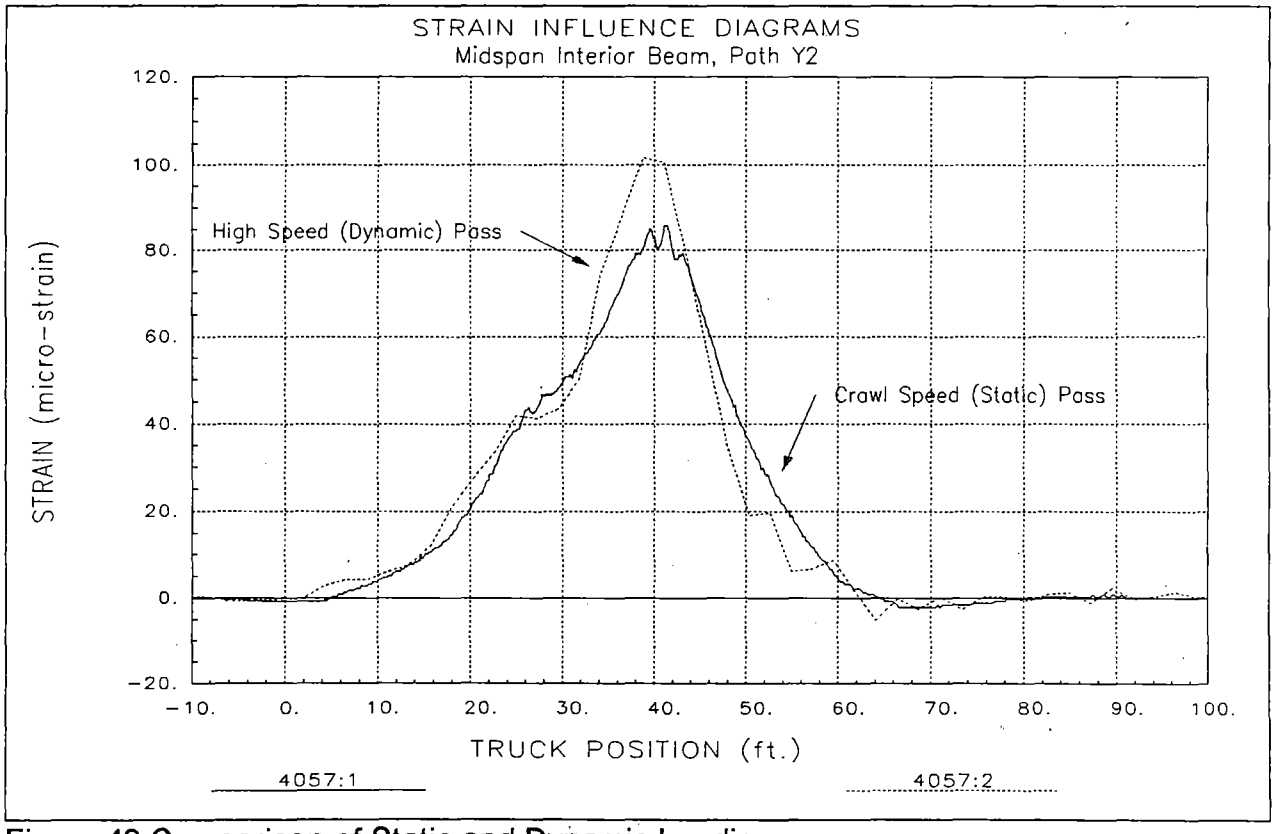

Figure 48 Comparison of Static and Dynamic Loading

Analysis and Model Calibration

Table 48 provides details regarding the structure model and analysis procedures. A discussion of the analysis results is provided along with conclusions regarding the structural performance.

Table 48 Analysis and model details – Eagle Creek crossing.

Analysis type	Linear-elastic finite element - stiffness method.
Model geometry	Plane grid matching framing plan (see Figure 42)
Model components	• RC slab represented by quadrilateral plate elements. • Beam elements corresponding to different sections.
Live-load	2-D footprint of test truck consisting of 10 vertical point loads. Truck paths simulated by series of load cases with truck moving at 10-foot increments.
Dead-load	Self-weight of beams, slab, curbs, and parapets with additional 15 psf to account for overlay not included in slab thickness. (Used for load rating only)
Data comparison	21 strain gage locations defined on model (longitudinal beams). Strains computed for 13 truck positions along each path. 21x13x4 = 1092 strain values. Strain records extracted from load test data files corresponding to analysis truck positions.
Model statistics	202 Nodes 393 Elements 11 Cross-section/Material types 52 Load Cases 21 Gage locations
Adjustable parameters for model calibration	1 Young's modulus of concrete for both original and widened sections (E_c - ksi) 2 Steel beam stiffness (I_y - in^4) 3 Exterior PS/C beam stiffness (I_y - in^4) 4 Interior PS/C beam stiffness (I_y - in^4) 5 Rotational end-restraint for steel and PS/C beams (k-in/in)

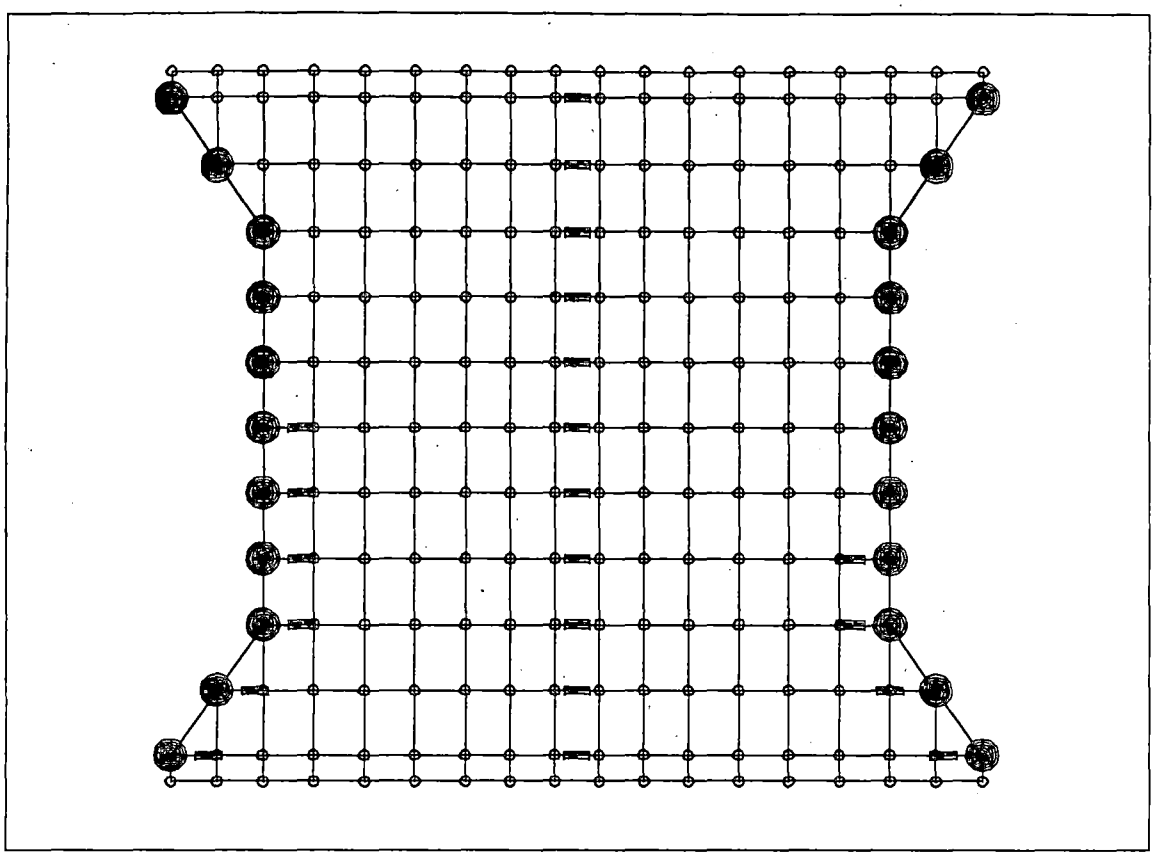

Figure 49 Finite Element Mesh – Eagle Creek

A model with the above parameters was defined and the analysis program simulated the load test process. The accuracy of the model was defined by comparing the 1092 computed and measured strain values. Selected parameters were modified to minimize the comparison error.

The ends of the beams were embedded in the concrete abutments, producing significant end restraints. This was simulated by adding rotational springs to the model and then optimizing their stiffness to best match the test data. The resulting concrete stiffnesses varied considerably between the original slab and the new slab. The modulus values are not considered to realistic values for the concrete itself. Rather they are the effect modulus values for flexure. The lower modulus of the original slab indicates that it is a higher degree of flexural cracking, additionally the effective span lengths are greater due to the differences in beam flange widths.

Table 49 contains the original stiffness parameters and the final values after the model calibration process. Statistical accuracy values associated with the initial and final models are provided in
Table 50.

Table 49 Adjustable Parameter Results

Stiffness Parameter	Units	Initial Value	Final Value
Original slab modulus E	ksi	3,600	1,325
Widened slab modulus E	ksi	3,600	3,400
Steel beam (I_y) - composite	in^4	9,917	8,800
Exterior PS/C beam (I_y)	in^4	106,309	212,180
Interior PS/C beam (I_y)	in^4	106,309	142,840
Rotational end restraint – PS/C bms	K-in/rad	0	648,380
Rotational end restraint – steel bms	k-in/rad	0	495,030

Table 50 Model Accuracy

Statistical Term	Initial Value	Final Value
Absolute Error	5079.4με	1601.4με
Percent Error	32.4%	3.4%
Scale Error	14.1%	3.5%
Correlation Coefficient	0.86	0.98

Load Rating Calculations

Load rating factors were computed for the longitudinal beams using the Load Factor method. A Load Factor of 1.3 was applied to all dead-load affects, while load factors 2.17 and 1.3 were applied to live-load responses for Inventory and Operating load ratings, respectively. Ultimate strength member capacities were computed, based on AASHTO specifications for steel beams. Positive moment capacities were obtained for midspan cross-sections and shear capacities were calculated for the sections near the face of the abutments.

Although the plans do not indicate that the bridge was designed to rely on composite behavior between the steel beams and the concrete deck, the field data shows that all beams acted compositely. Subsequently, the bridge was rated using the load factor method with the beam capacities being limited by yield stress of the composite sections.

A recommended means of checking the reliability of this unintended composite strength is to calculate the shear forces along the interface of the steel beam and the concrete deck using allowable stress parameters. A.G. Lichtenstein and Associates, Inc have suggested a horizontal shear stress of 100 psi as a reasonable limit for unintended composite action. The maximum calculated shear force, for HS-20 loading plus impact, was approximately 30% higher than the accepted value. However, the construction details show that any slippage of the interface is very unlikely. For this reason, the rating was performed on a model consisting of composite sections for both concrete and steel beams. Table 51 contains moment and shear capacity values for both steel and PS/C beam sections. The moment capacities were computed using non-composite action for dead load contribution, and composite action for positive live load moments.

Table 51 Ultimate strength capacities for beam sections.

Member	Ultimate Strength Capacity	
	Moment (K in)	Shear (Kips)
Steel Beams	9,057	223
PS/C Beams		
Exterior	9,770	105
Interior	10,087	114

Load rating calculations were performed for the HS-20 and the three Iowa rating vehicles by applying the truck configurations to the calibrated model. Due to the width of the roadway, three truck paths were defined. The first path was defined by placing a wheel line 2 feet from the face of the curb. The second and third truck paths were defined as being 12 feet from the previous paths. One of the three paths also provided critical loading for the interior steel beams. Single lane loading envelopes (critical responses) were generated for every model component by moving the applied rating truck at 2-foot intervals along the length of the bridge. Multiple lane load conditions were obtained by the principle of superposition. The response envelopes were added to generate two and three-lane loading response envelopes.

Dead load responses were obtained by computing the self-weight of the structure. The non-composite dead-load effects were subtracted from the member capacities prior to load rating. An additional 25 PSF was applied to the composite model to account for concrete overlay and guardrails. Table 52 contains computed dead-load and the various rating vehicle live-load forces for each critical beam section. Inventory and operating rating factors for each component are listed in Table 53.

Table 52 Dead load and maximum live load forces on critical beam sections.

Member	Units	Dead-Load	HS-20	Type 4	Type 3-3	Type 3S3
Steel Beam						
Moment	K in	1,710	1,334	1,169	976	1,097
Shear	Kips	18.9	22.0	17.7	16.9	17.1
Exterior PS/C Beam						
Moment	K in	3,099	1,994	1,730	1,619	1,556
Shear	Kips	19.1	14.0	10.8	11.6	13.4
Interior PS/C Beam						
Moment	K in	2,782	2,017	1,783	1,578	1,607
Shear	Kips	9.3	16.2	13.1	12.2	12.5

Table 53 Load Rating Factors – Eagle Creek.

Member	HS-20		Type 4		Type 3-3		Type 3S3	
	Inv.	Oper.	Inv.	Oper.	Inv.	Oper.	Inv.	Oper.
Steel Beam								
Moment	2.31	3.86	2.64	4.41	3.16	5.28	2.81	4.70
Shear	3.53	5.89	4.37	7.29	4.57	7.63	4.52	7.55
Exterior PS/C Beam								
Moment	1.62	2.71	1.87	3.12	2.00	3.33	2.08	3.48
Shear	2.55	4.25	3.30	5.51	3.06	5.10	3.13	5.23
Interior PS/C Beam								
Moment	1.67	2.79	1.89	3.16	2.14	3.57	2.10	3.50
Shear	2.42	4.04	2.98	4.98	3.20	5.34	3.14	5.24
Critical RF	**1.62**	**2.71**	**1.87**	**3.12**	**2.00**	**3.33**	**2.08**	**3.48**

Conclusions and Recommendations

Load rating factors for the steel beams are relatively high - to the extent that the controlling factor is the moment capacity of the exterior PS/C beams. The rating for the interior steel beams relies on two performance factors that were observed during the load test. First it was observed that the beams acted compositely with the RC deck even though the plans did not indicate any shear connectors. Due to the construction details and redundancy of the structure, it was determined that composite action was reasonable for rating purposes. The second observation was relatively fixed end-conditions provided by the embedded beam supports. The supports have the effect of significantly reducing midspan moments.

The condition of the end-diaphragm (beam supports) and the beam-deck interface should be examined thoroughly during future inspections to validate the rating assumptions provided here.

The load rating factors presented in this report are based on the structure's condition at the time of load testing. Any structural degradation must be considered in future load ratings. Note that no effort was made to assess the condition or capacity of the substructure elements such as the abutments or piers.

Bridge 9712.1R020 Elliot Creek - Parabolic RC T-beam

Description of Structure

Structure Identification	9712.1R020
Location	Us-20 over Elliot Creek – Woodbury County
Structure Type	3 span continuous RC t-beams. Variable depth beams (parabolic profile)
Span Lengths	44'-6", 61'-0", 44'-6"
Beam Spaces	9'-9 1/2", 10'-1 1/2", 9'-9 1/2" c.c.
Skew	Perpendicular
Structure/Roadway Widths	34'-8" / 28'-0"
Curb/Parapet Detail	RC curb integral with exterior beam and deck. RC parapet/guardrail directly above exterior beam web - not part of original structure. Parapet is continuous and no sign of distress.
Visual condition	Beams in good condition with minimal cracks. No spalling of concrete or exposed reinforcement.

Instrumentation and Load Test Details

Date	August 3rd, 1999
Structural Reference Point	X=0, Y= 0 at Southwest abutment beam bearing.
Test vehicle direction	East bound for all tests (positive X direction).
Start of data recording	All tests start with front axle at X = -15.4'
Truck position	Record truck position at every wheel revolution (10.8'). *Autoclicker* placed on driver side front wheel.
Lateral truck path(s)	2 truck paths were defined for the load test. The Y position refers to distance between driver side front wheel and centerline of south girder. Y1 = 10.5' Y2 = 26.4'
Measurements	(36) strain gages recorded at 33 Hz
Gage Placement	See Figure 43. Bottom beam gages placed at center of web. Upper beam gages located below bevel. Distance between gages varies.
Gage types	BDI Intelliducers with 18" extensions (21" gage length)
Number of test cycles	Data was recorded while the test truck crossed the bridge at crawl speed (5 mph). Each truck path was run twice to check reproducibility. One high-speed (45 mph) pass was also run along path Y2.

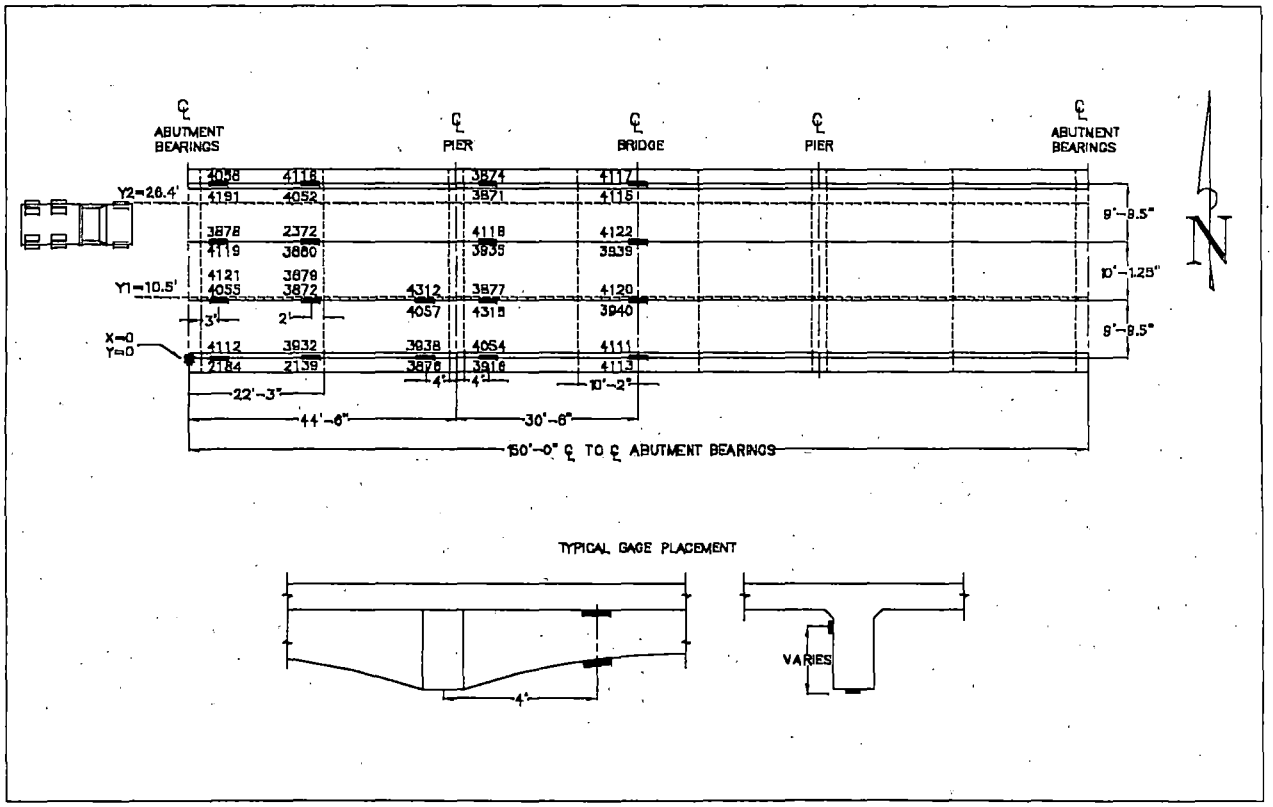

Figure 50 US-20 over Elliot Creek - Instrumentation Plan.

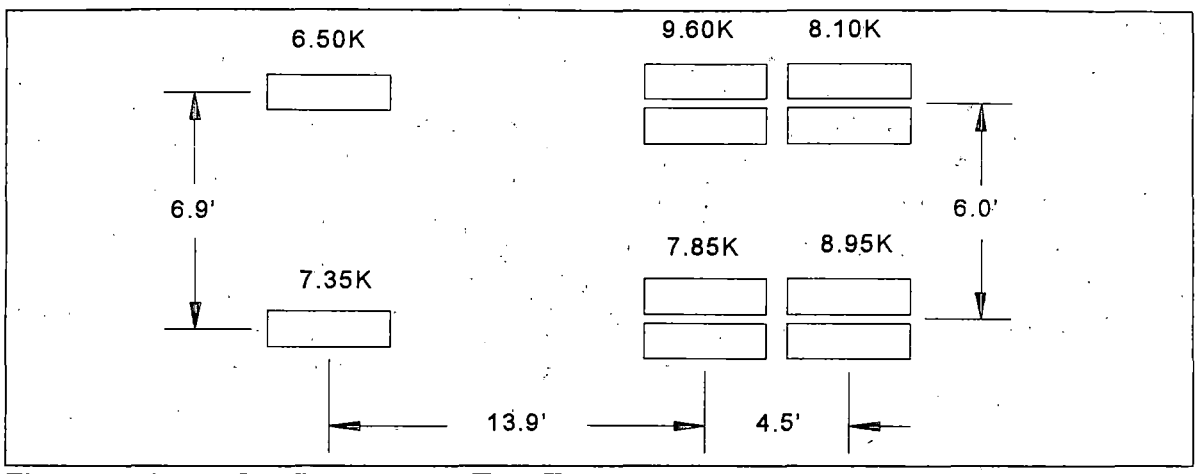

Figure 51 Load Configuration of Test Truck.

Table 54 Load Test Data Files

Truck Path	STS Data File	Comments
Y1	ELLIOT1.DAT	Passenger side wheel on south shoulder line - slow
Y1	ELLIOT2.DAT	Passenger side wheel on south shoulder line - slow
Y2	ELLIOT3.DAT	Driver side wheel on north shoulder line - slow
Y2	ELLIOT4.DAT	Driver side wheel on north shoulder line - slow
Y2	ELLIOT5.DAT	Driver side wheel on north shoulder line - fast 45 MPH

Preliminary Investigation of Test Results

A visual examination of the field data was performed to assess the quality of the data and to make a qualitative assessment of the bridge's live-load response. Conclusions made directly from the field data were:

- All responses were linear-elastic. Strains from all transducers returned to zero after each truck crossing.
- Reproducibility of data from identical truck passes was excellent as shown in Figure 52.
- Neutral axis measurements on exterior beam sections consistently higher than calculated for section consisting of web, deck and curb only. Indicates RC guardrail is contributing to stiffness of exterior beam. Figure 53 shows strains from upper and lower gages at midspan of southern exterior beam. Strains from both gages have the same sign indicating neutral axis well above upper gage position.
- Interior beam responses had a high degree of symmetry with the symmetrical load conditions as shown in Figure 54. Exterior beams were reasonably symmetric but not as consistent as the interior beams. This could be an indication that the exterior beams have a higher density of tension cracks in the concrete.

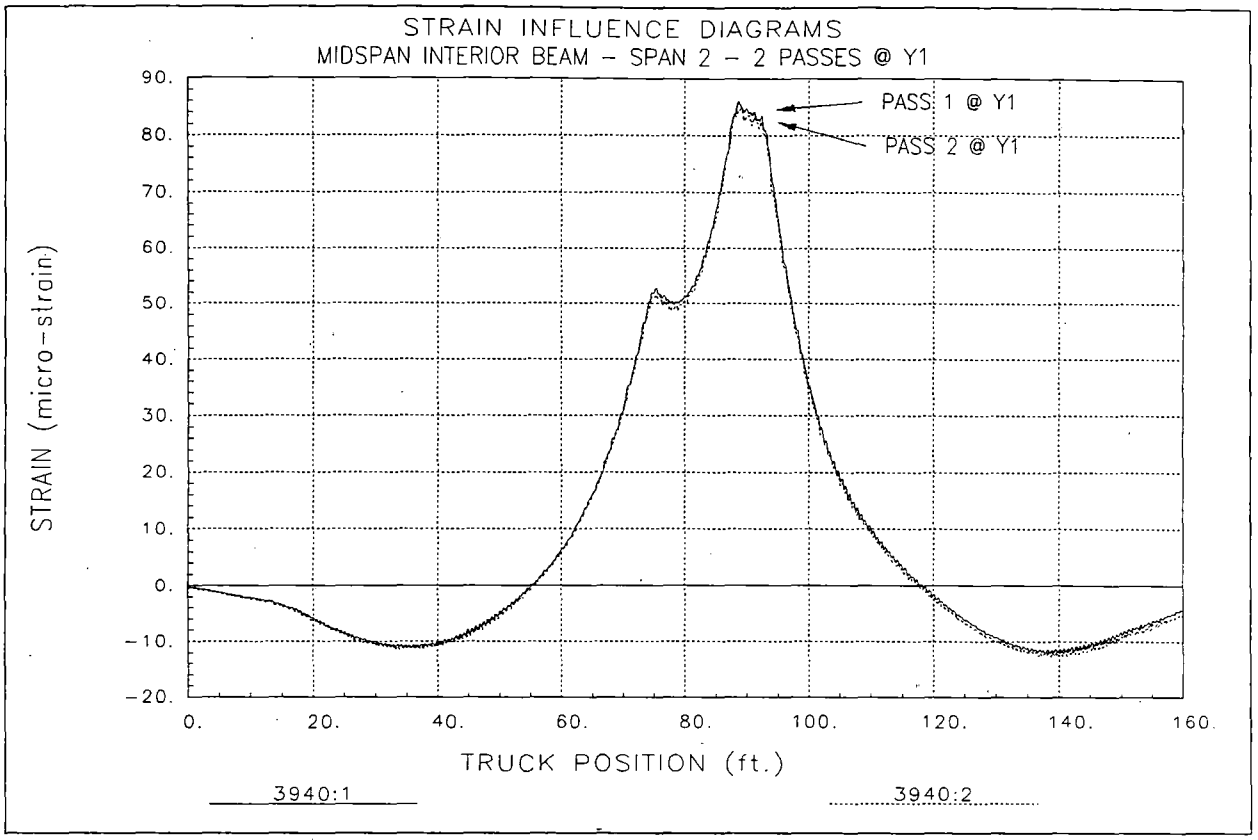

Figure 52 Reproducibility of strain responses - midspan Span 2.

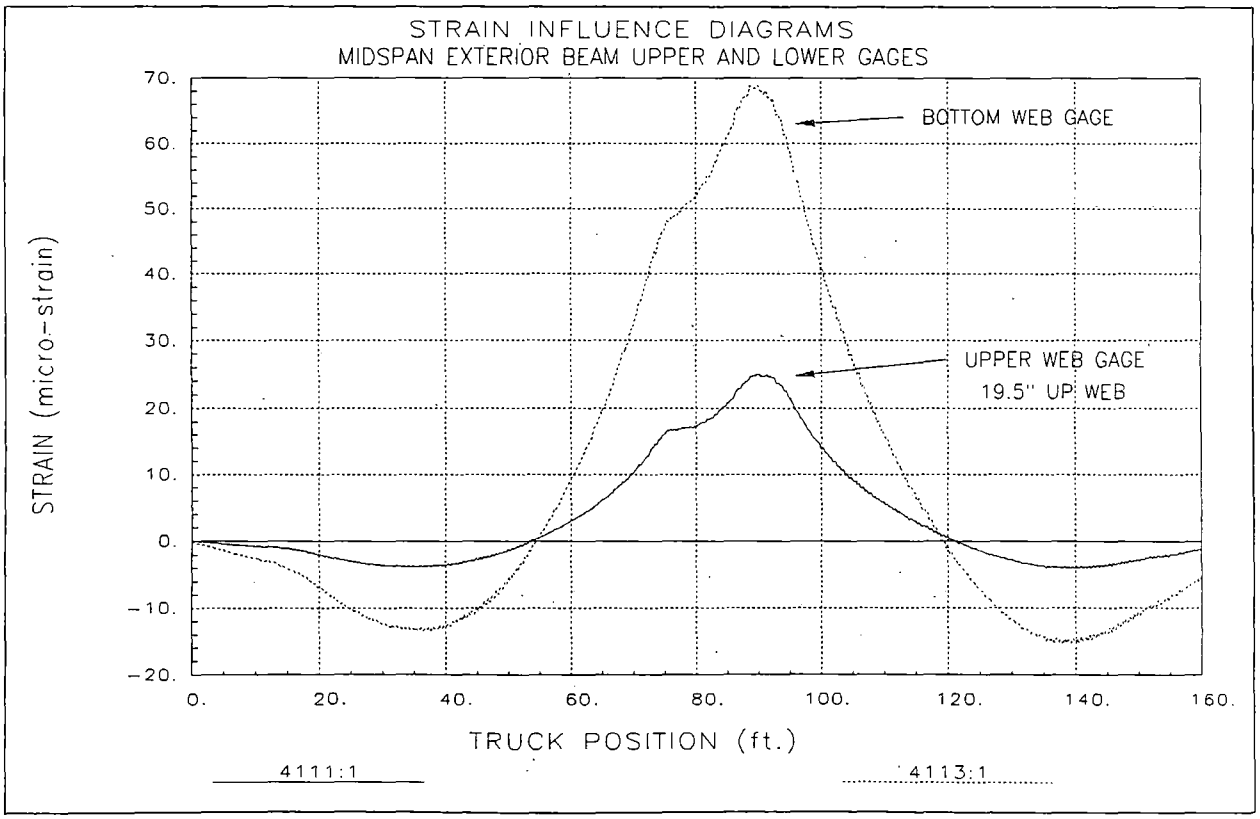

Figure 53 Strain histories indicating contribution of guardrail to exterior beam.

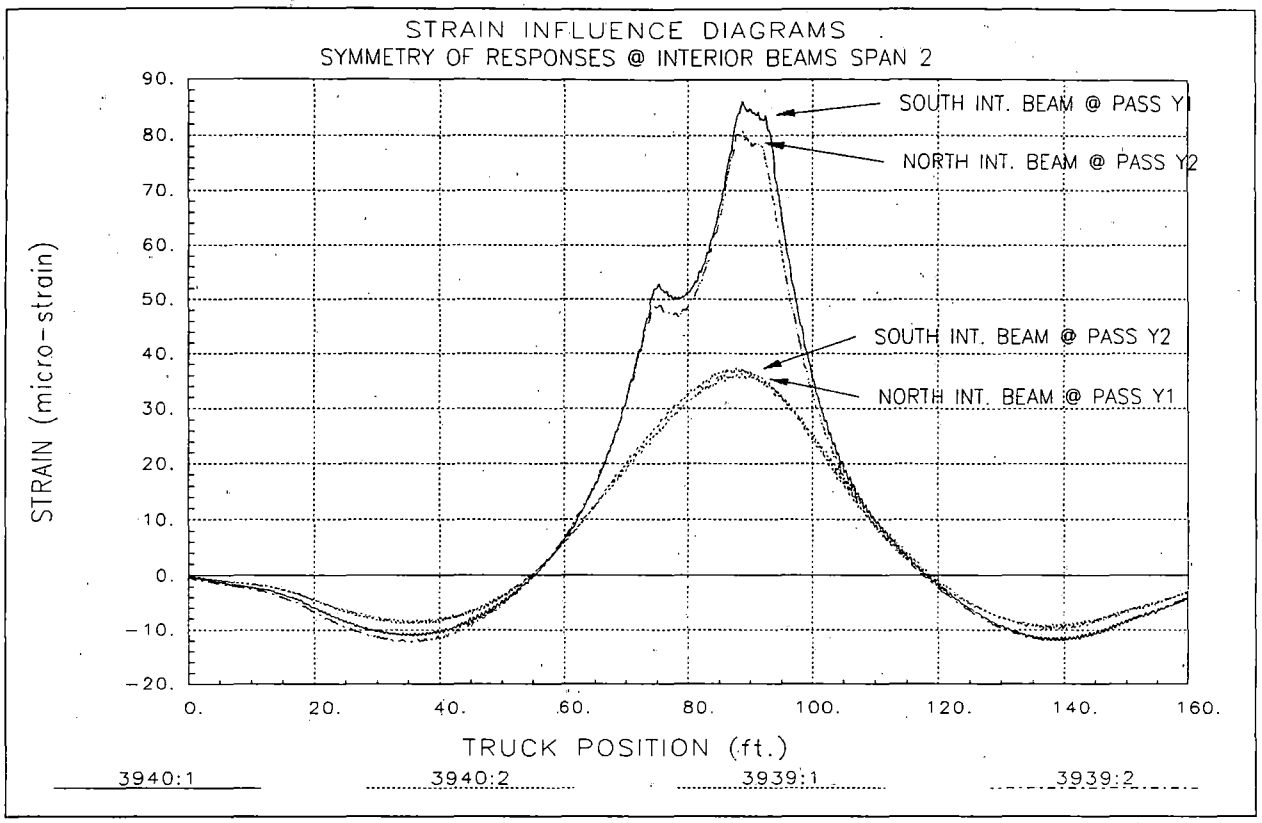

Figure 54 Symmetry of interior beam strains at midspan of span 2.

Analysis and Model Calibration

Table 5 provides details regarding the structure model and analysis procedures. A discussion of the analysis results is provided along with conclusions regarding the structural performance.

Table 55 Analysis and model details - Elliot Creek.

Analysis type	Linear-elastic finite element - stiffness method.
Model geometry	Plane grid matching structure framing plan (see Figure 6).
Model components	• Prismatic beam elements representing beam sections 1/12th span length in end-spans and 1/18th span length at middle span. Properties for each beam segment were based on average depth of beam segment. Figure 56 shows the depth of each beam segment relative to the bridge centerline. Actual beam depths vary due to crown of bridge deck. • Prismatic beam elements representing transverse diaphragms. • Quadrilateral plate elements representing deck - 3 plate elements between each beam.
Live-load	2-D footprint of test truck consisting of 10 vertical point loads. Truck paths simulated by series of load cases with truck moving at 5-foot increments.

Dead-load	Self-weight of slab, curbs, and parapets with additional 15 psf to account for overlay not included in slab thickness. (Used for load rating only)
Data comparison	18 longitudinal strain gage locations defined on model (bottom of T-beams). Strains computed for 29 truck positions along each path. 29x18x2 = 1044 strain values. Strain records extracted from load test data files corresponding to analysis truck positions.
Model statistics	430 Nodes 634 Elements 50 Cross-section/Material types 58 Load Cases 18 Gage locations
Adjustable parameters for model calibration	1 Young's modulus - span 1 Int. beam + moment (E_c - ksi) 2 Young's modulus - Int. beam near piers - moment (E_c - ksi) 3 Young's modulus - span 2 int. beam + moment (E_c - ksi) 4 Young's modulus - span 1 Ext. beam + moment (E_c - ksi) 5 Young's modulus - Ext. beam near piers - moment (E_c - ksi) 6 Young's modulus - span 2 Ext. beam + moment (E_c - ksi) 7 Young's modulus - regions of low moment (no cracks) (E_c - ksi)

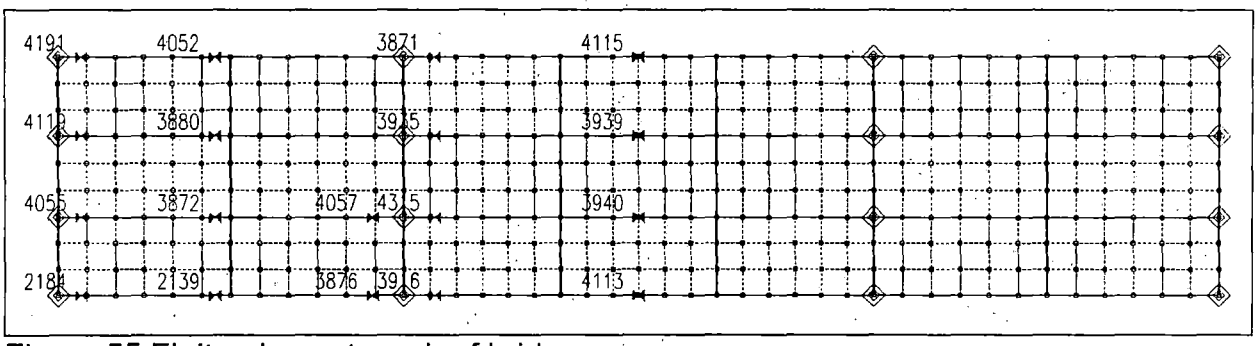

Figure 55 Finite element mesh of bridge.

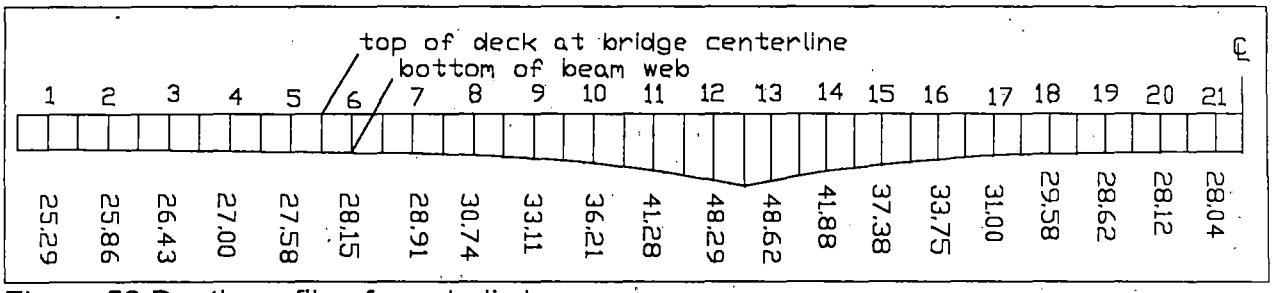

Figure 56 Depth profile of parabolic beams.

A model with the above parameters was defined and the analysis program simulated the load test process. The accuracy of the model was defined by comparing the 1044 computed and measured strain values. Selected parameters were modified to minimize the comparison error.

The general conclusions were that the RC guardrails did in fact contribute to the exterior beam stiffness. Beam cross-sections in the immediate vicinity of the piers and at midspan of Span 2 had stiffness below the gross concrete section indicating the presence of concrete tension cracks.

Table 56 contains the original stiffness parameters and the final values after the model calibration process. Statistical accuracy values associated with the initial and final models are provided in Table 57. The resulting accuracy terms were exceptionally good for RC slab structures. The relatively high accuracy is an indication that the bridge responses are very linear and that the measurements were not heavily influenced by flexural cracks in the concrete.

Table 56 Adjustable Parameter Results

Stiffness Parameter	Units	Initial Value	Final Value
Int. Bm Span 1+M Ec	ksi	3200	3246
Int. Bm Pier -M Ec	ksi	3200	2436
Int. Bm Span 2+M Ec	ksi	3200	2229
Int. Bm Span 1+M Ec	ksi	3200	3600
Int. Bm Pier -M Ec	ksi	3200	2667
Int. Bm Span 2+M Ec	ksi	3200	2208
Low Moment Ec	ksi	3200	3600

Table 57 Model Accuracy

Statistical Term	Initial Value	Final Value
Absolute Error	5578 με	1258 με
Percent Error	27.4%	2.5%
Scale Error	8.7%	1.7%
Correlation Coefficient	.92	.99

Load Rating Calculations

Load rating factors were computed for the structural components of the superstructure using the Load Factor method. A Load Factor of 1.3 was applied to all dead-load affects for both Inventory and Operating load ratings, while load factors 2.17 and 1.3 were applied to live-load responses. Ultimate strength member capacities, based on AASHTO specifications for reinforced concrete beams, were computed for positive and negative moment regions and shear near the supports. Positive moment capacities were obtained for several cross-sections near midspan and negative moment capacities were computed at nodal locations near the piers and abutments.

Since the guardrails were effective in load distribution, the additional concrete was included in the shear capacity and positive moment capacity of the exterior beams. Since the amount of steel in the parapets was unknown, it was assumed that they would not contribute to the negative moment capacity.

Table 58 contains shear and moment capacity calculations for various critical beam sections. Grade 40 reinforcement, with a minimum yield stress of 40 ksi, was assumed

based on the age of the structure. A concrete strength of 4 ksi was allowed due the relatively high concrete modulus obtained from the model calibration process.

Table 58 Ultimate strength capacities for beam cross-sections.

Member	Ultimate Strength Capacity	
	Moment (K in)	Shear (Kips)
Interior Beam Sections		
Int-1 (abutment)	-	143
Int-2	-	147
Int-3	16170	173
Int-4	18390	-
Int-5	18910	-
Int-6	19430	-
Int-7	18120	-
Int-8	12060	-
Int-10	-20890	-
Int-11	-27840	173
Int-12 adjacent to pier	-33910	202
Int-13 adjacent to pier	-34200	210
Int-14	-28360	209
Int-15	-21770	-
Int-20	19400	-
Int-21 (midspan 2)	19330	-
Exterior Beam Sections		
Ext-1 (abutment)	-	98**
Ext-2	-	99**
Ext-3	11810*	-
Ext-4	11940*	-
Ext-5	12070*	-
Ext-6	12200*	-
Ext-7	12370*	-
Ext-8	97470*	-
Ext-10	-11120	-
Ext-11	-15260	144**
Ext-12 adjacent to pier	-17850	162**
Ext-13 adjacent to pier	-17970	172**
Ext-14	-15490	145**
Ext-15	-11470	-
Ext-20	12190*	-
Ext-21 (midspan 2)	12180*	-

* RC Guardrail contributing to moment capacity of cross-section (b and d values)
** RC Guardrail contributing to shear capacity of cross-section $V_{GR}=2(f'c)^{0.5}bh$

Load rating calculations were performed for the HS-20 and the three Iowa rating vehicles by applying the truck configurations to the calibrated model. Due to the width of the roadway, three truck paths were defined. The first path was defined by placing a wheel line 2 feet from the face of the curb. Subsequent truck paths were defined at 12-

foot increments. Single lane loading envelopes (critical responses) were generated for every model component by moving the applied rating truck at 2-foot intervals along the length of the bridge. Multiple lane load conditions were obtained by the principle of superposition. The response envelopes were added to generate two and three-lane loading response envelopes. Three-lane load responses were reduced by 10% according to AASHTO specification 3.12.1.

Dead load responses were obtained by computing the self-weight of the structure and adding 15 PSF to account for concrete overlay not included in the deck model components. Because the guardrails were not part of the original structure, their stiffness was eliminated from the model for dead-load calculations. Therefore, the participation of the guardrails was only effective for live load. Table 59 and Table 60 contain maximum computed moment and shear for dead load and the various rating vehicles. Inventory and operating rating factors for each component are listed in Table 61 for moment ratings and Table 62 for shear ratings.

Table 59 Dead load and maximum live load moments on critical sections.

Section	Dead-Load M (k-in)	HS-20 M (k-in)	Type 4 M (k-in)	Type 3-3 M (k-in)	Type 3S3 M (k-in)
Interior Beam					
Int-3	2386	1952	1673	1453	1299
Int-4	2525	2095	1854	1554	1431
Int-5	2527	2085	1861	1547	1645
Int-6	2313	2047	1855	1493	1642
Int-7	1833	1901	1772	1447	1685
Int-8	854	1803	1695	1396	1624
Int-10	-4299	-2137	-1724	-1907	-1838
Int-11	-6933	-2260	-2109	-2315	-2293
Int-12	-9962	-3245	-2515	-2967	-3383
Int-13	-9975	-3256	-2578	-2993	-3374
Int-14	-7397	-2388	-1961	-1930	-2400
Int-15	-4821	-1928	-1635	-1591	-1512
Int-20	2912	2125	1928	1672	1842
Int-21	2977	2155	1897	1635	1774
Ext. Beam					
Ext-3	2106	2604	2111	2076	1739
Ext-4	2240	3061	2586	2394	2115
Ext-5	2083	3313	2875	2609	2502
Ext-6	2076	3307	2876	2609	2686
Ext-7	1640	3322	2996	2676	2670
Ext-8	746	2930	2632	2359	2337
Ext-10	-3536	-2841	-2303	-2461	-2314
Ext-11	-5310	-3088	-2498	-2744	-2593
Ext-12	-7798	-3095	-2517	-2777	-2645
Ext-13	-7490	-3207	-2600	-2831	-2661
Ext-14	-5384	-2157	-1776	-1831	-1794
Ext-15	-3724	-1716	-1451	-1415	-1272
Ext-20	2531	3442	2911	2834	2620
Ext-21	2646	3474	2950	2902	2786

Table 60 Dead load and maximum live load shear on critical sections.

Section	EL#	Dead-Load V (kips)	HS-20 V (kips)	Type 4 V (kips)	Type 3-3 V (kips)	Type 3S3 V (kips)
Interior Beam						
Int-1	43	-26.4	-25.6	-23.2	-20.9	-22.5
Int-2	44	-19.7	-21.3	-18.8	-16.5	-17.8
Int-11	53	58.7	32.0	24.5	24.0	29.0
Int-12	73	-69.2	-35.7	-30.0	-28.1	-29.2
Int-13	72	70.4	36.3	28.5	28.9	31.7
Int-14	56	-62.1	-33.3	-28.0	-27.5	-28.7
Ext. Beam						
Ext-1	1	-22.3	-23.2	-19.5	-18.5	-18.4
Ext-2	2	-17.0	-20.9	-18.2	-16.3	-16.3
Ext-11	32	-44.7	-25.7	-21.2	-20.8	-20.0
Ext-12	31	-50.5	-26.6	-22.0	-22.3	-21.4
Ext-13	13	-51.6	-31.1	-24.6	-28.0	-27.4
Ext-14	14	-46.2	-30.3	-24.2	-26.9	-26.4

Table 61 Load Rating Factors due to Moment - Elliot Creek.

Section	HS-20		Type 4		Type 3-3		Type 3S3	
	Inv.	Oper.	Inv.	Oper.	Inv.	Oper.	Inv.	Oper.
Interior Beam								
Int-3	2.41	4.02	2.81	4.69	3.24	5.40	3.04	5.07
Int-4	2.60	4.33	2.93	4.90	3.50	5.84	3.30	5.52
Int-5	2.70	4.50	3.02	5.05	3.64	6.07	3.41	5.69
Int-6	2.89	4.82	3.19	5.32	3.96	6.61	3.60	6.01
Int-7	2.98	4.98	3.20	5.34	3.92	6.54	3.36	5.61
Int-8	2.19	3.65	2.33	3.88	2.82	4.71	2.43	4.05
Int-10	2.58	4.30	3.20	5.33	2.89	4.82	3.00	5.00
Int-11	2.61	4.36	3.21	5.36	2.93	4.89	2.96	4.93
Int-12	2.32	3.87	3.00	5.01	2.48	4.14	2.19	3.65
Int-13	2.35	3.92	2.96	4.95	2.49	4.16	2.20	3.68
Int-14	2.83	4.72	3.44	5.74	3.47	5.79	2.81	4.69
Int-15	2.89	4.83	3.41	5.70	3.51	5.86	3.69	6.16
Int-20	2.65	4.42	2.92	4.87	3.36	5.61	3.05	5.09
Int-21	2.58	4.31	2.93	4.89	3.39	5.67	3.10	5.17
Ext. Beam								
Ext-3	1.25	2.09	1.55	2.58	1.57	2.63	1.88	3.14
Ext-4	1.06	1.77	1.26	2.10	1.36	2.27	1.54	2.57
Ext-5	1.02	1.70	1.17	1.96	1.29	2.16	1.35	2.25
Ext-6	1.03	1.73	1.19	1.99	1.31	2.19	1.35	2.25
Ext-7	1.11	1.85	1.23	2.05	1.38	2.30	1.38	2.30
Ext-8	1.08	1.80	1.20	2.00	1.34	2.24	1.35	2.26
Ext-10	.83	1.38	1.02	1.70	0.93	1.56	0.98	1.64
Ext-11	.97	1.63	1.20	2.00	1.10	1.83	1.16	1.94
Ext-12	.90	1.50	1.10	1.84	1.00	1.67	1.05	1.75
Ext-13	.92	1.54	1.13	1.89	1.03	1.71	1.08	1.80
Ext-14	1.42	2.37	1.72	2.87	1.67	2.79	1.63	2.73
Ext-15	1.39	2.32	1.64	2.75	1.69	2.82	1.88	3.13
Ext-20	.93	1.55	1.09	1.81	1.11	1.86	1.12	1.88
Ext-21	.91	1.51	1.06	1.77	1.08	1.81	1.12	1.88

Table 62 Load Rating Factors due to Shear - Elliot Creek.

Section	HS-20		Type 4		Type 3-3		Type 3S3	
	Inv.	Oper.	Inv.	Oper.	Inv.	Oper.	Inv.	Oper.
Interior Beam								
Int-1	1.53	2.55	1.69	2.81	1.87	3.13	1.74	2.91
Int-2	2.05	3.42	2.32	3.88	2.65	4.43	2.45	4.09
Int-11	1.09	1.82	1.27	2.12	1.39	2.32	1.20	2.01
Int-12	1.13	1.89	1.35	2.25	1.44	2.40	1.26	2.11
Int-13	1.17	1.96	1.35	2.26	1.38	2.30	1.32	2.21
Int-14	1.09	1.81	1.29	2.16	1.32	2.20	1.25	2.09
Ext. Beam								
Ext-1	1.07	1.79	1.27	2.12	1.34	2.23	1.35	2.25
Ext-2	1.33	2.22	1.53	2.55	1.71	2.85	1.70	2.84
Ext-11	1.20	2.01	1.46	2.43	1.49	2.48	1.54	2.57
Ext-12	1.30	2.17	1.57	2.62	1.55	2.59	1.61	2.69
Ext-13	1.22	2.04	1.54	2.57	1.35	2.26	1.38	2.31
Ext-14	1.01	1.68	1.26	2.11	1.13	1.89	1.16	1.93

Conclusions Recommendations

Load test results and model calibration procedures indicated that the RC guardrails provided a significant increase in the exterior beams stiffness. The effect of this is that more load is transferred to exterior beams. If contribution of the guardrails is included in the stiffness during load rating calculation it should also be included in the shear and moment capacity of the exterior beams. In the above ratings it was assumed to provide additional live-load capacity for positive moment and shear. In all cases the critical load ratings were controlled by negative moment of the exterior girders at a location approximately 9 feet from the piers. The condition of the guardrails should be thoroughly examined for cracking and attachment to the superstructure during future inspections.

If it is assumed that the RC guardrail cannot provide additional capacity, then the stiffening effects to the exterior girders should not be considered during load rating analyses. This condition was considered and the result was that the critical HS-20 Inventory rating factor was reduced to a factor of 0.6. The controlling factor was shear of the exterior girders near the piers.

The load rating factors presented in this report are based on the structure's condition at the time of load testing. Any structural degradation must be considered in future load ratings. Note that no effort was made to assess the condition or capacity of the substructure elements such as the abutments or piers.

Appendix A - Field Testing Procedures

The motivation for developing a relatively easy-to-implement field testing system was to allow short and medium span bridges to be tested on a routine basis. Original development of the hardware was started in 1988 at the University of Colorado under a contract with the Pennsylvania Department of Transportation (PennDOT). Subsequent to that project, the Integrated technique was refined on another study funded by the Federal Highway Administration (FHWA) in which 35 bridges located on the Interstate system throughout the country were tested and evaluated. Further refinement has been implemented over the last several years through testing and evaluating several more bridges, lock gates, and other structures.

The real key to being able to complete the field testing quickly is the use of strain transducers (rather than standard foil strain gages) that can be attached to the structural members in just a few minutes. These sensors were originally developed for monitoring dynamic strains on foundation piles during the driving process. They have been adapted for use in structural testing through special modifications, and have 3 to 4 percent accuracy, and are periodically re-calibrated to NIST standards.

In addition to the strain sensors, the data acquisition hardware has been designed specifically for field use through the use of rugged cables and military-style connectors. This allows quick assembly of the system and keeps bookkeeping to a minimum. The analog-to-digital converter (A/D) is an off-the-shelf-unit, but all signal conditioning, amplification, and balancing hardware has been specially designed for structural testing. The test software has been written to allow easy configuration (test length, etc.) and operation. The end result is a system that can be used by people other than computer experts or electrical engineers. Other enhancements include the use of an automatic remote-control position indicator. The Autoclicker, a device that electronically counts wheel revolutions, is mounted on the test vehicle over one of the wheels. As the test vehicle crosses the structure along the preset path, a communication radio sends a signal to the strain measurement system that receives it and puts a mark in the data. This allows the field strains to be compared to analytical strains as a function of vehicle position, not only as a function of time.

The use of a moving load as opposed to placing the truck at discrete locations has two major benefits. First, the testing can be completed much quicker, meaning there is less impact on traffic. Second, and more importantly, much more information can be obtained (both quantitative and qualitative). Discontinuities or unusual responses in the strain histories, which are often signs of distress, can be easily detected. Since the load position is monitored as well, it is easy to determine what loading conditions cause the observed effects. If readings are recorded only at discreet truck locations, the risk of losing information between the points is great. The advantages of continuous readings have been proven over and over again.

The following list of procedures has been reproduced from the BDI Structural Testing System (STS) Operation Manual. This outline is intended to describe the general procedures used for completing a successful field test on a highway bridge using the BDI-

STS. Other types of structures can be tested as well with only slight deviations from the directions given here.

Once a tentative instrumentation plan has been developed for the structure in question, the strain transducers must be attached and the STS prepared for running the test.

Attaching Strain Transducers

There are two methods for attaching the strain transducers to the structural members: C-clamping or with tabs and adhesive. For steel structures, quite often the transducers can be clamped directly to the steel flanges of rolled sections or plate girders. If significant lateral bending is assumed to be present, then one transducer may be clamped to each edge of the flange. If the transducer is to be clamped, insure that the clamp is centered over the mounting holes. In general, the transducers can be clamped directly to painted surfaces. However, if the surface being clamped to is rough or has very thick paint, it should be cleaned first with a grinder. The alternative to clamping is the tab attachment method outlined below.

1. Place two tabs in mounting jig. Place transducer over mounts and tighten the 1/4-20 nuts until they are snug (approximately 50 in-lb.). This procedure allows the tabs to mounted without putting stress on the transducer itself. When attaching transducers to R/C members, transducer extensions are used to obtain a longer gage length. In this case the extension is bolted to one end of the transducer and the tabs are bolted to the free ends of the transducer and the extension.

2. Mark the centerline of the transducer location on the structure. Place marks 1-1/2 inches on either side of the centerline and using a hand grinder remove paint or scale from these areas. If attaching to concrete, lightly grind the surface to remove any scale. If the paint is quite thick, use a chisel to remove most of it before grinding.

3. Very lightly grind the bottom of the transducer tabs to remove any oxidation or other contaminants.

4. Apply a thin line of adhesive to the bottom of each transducer tab.

5. Spray each tab and the contact area on the structural member with the adhesive accelerator.

6. Mount transducer in its proper location and apply a light force to the tabs (not the center of the transducer) for approximately 10 seconds.

If the above steps are followed, it should be possible to mount each transducer in approximately five minutes. When the test is complete, *carefully* loosen the 1/4-20 nuts from the tabs and remove transducer. If one is not careful, the tab will pop loose from the structure and the transducer may be damaged. Use vice grips to remove the tabs from the structure.

Assembly of System

Once the transducers have been mounted, they should be connected into an STS unit. The STS units should be placed near the transducer locations in such a manner to allow four transducers to be plugged in. Each STS unit can be easily clamped to the bridge girders. If the structure is concrete and no flanges are available to set the STS units on, transducer tabs glued to the structure and plastic zip-ties or small wire can be used to hold them up. Since the transducers will identify themselves to the system, there is no special order that they must follow. The only information that must be recorded is the transducer serial number and its location on the structure. Large cables are provided which can be connected between the STS units. The maximum length between STS units is 50ft (15m). If several gages are in close proximity to each other, then the STS units can be plugged directly to each other without the use of a cable. All connectors will "click" when the connection has been completed properly.

Once all of the STS units have been connected in series, one cable must be run and connected to the power supply located near the PC. Connect the 9-pin serial cable between the computer and the power supply. The position indicator is then assembled and the system connected to a power source (either 12VDC or 120-240AC). The system is now ready to acquire data.

Performing Load Test

The general testing sequence is as follows:

1. Transducers are mounted and the system is connected together and turned on.

2. The deck is marked out for each truck pass. Locate the point on the deck directly above the first bearing for one of the fascia beams. If the bridge is skewed, the first point encountered from the direction of travel is used and an imaginary line extended across and normal to the roadway. All tests are started from this line. In order to track the position of the loading vehicle on the bridge during the test, an X-Y coordinate system, with the origin at the selected reference point is laid out.

   In addition to monitoring the longitudinal position, the vehicle's transverse position must be known. The transverse truck position is kept uniform by first aligning the truck in the center of the lane where it would normally travel at highway speed. Next, a chalk mark is made on the deck locating the transverse location of the driver's side front wheel. By making a measurement from this mark to the reference point, the transverse ("Y") position of the truck is always known. The truck is aligned on this mark for all subsequent tests in this lane. For two lane bridges with shoulders, tests are run on the shoulder (driver's side front wheel along the white line) and in the center of each lane. If the bridge has only two lanes and very little shoulder, tests are run in the center of each lane only. If the purpose of the test is to calibrate a computer model, it is sometimes more convenient to simply use the lane lines as guides since it is easier for the driver to maintain a constant lateral position. Responses due to critical truck positions are then obtained by the analysis.

   The driver is instructed that the test vehicle must be kept in the proper location on the bridge. For example, the left front wheel needs to be kept on the white line for the

shoulder tests. Another important item is that the vehicles maintain a relatively constant rate of speed during the entire test. The process of converting data to a function of truck position assumes constant speed between each click mark.

Two more pieces of information are then needed: the axle weights and dimensions of the test vehicle. The driver generally provides the axle weights, after stopping at a local scale. However, a weight enforcement team can use portable scales and weigh the truck at the bridge site. Wheel base and axle width dimensions are made with a tape measure and recorded.

3. The program is started and the number of channels indicated is verified. If the number of channels indicated do not match the number of channels actually there, a malfunction has occurred and must be corrected before testing commences.

4. The transducers are initialized (zeroed out) with the Balance option. If a transducer cannot be initialized, it should be inspected to ensure that it has not been damaged.

5. The desired test length, sample rate, and output file name are selected. In general, a longer test time than the actual event is selected. For most bridge tests, a one or two-minute test length will suffice since the test can be stopped as soon as the truck crosses completely over the structure.

6. To facilitate presenting data as a function of load position, rather than time, two items describing the PI information must be defined. The starting position and PI interval distance allow the data to be plotted using position coordinates that are consistent with a numeric analysis. The starting position refers to the longitudinal position of the load vehicle in the model coordinate system when the data recording is started. The interval distance is the circumference of the tire that is being used by the Autoclicker. It is important that this information be clearly defined in the field notes.

7. If desired, the Monitor option can be used to verify transducer output during a trial test. Also, it is useful to run a Position Indicator (PI) test while in Monitor to ensure that the clicks are being received properly.

8. When all parties are ready to commence the test, the Run Test option is selected which places the system in an activated state. The Autoclicker is positioned so that the first click occurs at the starting line. This first click starts the test. The Autoclicker also puts one mark in the data for every wheel revolution. An effort should be made to get the truck across with no other traffic on the bridge. There should be no talking over the radios during the test, as a "position" will be recorded each time the microphones are activated.

9. When the test has been completed, and the system is still recording data, hit "S" to stop collecting data and finish writing the recorded data to disk. If the data files are large, they can be compressed and copied to floppy disk.

10. It is important to record the field notes very carefully. Having data without knowing where it was recorded can be worse than having no data at all. Transducer location and

serial numbers must be recorded accurately. All future data handling in BDI-GRF is then accomplished by keying on the transducer number. This system has been designed to eliminate the need to track channel numbers by keeping this process in the background. However, the STS unit and the transducer's connector number are recorded in the data file if needed for future hardware evaluations.

Appendix B - Modeling and Analysis: The Integrated Approach

Introduction

In order for load testing to be a practical means of evaluating short- to medium-span bridges, it is apparent that testing procedures must be economic to implement in the field and the test results translatable into a load rating. A well-defined set of procedures must exist for the field applications as well as for the interpretation of results. An evaluation approach based on these requirements was first developed at the University of Colorado during a research project sponsored by the Pennsylvania Department of Transportation (PennDOT). Over several years, the techniques originating from this project have been refined and expanded into a complete bridge rating system.

The ultimate goal of the Integrated Approach is to obtain realistic rating values for highway bridges in a cost-effective manner. This is accomplished by measuring the response behavior of the bridge due to a known load and determining the structural parameters that produce the measured responses. With the availability of field measurements, many structural parameters in the analytical model can be evaluated that are otherwise conservatively estimated or ignored entirely. Items that can be quantified through this procedure include the effects of structural geometry, effective beam stiffnesses, realistic support conditions, effects of parapets and other non-structural components, lateral load transfer capabilities of the deck and transverse members, and the effects of damage or deterioration. Often, bridges are rated poorly because of inaccurate representations of the structural geometry or because the material and/or cross-sectional properties of main structural elements are not well defined. A realistic rating can be obtained, however, when all of the relevant structural parameters are defined and implemented in the analysis process.

One of the most important phases of this approach is a qualitative evaluation of the raw field data. Much is learned during this step to aid in the rapid development of a representative model.

Initial Data Evaluation

The first step in structural evaluation consists of a visual inspection of the data in the form of graphic response histories. Graphic software was developed to display the raw strain data in various forms. Strain histories can be viewed in terms of time or truck position. Since strain transducers are typically placed in pairs, neutral axis measurements, curvature responses, and strain averages can also be viewed. Linearity between the responses and load magnitude can be observed by the continuity in the strain histories. Consistency in the neutral axis measurements from beam to beam and as a function of load position provides great insight into the nature of the bridge condition. The direction and relative magnitudes of flexural responses along a beam line are useful in determining if end restraints play a significant role in the response behavior. In general, the initial data inspection provides the engineer with information concerning modeling requirements and can help locate damaged areas.

Having strain measurements at two depths on each beam cross-section, flexural curvature and the location of the neutral axis can be computed directly from the field data. Figure 57 illustrates how curvature and neutral axis values are computed from the strain measurements.

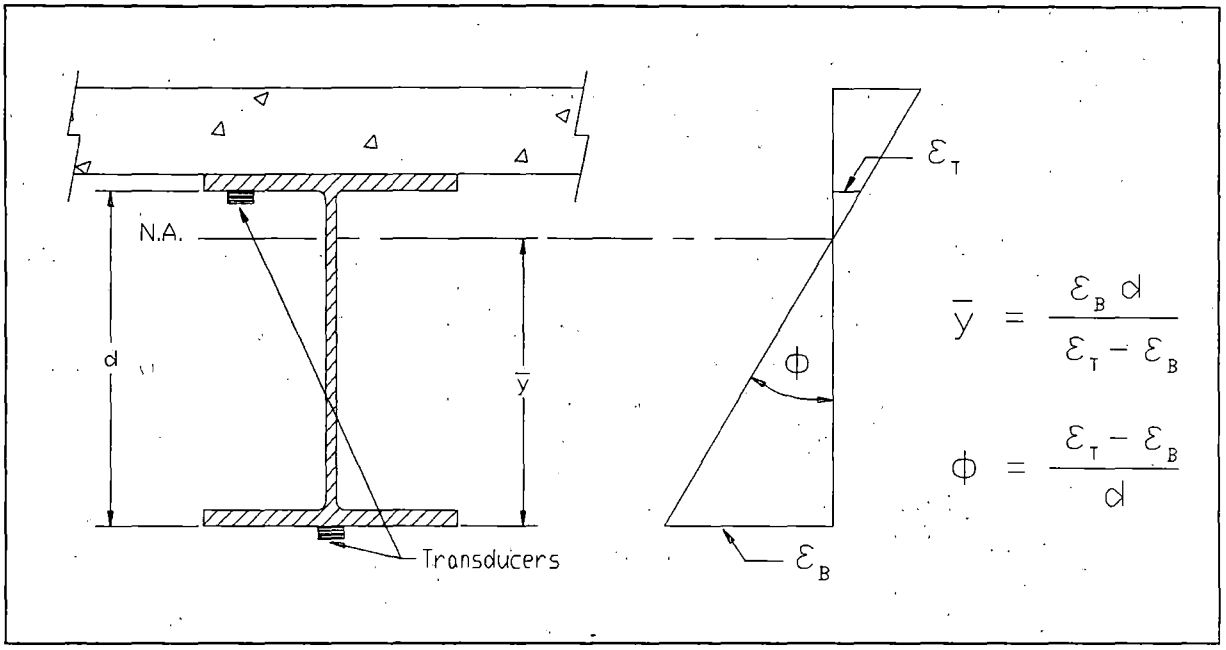

Figure 57 Illustration of Neutral Axis and Curvature Calculations

The consistency in the N.A. values between beams indicates the degree of consistency in beam stiffnesses. Also, the consistency of the N.A. measurement on a single beam as a function of truck position provides a good quality check for that beam. If for some reason a beam's stiffness changes with respect to the applied moment (i.e. loss of composite action or loss of effective flange width due to a deteriorated deck), it will be observed by a shift in the N.A. history.

Since strain values are translated from a function of time into a function of vehicle position on the structure and the data acquisition channel and the truck position tracked, a considerable amount of book keeping is required to perform the strain comparisons. In the past, this required manipulation of result files and spreadsheets which was tedious and a major source of error. This process in now performed automatically by the software and all of the information can be verified visually.

Finite Element Modeling and Analysis

The primary function of the load test data is to aid in the development of an accurate finite element model of the bridge. Finite element analysis is used because it provides the most general tool for evaluating various types of structures. Since a comparison of measured and computed responses is performed, it is necessary that the analysis be able to represent the actual response behavior. This requires that actual geometry and boundary conditions be realistically represented. In maintaining reasonable modeling efforts and computer run times, a certain amount of simplicity is also required, so a planar grid model is generated for most structures and linear-elastic responses are assumed. A grid of frame elements is assembled in the same geometry as the actual structure. Frame

elements represent the longitudinal and transverse members of the bridge. Plate elements attached to the grid provide the load transfer characteristics of the deck. When end-restraints are determined to be present, elastic spring elements having both translational and rotational stiffness terms are inserted at the support locations.

The connection between the beams and the deck plates can be handled in various ways. The simplest, and generally the most accurate, method is to assume all of the beam neutral axes lie in a single plane. Any contribution of the deck resulting in composite action is then accounted for by the beam moment-of-inertia values. This method is most suitable when the primary beam load response is flexure.

An alternate approach, providing a more realistic model of the beam/deck interaction, is the use of eccentricity terms in the beam elements. This is a quasi 3-D modeling technique that separates the plane of the beam neutral axes with the plane of the deck. It is useful when modeling composite beam/slab structures with a variety of different beam cross-sections such that a single plane cannot be assumed. While the geometry of this model is technically more realistic, a much finer mesh is required because flexural responses are partially resisted by first-order axial terms of the beam elements. The resulting moment and axial force responses are much more discretized than with the pure planar model. Another draw back to the quasi 3-D model becomes apparent during data processing of the analysis results because beam stresses are a function of beam flexure and axial deformation.

Depending on the structure's geometry, a planar model may not be sufficient. For example trusses, box girders, and structures containing beams with depth-to-span ratios greater than 10 generally required 3-D modeling techniques to accurately represent load transfer characteristics. The method of modeling is therefore dependent on the complexity of the structure, the type of information that is sought, and the preference of the engineer.

Loads are applied in a manner similar to the actual load test. A model of the test truck, defined by a two-dimensional group of point loads, is placed on the structure model at discrete locations along the same path that the test truck followed during the load test. Gage locations identical to those in the field are also defined on the structure model so that strains can be computed at the same locations under the same loading conditions.

Model Correlation and Parameter Modifications

The accuracy of the model is determined numerically by the analysis using several statistical relationships and through visual comparison of the strain histories. The numeric accuracy values are useful in evaluating the effect of any changes to the model, where as the graphical representations provide the engineer with the best perception for why the model is responding differently than the measurements indicate. Member properties that cannot be accurately defined by conventional methods or directly from the field data are evaluated by comparing the computed strains with the measured strains. These properties are defined as variable and are evaluated such that the best correlation between the two sets of data is obtained. It is the engineer's responsibility to determine which parameters need to be refined and to assign realistic upper and lower limits to each parameter. The evaluation of the member property is accomplished with the aid of a parameter identification process (optimizer) built into the analysis. In short, the process consists of an

iterative procedure of analysis, data comparison, and parameter modification. It is important to note that the optimization process is merely a tool to help evaluate various modeling parameters. The process works best when the number of parameters is minimized and reasonable initial values are used.

During the optimization process, various error values are computed by the analysis program that provide quantitative measure of the model accuracy and improvement. The error is quantified in four different ways, each providing a different perspective of the model's ability to represent the actual structure; an absolute error, a percent error, a scale error and a correlation coefficient.

The **absolute error** is computed from the absolute sum of the strain differences. Algebraic differences between the measured and theoretical strains are computed at each gage location for each truck position used in the analysis, therefore, several hundred strain comparisons are generally used in this calculation. This quantity is typically used to determine the relative accuracy from one model to the next and to evaluate the effect of various structural parameters. It is used by the optimization algorithm as the objective function to minimize. Because the absolute error is in terms of micro-strain ($m\varepsilon$) the value can vary significantly depending on the magnitude of the strains, the number of gages and number of different loading scenarios. For this reason, it has little conceptual value except for determining the relative improvement of a particular model.

A **percent error** is calculated to provide a better qualitative measure of accuracy. It is computed as the sum of the strain differences squared divided by the sum of the measured strains squared. The terms are squared so that error values of different sign will not cancel each other out, and to put more emphasis on the areas with higher strain magnitudes. A model with acceptable accuracy will usually have a percent error of less than 10%.

The **scale error** is similar to the percent error except that it is based on the maximum error from each gage divided by the maximum strain value from each gage. This number is useful because it is based only on strain measurements recorded when the loading vehicle is in the vicinity of each gage. Depending on the geometry of the structure, the number of truck positions, and various other factors, many of the strain readings are essentially negligible. This error function uses only the most relevant measurement from each gage.

Another useful quantity is the **correlation coefficient** which is a measure of the linearity between the measured and computed data. This value determines how well the shape of the computed response histories match the measured responses. The correlation coefficient can have a value between 1.0 (indicating a perfect linear relationship) and -1.0 (exact opposite linear relationship). A good model will generally have a correlation coefficient greater than 0.90. A poor correlation coefficient is usually an indication that a major error in the modeling process has occurred. This is generally caused by poor representations of the boundary conditions or the loads were applied incorrectly (i.e. truck traveling in wrong direction).

The following table contains the equations used to compute each of the statistical error values:

Table 63. Error Functions

ERROR FUNCTION	EQUATION
Absolute Error	$\Sigma\lvert\varepsilon_m - \varepsilon_c\rvert$
Percent Error	$\Sigma(\varepsilon_m - \varepsilon_c)^2 \;/\; \Sigma(\varepsilon_m)^2$
Scale Error	$\dfrac{\Sigma \max\lvert\varepsilon_m - \varepsilon_c\rvert_{gage}}{\Sigma \max\lvert\varepsilon_m\rvert_{gage}}$
Correlation Coefficient	$\dfrac{\Sigma(\varepsilon_m - \overline{\varepsilon_m})(\varepsilon_c - \overline{\varepsilon_c})}{\Sigma\sqrt{(\varepsilon_m - \overline{\varepsilon_m})^2(\varepsilon_c - \overline{\varepsilon_c})^2}}$

In addition to the numerical comparisons made by the program, periodic visual comparisons of the response histories are made to obtain a conceptual measure of accuracy. Again, engineering judgment is essential in determining which parameters should be adjusted so as to obtain the most accurate model. The selection of adjustable parameters is performed by determining what properties have a significant effect on the strain comparison and determining which values cannot be accurately estimated through conventional engineering procedures. Experience in examining the data comparisons is helpful, however, two general rules apply concerning model refinement. When the shapes of the computed response histories are similar to the measured strain records but the magnitudes are incorrect this implies that member stiffnesses must be adjusted. When the shapes of the computed and measured response histories are not very similar then the boundary conditions or the structural geometry are not well represented and must be refined.

In some cases, an accurate model cannot be obtained, particularly when the responses are observed to be non-linear with load position. Even then, a great deal can be learned about the structure and intelligent evaluation decisions can be made.

Appendix C - Load Rating Procedures

For borderline bridges (those that calculations indicate a posting is required), the primary drawback to conventional bridge rating is an oversimplified procedure for estimating the load applied to a given beam (i.e. wheel load distribution factors) and a poor representation of the beam itself. Due to lack of information and the need for conservatism, material and cross-section properties are generally over-estimated and beam end supports are assumed to be simple when in fact even relatively simple beam bearings have a substantial effect on the midspan moments. Inaccuracies associated with conservative assumptions are compounded with complex framing geometries. From an analysis standpoint, the goal here is to generate a model of the structure that is capable of reproducing the measured strains. Decisions concerning load rating are then based on the performance of the model once it is proven to be accurate.

The main purpose for obtaining an accurate model is to evaluate how the bridge will respond when standard design loads, rating vehicles or permit loads are applied to the structure. Since load testing is generally not performed with all of the vehicles of interest, an analysis must be performed to determine load-rating factors for each truck type. Load rating is accomplished by applying the desired rating loads to the model and computing the stresses on the primary members. Rating factors are computed using the equation specified in the AASHTO Manual for Condition Evaluation of Bridges - see Equation (1).

It is important to understand that diagnostic load testing and the integrated approach are most applicable to obtaining Inventory (service load) rating values. This is because it is assumed that all of the measured and computed responses are linear with respect to load. The integrated approach is an excellent method for estimating service load stress values but it generally provides little additional information regarding the ultimate strength of particular structural members. Therefore, operating rating values must be computed using conventional assumptions regarding member capacity. This limitation of the integrated approach is not viewed as a serious concern, however, because load responses should never be permitted to reach the inelastic range.

Operating and/or Load Factor rating values must also be computed to ensure a factor of safety between the ultimate strength and the maximum allowed service loads. The safety to the public is of vital importance but as long as load limits are imposed such that the structure is not damaged then safety is no longer an issue.

Following is an outline describing how field data is used to help in developing a load rating for the superstructure. These procedures will only complement the rating process, and must be used with due consideration to the substructure and inspection reports.

1. **Preliminary Investigation:** Verification of linear and elastic behavior through continuity of strain histories, locate neutral axis of flexural members, detect moment resistance at beam supports, qualitatively evaluate behavior.

2. **Develop representative model:** Use graphic pre-processors to represent the actual geometry of the structure, including span lengths, girder spacing, skew, transverse

members, and deck. Identify gage locations on model identical to those applied in the field.

3. **Simulate load test on computer model:** Generate 2-dimensional model of test vehicle and apply to structure model at discrete positions along same paths defined during field tests. Perform analysis and compute strains at gage location for each truck position.

4. **Compare measured and initial computed strain values:** Various global and local error values at each gage location are computed and visual comparisons made with post-processor.

5. **Evaluate modeling parameters:** Improve model based on data comparisons. Engineering judgment and experience is required to determine which variables are to be modified. A combination of direct evaluation techniques and parameter optimization are used to obtain a realistic model. General rules have been defined to simplify this operation.

6. **Model evaluation:** In some cases it is not desirable to rely on secondary stiffening effects if it is likely they will not be effective at higher load levels. It is beneficial, though, to quantify their effects on the structural response so that a representative computer model can be obtained. The stiffening effects that are deemed unreliable can be eliminated from the model prior to the computation of rating factors. For instance, if a non-composite bridge is exhibiting composite behavior, then it can conservatively be ignored for rating purposes. However, if it has been in service for 50 years and it is still behaving compositely, chances are that very heavy loads have crossed over it and any bond-breaking would have already occurred. Therefore, probably some level of composite behavior can be relied upon. When unintended composite action is allowed in the rating, additional load limits should be computed based on an allowable shear stress between the steel and concrete and an ultimate load of the non-composite structure.

7. **Perform load rating:** Apply HS-20 and/or other standard design, rating and permit loads to the calibrated model. Rating and posting load configuration recommended by AASHTO are shown in Figure 58.The same rating equation specified by the **AASHTO - Manual for the Condition Evaluation of Bridges** is applied:

$$RF = \frac{C - A_1 D}{A_2 L(1 + I)} \qquad (1)$$

where:

RF = Rating Factor for individual member.
C = Member Capacity.
D = Dead-Load effect.
L = Live-Load effect.
A_1 = Factor applied to dead-load.
A_2 = Factor applied to live-load.
I = Impact effect, either AASHTO or measured.

The only difference between this rating technique and standard beam rating programs is that a more realistic model is used to determine the dead-load and live-load effects. Two-dimensional loading techniques are applied because wheel load distribution factors are not applicable to a planar model. Stress envelopes are generated for several truck paths, envelopes for paths separated by normal lane widths are combined to determine multiple lane loading effects.

8. **Consider other factors:** Other factors such as the condition of the deck and/or substructure, traffic volume, and other information in the inspection report should be taken into consideration and the rating factors adjusted accordingly.

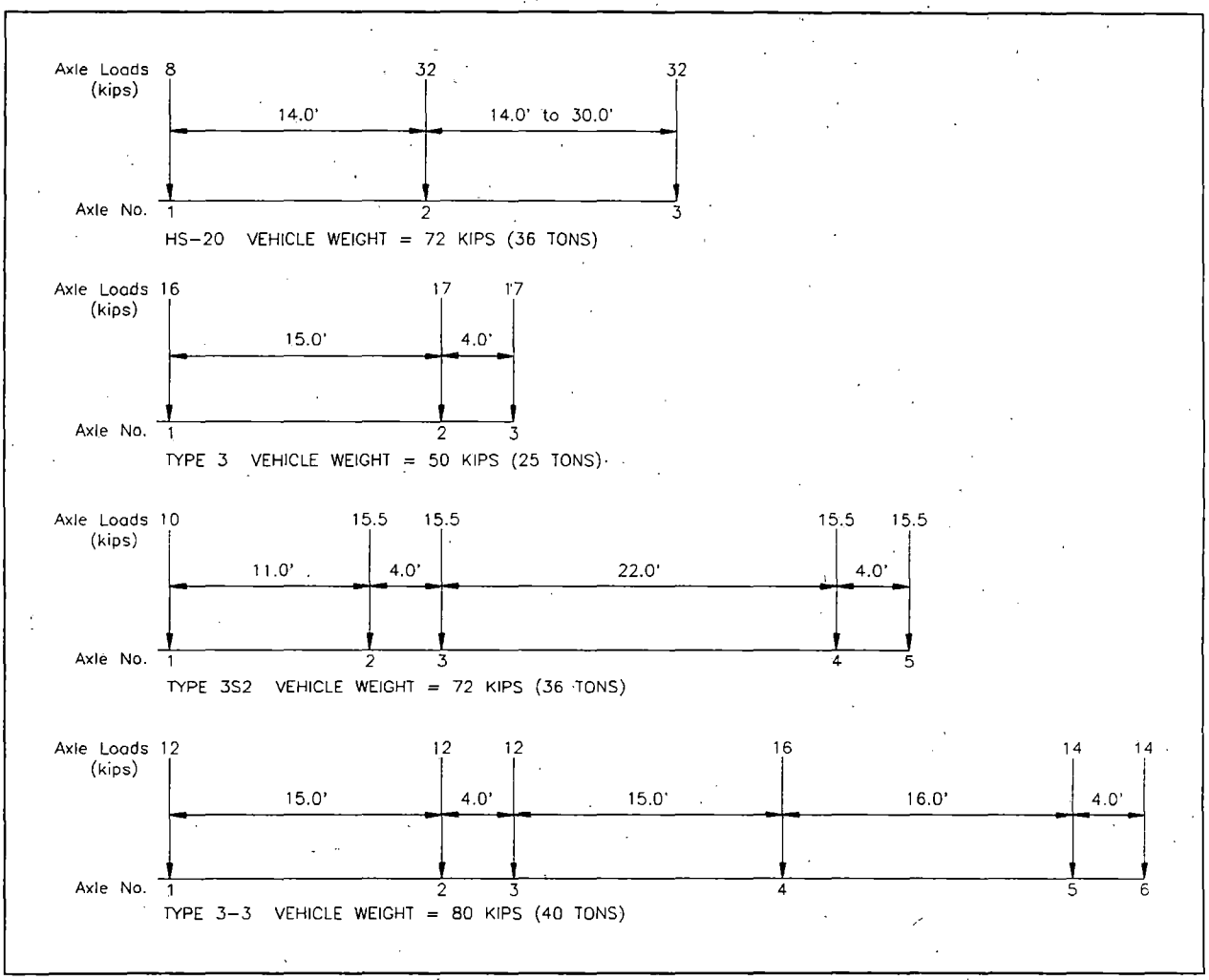

Figure 58 AASHTO rating and posting load configurations.

Appendix D - References

AASHTO (1989). "Standard Specification for Highway Bridges." Washington,D.C.

AASHTO, (1994). "Manual for the Condition Evaluation of Bridges", Washington,D.C.

Commander,B., (1989). "An Improved Method of Bridge Evaluation: Comparison of Field Test Results with Computer Analysis." Master Thesis, University of Colorado, Boulder, CO.

Gerstle, K.H., and Ackroyd,M.H. (1990). "*Behavior and Design of Flexibly-Connected Building Frames.*" Engineering Journal, AISC, 27(1),22-29.

Goble,G., Schulz,J., and Commander,B. (1992). "Load Prediction and Structural Response." Final Report, FHWA DTFH61-88-C-00053, University of Colorado, Boulder, CO.

Lichtenstein,A.G.(1995). "Bridge Rating Through Nondestructive Load Testing." Technical Report, NCHRP Project 12-28(13)A.

Schulz,J.L. (1989). "Development of a Digital Strain Measurement System for Highway Bridge Testing." Masters Thesis, University of Colorado, Boulder, CO.

Schulz,J.L. (1993). "In Search of Better Load Ratings." *Civil Engineering*, ASCE 63(9),62-65.